NASA Contractor Report 175021

NASA-CR-175021
19860008318

# Closure of Fatigue Cracks at High Strains

N.S. Iyyer and N.E. Dowling
*Virginia Polytechnic Institute and State University*
*Blacksburg, Virginia*

December 1985



Prepared for the
Lewis Research Center
Under Grant NAG 3–438

National Aeronautics and
Space Administration

TABLE OF CONTENTS

# CHAPTER 1

# INTRODUCTION AND LITERATURE REVIEW

The present day concern of fracture mechanics is the study of critical crack sizes which have a significant effect on the life of a component. The failure of a structure or a component is often due to the presence of a crack of critical size. Fatigue, which causes failure of materials by the incipient growth of flaws, is the most important cause. Thus, understanding the behavior of microcracking and growth of small cracks in fatigue leads to the development of improved methods of predicting lives of components.

Failure of materials under fatigue involves [1] the following:

1. Initial cyclic damage (cyclic hardening or softening)
2. Formation of initial microscopic flaws (microcrack initiation)
3. Microcrack coalescence to form a propagating flaw (microcrack growth)
4. Macroscopic propagation of this flaw (macrocrack growth)
5. Failure instability

Often steps 1 and 2 described above are referred to as crack initiation, 3 and 4 as crack propagation.

## 1.1 SHORT CRACKS AND THEIR IMPORTANCE

The definition of a short crack depends on the nature of the problem being considered. Reference 2 lists various considerations for defining short cracks, such as the following:

1. Relative size of the crack with respect to the microsructure (grain size etc., $0.4 \times 10^{-6}$ in to $2 \times 10^{-3}$ in.)
2. Relative size of the crack with respect to the plastic zone (typically 0.004 in. in high strength materials, or 0.04 in. to 0.4 in. in low strength materials, and varying with stress level)
3. Size of the crack with respect to thickness (constraint)
4. Size of the crack with respect to the applicability of linear elastic fracture mechanics, LEFM.
5. Crack detecting capability i.e., cracks that are so small that they are difficult to find (0.004 in. to 0.04 in.)

Thus, an exact definition of a short crack cannot be made. The size of a crack to be considered as short (small) depends on the perspective of the problem that one is faced with.

A reasonable and improved estimate of the life of a component can be made by the study of short crack initiation and growth. Since most service failures are caused by cyclically varying stresses which cause progressive failure of a component, the short crack problem in fatigue is of major concern. Advances in the understanding of short crack growth have enabled increasingly quantitative studies to be pursued into the specific mechanisms that affect initiation and growth. Manufacturing related problems associated with small cracks that affect the lives of structural components have been identified [3]. References [4,5,6] discuss the importance of the short crack problem.

Since the similitude relative to the metallurgical structure breaks down for short cracks, the local effects will be dominant in the materials response. Material inhomogenieties, such as crack front irregularities, second phase particles or inclusions, and grain boundaries play a vital part in affecting the local stress field and hence the materials response. In the case of long cracks, all these effects are integrated and averaged over many grains. But in the short crack case, the following are important: applied stress, yield stress and yield properties, crystallographic anisotropy, homogeneity, and environment.

The behavior of short cracks as to their propagation is different from that of long cracks, which can be generally handled by LEFM. The literature indicates that study of short cracks should consider the following aspects:

1. Fracture mechanics characteristics involving elastic-plastic fracture mechanics, and
2. Physics of crack propagation involving microstructure, environment, crack closure, crack extension, crack size, and crack shape.

## 1.2 FATIGUE CRACK PROPAGATION

Rice [7] and Hult and McClintock [8] used plastic superposition methods which are valid in cases where plastic strains are in constant proportion to one another and where total strain theories can be applied. These are ideal cases, and in reality, there are

deviations from proportional flow. The ideal case assumed by Rice [7] permits a general treatment of the reponse to unloading, reloading and cyclic loading.

Small scale yielding solutions for cyclic loading are obtained directly by replacing the stress intensity factor by its variation and doubling the yield stress, $\sigma_y$, and yield strain, $\varepsilon_y$. One of the important results from analyzing the elastic-plastic models for small scale yielding is that plastic deformation is entirely determined by the history of variation of the stress intensity factor, K. Thus, two different cracked bodies will exhibit identical fatigue crack extensions if each is subjected to the same variations of K.

But in large scale yielding, especially when the crack itself is small, no single parameter is known that plays the role of the elastic stress intensity factor in determining crack tip plasticity. Large scale yielding analyses are not available for all cases, since with perfect plasticity models, unrestricted flow occurs. Thus, crack propagation under repeated overall plastic straining has not been analyzed mathematically because of the complexities involved.

LEFM is based on the result that the strength of the elastic stress field singularity at the crack tip is expressed by K, which is a function of the applied load and geometry [9,10]. The resistance of metals to fracture under static and cyclic loading can be described by this stress intensity factor in a geometry independent

atigue crack growth models also do not
ities of the long crack behavior. Hence,
this method of using LEFM for predicting
limited. Kanninen [12] observes that crack
crack tip plasticity, but the result is not
ties involving similitude. Thus, for short
litude does not usually exist, LEFM based
ed.

scale yielding, crack growth rate is
h as the J-integral [13,14,15], crack
16,17,18], and the size of the plastic
d on small scale yielding generally
rates, especially when the crack length

f short cracks can thus be atrributed to

ium mechanics assumption used with LEFM,
elasticity assumption.

l compared to the plastic zone, cracks are
n expected from the long crack LEFM
ed to inappropriate use of LEFM analysis
. One approach is to remove the
id long cracks in the use of the J-

DISPLAY 16/6/1
86N17788*# ISSUE 8 PAGE 1292 CATEGORY 39 RPT#: NASA-CR-175021 NAS
1.26:175021 CNT#: NAG3-438 85/12/00 159 PAGES UNCLASSIFIED DOCUMENT
UTTL: Closure of fatigue cracks at high strains TLSP: Final Report
AUTH: A/IYYER, N. S.; B/DOWLING, N. E.
CORP: Virginia Polytechnic Inst. and State Univ., Blacksburg. CSS: (Dept. of Engineering Science and Mechanics.)
SAP: HC A08/MF A01 AVAIL.NTIS
CIO: UNITED STATES
MAJS: /*CRACK CLOSURE/*CRACK PROPAGATION/*CYCLIC LOADS/*FATIGUE (MATERIALS)/*J INTEGRAL/*MICROCRACKS/*STRAIN MEASUREMENT
MINS: / CRACK INITIATION/ LOADS (FORCES)/ PLASTIC DEFORMATION
ABA: Author

Ritchie [2] lists the following factors which have significant impact on short crack growth behavior:

1. Plasticity at stress raisers (notches)
2. Microplasticity
3. Grain boundary blocking of slip bands
4. Cessation of growth and crystallographic reorientation of growth at grain boundaries.
5. Crack closure

## 1.3 CRACK CLOSURE

Since Elber [20] showed that fatigue cracks can be partially closed even under tensile loading, crack closure has been widely investigated and recognized as an important factor affecting fatigue crack propagation behavior. Briefly, crack closure can be induced by plasticity, crack surface roughness, or oxide wedging.

### 1.3.1 PLASTICITY INDUCED CLOSURE

A schematic illustration of the mechanism of plasticity induced closure is shown in Fig. 1.

Plasticity induced closure is due to the contained plasticity and due to the residual tensile strains left behind the crack tip. As the load is applied, the material ahead of the crack tip yields due to the stress concentration, even if the applied stress on the specimen is below the yield stress. The size of the plastic zone is related to the crack length and applied stress [9]. The material

surrounding the plastic zone remains elastic, and as the load is decreased, compressive stresses build up in the region of the crack tip. This compressive stress must be overcome before the crack tip can open on reloading.

The other mechanism which causes crack closure behavior is due to the residual strains that exist in the wake of the moving crack tip. There exists a region of residual tensile strains (deformations) which are left in the material behind the crack tip. These are illustrated schematically in Fig. 2. These residual strains existing inside of the envelope of all previous plastic zones are also responsible for crack closure [20,21]. These cause the crack surfaces to come into contact before the minimum stress level in the cyle is reached. Upon loading, the crack will open only when the applied stresses overcome the residual compressive stresses between the crack surfaces. Since crack growth can occur only when the crack tip is open, an effective stress intensity is defined to correlate crack growth rates. Elber [21] defines an effective stress range as

$$\Delta\sigma_{eff} = \sigma_{max} - \sigma_{op} \tag{1}$$

where $\sigma_{max}$ is the maximum stress level and $\sigma_{op}$ is the opening level. Defining

$$U = \frac{\sigma_{max} - \sigma_{op}}{\sigma_{max} - \sigma_{min}} = \frac{\Delta\sigma_{eff}}{\Delta\sigma} \tag{2}$$

Elber obtained the following crack propagation equation for an aluminum alloy:

$$\frac{da}{dN} = C(\Delta K_{eff})^n = C(U\Delta K)^n \tag{3}$$

where da/dn is the crack growth rate and $\Delta K_{eff}$ is the effective stress intensity range. By his results, he fitted an emperical relation for U as

$$U = 0.5 + 0.1R + 0.4R^2 \tag{4}$$

where R is the ratio of the minimum stress level to the maximum stress level.

Some other relations developed for U by various workers are given as

$$U = 0.68 + 0.91\ R \qquad \text{(Ref. 22)} \tag{5}$$

$$U = \frac{1 - C_f}{1 - R}\ ;\ C_f = \frac{\sigma_{op}}{\sigma_{max}} \qquad \text{(Ref. 23)} \tag{6}$$

$$U = \frac{K_{max}}{100}\,[880R + 6.0] + 1.30R + 0.2 \qquad \text{(Ref. 24)} \tag{7}$$

Equations (4) - (7) can be expressed in the general form

$$U = f(R,\ K_{max},\ \text{material}) \tag{8}$$

Crack closure is thus a complicated process influenced by cracking mode (I, II, or III) environment, and microstructure.

From the various reported work, the following, not fully consistent, observations have been made:

1. U = f(R) for a material is independent of other parameters [22,23]
2. U increases with increase in R in all cases, whereas the relationship of U with $K_{max}$ is not usually the same.
3. No crack closure is observed at higher values of R, i.e., U becomes more than unity [24].
4. Crack closure measurement technique is found to influence the value of U.

The role of compressive stress in the plastic zone envelope in the wake of the crack would be limited for a small crack of length comparable to the plastic zone size ahead of the crack tip. This may be one of the reasons why short cracks can grow at a level below the threshold stress-intensity range.

Analytical work [25,26] has been done to predict the crack opening load. These results may give closure loads which differ from the opening load [27]. Budiansky and Hutchinson [25] have determined the residual stresses and crack opening and closure loads for $R > 0$ loading in plane stress situations. Recently, Nakai, et.al. [28] have published results based on Budiansky and Hutchinson's analysis which can be extended to $R < 0$, also for small scale yielding situations.

In their analytical work, Budiansky and Hutchinson [25] solved a boundary value problem at $K_{min}$ with a residual displacement $\delta_r$ along the contact region $(-\infty,o)$, a compressive yield stress, $-\sigma_y$ over the reversed plastic zone, $\Delta\omega$, in $(o,a)$, and with a displacement $\delta=\delta_M$, between reversed and maximum plastic zone size $(a,w)$. The crack tip parameters that were used in their analysis are shown in Fig. 3. As is indicated in their work, the Dugadale model which has been used is most appropriate for plane stress problems, whereas plane strain conditions are more relevant to fatigue crack growth. It is also noticed that cyclic hardening produces increased closure effects. Dill et.al. [29,30] obtained an integral equation formulation to determine the contact stresses and effective stress intensity by a different approach.

Thus it is observed that most of the work on crack closure has been focused on long cracks and small scale yielding conditions. Newman [26,31,32] has developed a model based on the Dugdale model, leaving the plastically deformed material in the wake of an advancing crack tip. The advantage of using this model is that plastic zone size and crack surface displacements are obtained by superposition of two elastic problems. Ohji et.al [33,34] also have used finite element tecniques based on a Dugdale type model to study closure behavior. Newman has used elements, which behave as perfectly plastic material for any applied load. These elements can be either

intact ahead of the crack tip, or broken behind it, to represent residual plasticity effects. The elements which are not in contact are used to calculate $\sigma_{op}$. Using the effective stress-intensity, Newman [26] has used plasticity corrected K values in his calculations. Figure 4 describes the crack surface displacements and stress distributions along a crack line with the elements as used by Newman [26].

It is important to observe from Newman's analysis that at equal K values, the applied stress needed to open a small crack is less than that required to open a large crack. Consequently, $\Delta\sigma_{eff}$ is greater for small cracks. This correlates well with the high crack growth rates for short cracks. Thus, the short crack effect may be at least partly a result of the differences in the crack closure effect between long and short cracks [26]. The effects of the stress ratio, R, peak stress, $\sigma_{max}$, and the degree of constraint at the crack tip can all be included in Newman's analysis.

### 1.3.2 ROUGHNESS INDUCED CLOSURE

In shear mode (II or III) extension of the crack, the rough irregular fracture surfaces [35,36] induce roughness induced closure. In these cases, crack closure will be strongly dependent upon crack size [36,37]. In the case of short cracks, roughness induced closure is less significant because of the near zero crack lengths. A schematic diagram of roughness induced closure is shown in Fig. 5. The amount of crack closure has been observed to

correlate with increasing fracture surface roughness and the degree of crack path deviation from a straight line [46]. Thus, for long cracks, a zig-zag path of the crack should be considered along the crack front because of the pronounced crack deflection. The extent and angles of these deflections and concurrent stresses are thought to be related to texture and grain size.

### 1.3.3 OXIDE INDUCED CLOSURE

There are situations in which crack closure occurs because of a wedging action from oxidation or corrosion products [38]. A schematic diagram of the oxide induced closure is shown in Fig. 6. A number of workers have studied oxide induced closure and have offered explanations for near threshold corrosion fatigue crack growth behavior.

### 1.3.4 DISCUSSION OF CRACK CLOSURE EFFECTS

Since short cracks possess a limited wake, it is to be expected that in general such cracks will be subjected to less closure. There are difficulties in experimental techniques to observe closure as such. The experimental techniques reported in the literature on crack opening/closure measurements vary from one investigator to another. The location of the crack opening displacement has also been shown to influence the results significantly [47]. As observed in Newman's analysis, residual stresses at $\sigma_{min}$ have been estimated, and crack opening loads to overcome them have been calculated. The

other analytical work on crack closure has mostly been done for $R > 0$ loading.

Sehitoglu [27] has observed a difference between crack opening and closure levels, while in most experimental studies crack opening and closure levels were assumed to be equal. The level of crack closure is lower than the opening level, so that use of the closure level results in conservative values of $\Delta K_{eff}$.

Because of the inadequate characterization of the crack tip stress and deformation fields and surface interaction effects, crack closure studies are not complete. Reference [39] reports a crack that was open throughout the entire cycle under R=-1 loading. Similar observations have been made under large scale yielding. No solution yet exists to analyze closure effects in the case of general yielding.

In most previous work, a Dugdale type of model is used, where the plastic strain gradient perpendicular to the crack axis is considered by assuming all the sample to be elastic except a small strip in the weakest cross section. This severely strained region is considered to model the redistribution process due to the elastic material response on its boundary. From this viewpoint, the shape of the plastic zone is less significant compared to its extent along the crack axis. Thus, this type of model can be applied only to a special case of elastic-plastic fracture mechanics problems and cannot be generalized to completely describe real fatigue crack

growth behavior. Added to these complexities is the three-dimensional nature of the crack, where plane strain conditions exist in the interior and plane stress conditions at the surface. Since most experimental techniques measure closure by observing surface cracks, they may not give good insight into the actual crack closure phenomenon.

From the various reported work, it has been observed that study of crack closure effects has been limited to mostly elastic analysis, i.e., small scale yielding. Crack closure observations in completely reversed cycling at high strains have not been reported. The effect of plastic strain on the crack closure behavior is thus poorly understood. For a better understanding of the crack growth behavior, experiments are to be conducted at different strain levels, at different R ratios, and on different grain sizes. This in turn will result in a more general elastic-plastic analysis describing the crack growth behavior in all cases. This study concentrates on the closure behavior of cracks at high strains. The experimental results of this study is hoped to reveal the effects of the residual crack tip plasticity and its manifestations, i.e., crack closure in a broader perspective.

# CHAPTER 2

# EXPERIMENTAL PROGRAM

Controlled strain tests were conducted on uniaxial test specimens, and detailed observations of crack opening and closing were made. The details and scope of the testing procedures and methods are described here.

## 2.1 MATERIAL

The experiments are conducted on strengthened metal alloy AISI 4340 steel. The chemical composition and the mechanical properties are tabulated in tables 1 and 2, respectively. The material was obtained in thick section to obtain the most isotropic and homogeneous state possible, and was heat treated in slabs sufficiently thin to obtain through hardening, specifically 2 inches. Also, the material was relatively free of any crack arresters such as large nonmetallic inclusions. Reference [40] illustrates typical inclusions and their sizes. The presence of such crack arresters would invalidate the results, since measurements are made on surface cracks, which propagate through the thickness also. The AISI 4340 steel chosen for the study has a mean prior austenite grain size of 0.00063 in. Cyclic stress-strain and low cycle fatigue data for this material are shown in Figs. 7 and 8 [40]. The data obtained from the present study are also shown on

these figures, and these correlate well with the previous work of Dowling [40] on the same material.

## 2.2 SPECIMEN DESIGN AND GEOMETRY

Smooth unnotched axial specimens are used in the present study. The specimen geometry is shown in Fig. 9. Material for these specimens was obtained from a 7.5 in. diameter bar, the axis of the specimens being parallel to the axis of the circular bar. In the low cycle fatigue region, surface finish in the reduced section is not that important. A good surface finish of $4 \times 10^{-6}$ in.) was nevertheless used in the reduced section to help in differentiating the crack from polishing or grinding marks. Since longitudinal strains are measured with a 0.5 in. gauge length, straight gage sections were employed. To minimize buckling problems, we have employed a length to diameter ratio of 2.0. We have been able to reach strains of 0.02 in/in without buckling. The secimen with straight gage section helped us in the surface topographical studies and provided an ample amount of equally strained, bulk material. All marks from the final polishing were required to be longitudinal, i.e., parallel to the axis of the specimen, since cracks grow on planes generally perpendicular to the axis of the specimen.

## 2.3 TEST EQUIPMENT

All the tests were conducted on a closed loop, servo controlled hydraulic MTS testing system of 20 kips capacity. To arrest the

lateral motion of the hydraulic actuator (ram) during its travel, a fixture was designed to stiffen the hydraulic actuator against lateral motion. This fixture is shown in Fig. 10. This ensures alignment and also minimizes the problem of specimen buckling. This fixture essentially consists of a sleeve shrunk fit on the actuator, which slides inside a bronze plated demountable bushing, which is in turn fixed in position by a bottom plate secured to the bottom platen of the MTS machine.

To avoid extraneous bending and to obtain high quality test results meeting ASTM standards for alignment, special grips were designed. An assembled view of the grip and the detailed drawings are shown in Figs. 11 and 12, respectively. The grips were made out of Carpenter Custom 450 stainless steel of hardness $R_C42$. The grips are hydraulically operated, and the piston is designed for a maximum of 3000 psi of hydraulic pressure. An essential feature of the grips is that, once the grips themselves are centered and aligned, each test specimen is then automatically centered and aligned when gripped. Operation of these grips involves the movement of the piston upward due to hydraulic pressure applied at the bottom oil port, forcing the collet to squeeze on the grip ends of the specimen. This ensures that the specimen end surfaces are held evenly by the collet. The collet ends were smoothed and given a small radius to avoid any fretting problems. Releasing the grips is also by hydraulic pressure, the piston being made to move downward by

oil pressure applied from the top port. Proper sealant (o-rings) were used in the grips to preserve oil and to avoid any leakage.

These grips are found to be effective in testing smooth specimens with circular ends. Although these grips are intended for 0.5 in. diameter specimen ends, compatible collets with different inside diameters are available for testing different specimens. Several advantages of this gripping arrangement are as follows:

1. specimen alignment and centering are automatic
2. there is no backlash in the grip,
3. total mounting time is less, and
4. it can be used for other tests, such as tension testing, etc.

## 2.4 MOUNTING THE SPECIMEN AND ALIGNMENT

Alignment and centering of the grip is checked as follows: With the head of the hydraulic ram retracted, a specimen is gripped in the top grip. A dial gage indicator of high resolution (0.0001 in.) is mounted on the bottom grip, such that the dial gage stylus is in contact with the test section of the specimen. By moving the ram upward and downward, the parallelism of the test section with the grip axis is checked, specifically by noting any deflection on the dial gage. If the gage deflection is greater than 0.0005 in. over the test section, then the parallelism is not satisfactory. To obtain good parallelism, circular bevelled shims which give proper tilt, are to be provided beneath the bearing area of the top grip.

The concentricity of the specimen axis with respect to the grip

axis is checked by rotating the ram 360° and noting the maximum and minimum of the readings on the dial gage. It should be noticed that the maximum and minimum occur at opposite ends of the specimen diameter. The offset, which is half the difference between the readings, is then adjusted by loosening the locking nut on top of the crosshead and moving gently in the direction where correction is required.

This initial alignment procedure is absolutely necessary to avoid bending strains and specimen buckling. A further check is made using a specimen with 6 strain gages mounted on it, 3 gages 120° apart on top of the test section, and 3 on bottom of the test section. First, this specimen is held in the top grip and the strain readings adjusted to zero. After gripping the lower end, the strain readings of all six gages are noted. The difference between he readings before and after gripping for the same strain gauge should not exceed $40 \times 10^{-6}$ in/in. which corresponds to the maximum bending strain. Otherwise, the initial alignment procedure is to be repeated and checked again.

Next, the specimen is cycled at a low stress level, and plots of strain versus load for each of the gages are then obtained. If the slopes on the plots do not differ more than 2%, then alignment is considered satisfactory, and the system is ready for testing. Alignment checks are not considered necessary for individual specimens, further checks being done only at infrequent intervals.

## 2.5 TEST PROCEDURES AND METHODS

Constant amplitude controlled strain tests were carried out in the present study. Although the closed-loop hydraulic testing machine is capable of frequencies upto 100 Hz, the recording equipment, the dynamic characteristics of the clip gage, and heat generation in the sample limits the actual testing frequency to the range 0.01 to 5 Hz. Our strain controlled tests were carried out at a cyclic frequency given by an ampirical relation [41]

$$f = \varepsilon_{pa}/0.0008 \qquad (9)$$

where f is the frequency and $\varepsilon_{pa}$ is the stable plastic strain amplitude estimated prior to the test.

Note that use of the above implies a constant average plastic strain rate in a cycle. Thus, at higher strain levels, where the life of the specimen is less than $10^3$ cycles, a frequency of 0.01 to 0.5 Hz is employed, and up to 5 Hz is used for greater lives corresponding to low strain levels. At low strain amplitudes where the life is expected to exceed $10^5$ cycles, the tests are usually carried out in stress control, which allows a higher cyclic frequency up to about 20 Hz. This modest change in frequency above 5 Hz is not expected to affect the behavior. Since approximately isothermal conditions are maintained in the normal room temperature testing, and since no other significant effect of frequency on life is known to exist in this material at room temperature, the effect of frequency

on the life is not included in the study.

Since it is desired to follow crack growth with a large degree of plastic strain, two pairs of identical tests are conducted. The first of these involves controlling the grip deflection using a longer clip gage mounted across the grip ends along with a smaller clip gage mounted on the test section. This is shown in Fig. 13. Use of this pair of gages provides a correlation between the test section strain nd grip deflection. Such a correlation is shown in Fig. 14 along with a schematic diagram of strain measurements. In particular, there is a correlation between the test section plastic strain range, $\Delta\varepsilon_{p2}$, and the plastic strain range on the grip ends, $\Delta\varepsilon_{p1}$. It is observed from the plot of $\Delta\varepsilon_{p1}$ versus $\Delta\varepsilon_{p2}$ that the relation between the two strain ranges is almost linear (on a log-log plot) at higher levels and nonlinear at lower levels. The plastic strain in the test section is then estimated from the correlation of Fig. 14, and the elastic strain, known from the measured stress, is then added to obtain the total strain [13].

The second of these tests has the longer clip gauge mounted across the grip ends, with the smaller clip gage not present, as shown in Fig. 15. This is done so as to have access for surface crack measurements. This type of test allows crack growth data to be obtained under conditions of known large plastic strains.

Cracks are either naturally initiated or are initiated from artificial defects. The growth behavior is then monitored by surface

crack measurements using cellulose acetate replicas. In the earliest experiments, defects in the specimen were made by drilling a hemispherical hole of diameter 0.004 to 0.012 in. In one case, the crack was initiated by creating a region of residual tensile stresses by piercing the surface of the specimen with the tip of a sharp needle. Although this is not highly recommended, we tried this as an expedient. However, the best approach was found to be a small pit made by electro-discharge machining, EDM. The smallest crack length that could be observed had to be limited to 0.01 inches, which includes the size of the artificial flaw, so that the results were not affected by the proximity of the crack tip to the artificial flaw.

A dense array of cracks was observed at higher levels of strain greater than 0.02 in/in. Since the cracks were close to one another, affecting the stress/strain field and complicating the interpretation of the data, the tests were mostly limited to a maximum of 0.015 strain amplitude.

Cellulose acetate replica tapes were used to monitor the crack growth. The replicating tape thickness used was 0.005 in. and acetone was employed to soften the tape. The tape was wrapped firmly around the specimen, taking care not to allow excessive air bubbles inside the area between the specimen and the tape. The tape was removed after it dried, so as to obtain the impression of the surface. Two or three replicas were taken to cover the entire test

section of the specimen.

A low power microscope (up to 280X) was fitted to the system as shown in Fig. 15. This aided in observing the cracks. Since the crack could start anywhere in the test section, the microscope mounted from the top grip could be swivelled 360° around the specimen, enabling detection of cracks on the test section in any region.

The replicas thus obtained provided a permanent record of crack growth and its measurements, and cracks of smaller lengths could be traced back. Crack lengths and closure measurements were then made by examining and measuring the replicas under a microscope. Typical crack length versus cycles data obtained from surface replicas are shown in Fig. 16. Crack growth rate, da/dn, versus stress intensity range, $\Delta K$, as obtained by Dowling [40] on the same material is shown in Fig. 17. Note that the earlier work of Dowling on this material did not include closure measurements.

Crack closure measurements are made by measuring the offset of an inclined scribe line intersecting the crack [42]. This is illustrated in Fig. 18. A scribe line at an angle to the crack axis is drawn across the crack at the minumum stress level. As the load level is increased in the cycle, the crack opens. Thus, there results an offset between the lines. By measuring this offset, the crack opening displacement, COD, was computed. Lines drawn at several points along the crack give rise to COD measurements at

various points along the crack. In a few cases, when the crack was very nearly parallel to the scribe line, it sometimes became necessary to compute COD from enlarged pictures, by direct measurement of the width of the crack surfaces.

# CHAPTER 3

# EXPERIMENTAL RESULTS AND DISCUSSION

## 3.1 EXPERIMENTAL RESULTS

The experiments were conducted to observe the closure behavior of small cracks. The term small crack in our present study is used to indicate a crack which is physically small, but which can be easily observed in detail under a microscope at a magnification of 100X. Thus, the short cracks in this context fall in the region of 0.01 to 0.1 inches of crack length.

Constant amplitude controlled deflection was used with a completely reversed (R=-1.0) sinusoidal wave form. Tests were conducted at four different values of test section strain, by employing four different deflection amplitudes on the grip ends. The four different strain amplitude levels, $\varepsilon_a$, chosen for the study are 0.0125, 0.0066, 0.0042, and 0.0024 in/in. These cover conditions from predominantly elastic to grossly plstic strain. At each of the strain levels, crack closure measurements were made at 3 or more different crack lengths. Crack closure measurements are made by the offset technique as described in chapter 2. The COD, crack opening displacement, was obtained at various points along the crack length. A typical observation of the crack at various levels of stress (strain) in one cycle is shown in Fig. 19.

Figures 20-38 illustrate the variation during a cycle of the

crack opening displacement with the stress and strain at various points along the crack length. Along with this also is shown the load versus displacement loop obtained from the longer clip gauge mounted across the grip ends. Data for both loading and unloading are shown in each case. It is noteworthy that here we are measuring crack opening displacement, at the indicated positions, since it is difficult to measure the crack tip opening displacement, CTOD. Fig. 39 indicates typical loading and unloading paths in COD vs stress, and COD vs. strain plots.

The determination of the crack opening stress level is shown in Fig. 40. A scatter of $\pm 0.05(COD_{max})$ is attached to each of the points on the loading part of the cycle, where $COD_{max}$ is the largest value in the cycle. A corresponding scatterband is then drawn as shown in Fig. 40. The crack opening stress level, $\sigma_{op}$, is then defined as the stress level where the center of the scatterband crosses a COD value of zero. Similarly, the crack opening strain level, $\varepsilon_{op}$, is defined as the strain which occurs at the same time as $\sigma_{op}$.

A plot of $\sigma_{op}/\sigma_{max}$ versus crack length is shown in Fig. 41 for the different strain amplitudes chosen for the study. Figure 42 illustrates a similar plot of $\varepsilon_{op}/\varepsilon_{max}$ versus crack length.

## 3.2 DISCUSSION OF THE RESULTS

The work of Elber [20] suggested that the plastic zone left in the wake of the advancing crack tip causes the crack to be closed

after unloading even under tension-tension loading. But as observed from the present study at R=-1.0, i.e., at completely reversed cycling, no closure could be observed at zero load. The crack closed only as the lowest stress level, $\sigma_{min}$, was approached. However, the crack opening was delayed, but still occurred in the compressve part of the loading cycle. Thus, there is a significant difference observed between the closure and opening levels of the crack, while some of the other work in the literature assumes the crack opening and closure levels to be the same. For the contained plasticity problem, not involving wake effects, Newman [26] calculates that cracks are open for approximately 1/4 of the total cycle, i.e., half of the tensile loading part of the cycle. A similar result was obtained by Budiansky and Hutchinson [25], who included the plastic wake effect. In the present study, it is observed that the crack is open more than 1/2 of the loading portion of the cycle. This drastic difference in behavior is almost certainly due to the large scale plasticity involved in the present tests.

### 3.2.1 AN ESTIMATE AND THE MODEL OF BUDIANSKY AND HUTCHINSON

In the case of small scale yielding, a first order estimate for crack closure levels can be made. The following is based on Budiansky and Hutchinson's [25] analysis. Recalling Fig. 3, the crack tip opening displacement, $\delta_o$, which is calculated using the Dugdale strip yield model, corresponding to an applied maximum load, $\sigma_{max}$, is

$$\delta_o = K_{max}^2/E\sigma_y \tag{10}$$

where $\sigma_y$ is the ideally plstic tensile yield stress, and E is the elastic modulus.

The corresponding plastic zone size, $\omega$, is given by

$$\omega = \frac{\pi}{8}\left(\frac{K_{max}}{\sigma_y}\right)^2 \tag{11}$$

Thus, crack tip opening displacement is given by

$$\delta_o = \frac{K_{max}^2}{E\sigma_y} = \frac{8\ \sigma_y\ \omega}{\pi E} \tag{12}$$

The plastic stretch variation, or the crack opening displacement from the weight function analysis, is then given by

$$\delta = \delta_o\ g(\eta) \tag{13}$$

where

$$\eta = x/\omega$$

and

$$g(\eta) = \sqrt{1-\eta} - \eta/2\ \ell n\left|\frac{1+\sqrt{1-\eta}}{1-\sqrt{1-\eta}}\right| \tag{14}$$

It should be noted that the above equation is valid only for small scale yielding. The crack tip displacement variations, upon unloading to a level K from $K_{max}$, then is

$$\Delta\delta = f(\Delta K) = \frac{(K_{max} - K)^2}{2E\ \sigma_y}\ g(x/\omega) \tag{15}$$

This is based on Rice's [7] work where the plastic flow is proportional, and the plastic strains are in proportion to one

another.

Similarly, the variation of the plastic zone size, $\Delta\omega$, is

$$\Delta\omega = \frac{\pi}{8}\left(\frac{(K_{max} - K)^2}{2\sigma_y}\right) \tag{16}$$

Defining, $\zeta = \frac{\Delta\omega}{\omega}$, then

$$\zeta = \frac{\Delta\omega}{\omega} = \frac{1}{4}\left(1 - \frac{K}{K_{max}}\right)^2 \tag{17}$$

The function $g(x/\Delta\omega)$ similarly takes the form

$$g(x/\Delta\omega) = g\left(\frac{x/\omega}{\Delta\omega/\omega}\right) = g\ (\eta/\zeta),$$

$$g\left(\frac{\eta}{\zeta}\right) = \sqrt{1 - \eta/\zeta} - \frac{\eta}{2\zeta}\ \ell n\left|\frac{1 + \sqrt{1 - \eta/\zeta}}{1 - \sqrt{1 - \eta/\zeta}}\right| \tag{18}$$

If the crack is assumed to have a residual displacement of $\delta_r$ appended to its surfaces, then the crack closure can be assumed to occur at the tip to get a lower bound on $(K_{clos}/K_{max})$, when

$$\delta - \Delta\delta - \delta_R = 0 \tag{19}$$

Normalizing with respect to crack tip opening displacement, $\delta_o$

$$\frac{\delta}{\delta_o} - \frac{\Delta\delta}{\delta_o} - \frac{\delta_R}{\delta_o} = 0 \tag{20}$$

Observing the crack tip displacement, at $\eta=0$ i.e., when $\delta=\delta_o$, $\eta=0$

$$1 - \frac{\Delta\delta}{\delta_o} - \frac{\delta_R}{\delta_o} = 0 \tag{21}$$

$$\left.\frac{\Delta\delta}{\delta_o}\right|_{x=0} = \left[\frac{(K_{max} - K_{clos})^2}{2E\sigma_y}\ g(x/\Delta\omega)\right] \Big/ \left.\frac{K_{max}^2}{E\sigma_y}\right|_{x=0}. \tag{22}$$

Since $g(x/\Delta\omega)|_{x=0} = 1$ we get

$$\frac{\Delta\delta}{\delta_o} = \frac{1}{2}\left(1 - \frac{K_{clos}}{K_{max}}\right)^2 \tag{23}$$

Equation (13) becomes

$$1 - \frac{1}{2}\left(1 - \frac{K_{clos}}{K_{max}}\right)^2 - \frac{\delta_R}{\delta_o} = 0 \tag{24}$$

or

$$\frac{K_{clos}}{K_{max}} = 1 - \sqrt{2\left(1 - \frac{\delta_R}{\delta_o}\right)} \tag{25}$$

This closure level is for the crack tip, but first contact of cracks may occur behind the crack tip, as is the case in Budiansky and Hutchinson's [25] analysis. A similar form of the equation for the first contact closure level has been shown [25,27] to be

$$\frac{K_{clos}}{K_{max}} = 1 - \sqrt{1 - \left(\frac{\delta_R}{\delta_o}\right)^2} \tag{26}$$

During the reloading process, the crack starts opening, and the value if $K_{open}$ when the crack has been fully opened up has been calculated as for R=0 loading as [25]

$$\frac{K_{open}}{K_{max}} = 0.557 \tag{27}$$

The above equations have been derived based on the assumptions of small scale yielding, ideally plastic materials, and plane stress situations.

From equations (25) and (26) it is observed that the K level at the contact in the crack tip region and at first contact anywhere are

different. In their analysis, Budiansky and Hutchinson showed that first contact occurs behind the crack tip. Contrary to this, it has been observed that in our study, within the resolution experimentally possible, that contact of cracks occurs first at the tip, in agreement with the analysis of Newman [26]. It was also observed in one case only that the crack front irregularities enabled the crack to close behind the crack tip in a manner consistent with roughness induced closure.

### 3.2.2 MODELS OF NEWMAN AND OF NAKAI

An analytical fatigue crack closure model was developed by Newman [26] which is based on the Dugdale model, but modified to leave plastically deformed material in the wake of the advancing crack tip. A fatigue crack growth analysis program (FASTRAN) developed by Newman calculates the crack opening stresses under simulated plane stress and plane strain conditions. The model developed cannot handle general yielding conditions but is quite representative of small scale yielding conditions. A simulated plane strain situation is chosen and the results of Newman's analysis are shown in Fig. 43.

Recently Nakai et.al. [28] extended Budiansky and Hutchinson's analysis to short cracks growing from notches under small scale yielding conditions, and they arrived at an equation for opening the stress as

$$\frac{K_{open}}{K_{max}} = \frac{2}{\pi}\left(\frac{-\zeta h}{\zeta - h}\right)^{1/2} I\sqrt{\left\{\frac{\zeta}{\zeta - h}\right\}} + \frac{2R}{\pi}\tan^{-1}\left(\frac{\zeta}{-h}\right)^{1/2}$$

$$+ \frac{1}{\pi}\int_{\zeta}^{1}\frac{1}{2}\left[1 - \frac{2}{\pi}\tan^{-1}\left\{\left(\frac{-\zeta\,(\eta-h)}{h(\eta-\zeta)}\right)^{1/2}\right\}\right]\ell n\left|\frac{1 + (1-\eta)^{1/2}}{1 - (1-\eta)^{1/2}}\right|\frac{d\eta}{\sqrt{\eta}} \quad (28)$$

where $\zeta = \Delta\omega/\omega$ is the reversed plastic zone ratio at $K_{min}$, $h=\ell/\omega$, $\ell$, being the crack length, and R is the ratio of the minimum stress level to the maximum stress level. The term $I\{\sqrt{\frac{\zeta}{\zeta-h}}\}$ is a first order elliptical integral, which is read from mathematical tables. The reversed plastic zone ratio, $\zeta$ at $K_{min}$ has been obtained [27] from Budiansky-Hutchinson's analysis. Such as

$$R = -\frac{1}{2}\int_{0}^{\zeta}\left(\frac{\eta-h}{(\zeta-\eta)\eta}\right)^{1/2} d\eta + \frac{1}{\pi}\int_{\zeta}^{1}\left(\frac{\eta-h}{(\eta-\zeta)\eta}\right)^{1/2}\frac{1}{2}\ell n\left|\frac{1 + (1-\eta)^{1/2}}{1 - (1-\eta)^{1/2}}\right| d\eta \quad (29)$$

Solving this equation numerically for $\zeta$ for representative cases similar to the crack size and plastic zone sizes in our study, the results are depicted in the crack opening map of Fig. 43. It is to be noted that the above equations are obtained for small scale yielding and for cracks growing from nothces where closure cannot occur over the notch.

Along with these results, values obtained from Elber's estimated empirical relation (equation 2) is also shown in Fig. 43. The results from the present study are also indicated in the same fig. 43.

### 3.2.3 COMPARISON OF EXPERIMENTAL RESULTS WITH EXISTING MODELS

The effective stress intensity opening ratio, U, has been found to increase as the crack length becomes shorter and approaches unity. When the crack is open throughout the unloading part of the cycle, closing only at the minumum stress level, the the effective stress intensity range, defined by

$$\Delta K_{eff} = U\,\Delta K = \left(\frac{1 - K_{clos}/K_{max}}{1 - R}\right) \tag{30}$$

becomes equal to $\Delta K$, the overall stress-intensity range. From our present experimental results, conducted at R=-1 at different strain levels, it is observed that the crack closes first at the lowest stress in the cycle, $\sigma_{min}$, and remains closed for a part of the loading cycle till it opens at a value $\sigma_{op}$ ($\sigma_{op} > \sigma_{min}$) . This can be seen from the Figures 20-38. If we apply these results to the equation for crack closure obtained earlier in equation (26) we observe that

$$\frac{K_{clos}}{K_{max}} = 1 - \sqrt{1 - \left(\frac{\delta_R}{\delta_o}\right)^2} \tag{31}$$

since $\delta_R/\delta_o \to 1$ as $R \to 1$, and $\delta_R/\delta_o \to 0$ as $R \to -\infty$, a reasonable choice for the estimate of $\delta_R/\delta_o$ could not be made from our present study, since closure of the cracks was first observed at $\sigma_{min}$, corresponding to $K_{min}$. (For R=0 loadings, Budiansky and Hutchinson [25] have estimated the $\delta_R$ value as $0.85\delta_o$).

Crack closure and opening stress level analysis for cracks subjected to stress beyond the yield stress does not exist in the literature. Following the elastic, small scale yielding analysis gives inconsistent results. This is observed in fig. 43 where the present data is pictured along with the analytical results.

Our observation that crack closure occurs only at $\sigma_{min}$, suggests that $\delta_R/\delta_o = -1$, (from eqn. 25) which is not meaningful. If $\delta_R$ taken to be zero then,

$$\Delta K_{eff} = \Delta K \quad \text{since} \quad U = \left(\frac{1 - \frac{K_{clos}}{K_{max}}}{1 - R}\right) = 1 \tag{32}$$

Thus, for short cracks which are subjected to stresses beyond yield, the crack closure level which occurs at $\sigma_{min}$, and the crack opening level, $\sigma_{op}$, may both have significant effects on the growth behavior of the crack. Since the crack tip advances only in the loading part of the cycle, the crack opening level, $\sigma_{op}$, may be relatively more important. If we define the effective stress intensity as

$$\Delta K_{eff} = U' \Delta K \tag{33}$$

where, $U'$ is defined as

$$U' = \left[\frac{1 - K_{op}/K_{max}}{1 - R}\right] \tag{34}$$

then, we observe that the increased plastic deformations, the value of $K_{op}/K_{max}$ decreases and approaches the value of R making the value of $U'$ to approach unity. From this definition of effective stress

intensity we observe that for shorter cracks, under large scale deformations, the value of the effective stress intensity, $\Delta K_{eff}$, is significantly different from the earlier definition of the effective stress intensity.

From our present results it is observed in most of the cases that the crack opened in the compressive part of the loading cycle. This revealed the significant difference in the crack closure and opening levels, and these do not occur at the same stress level as assumed in some studies.

From the crack opening displacement versus strain plots in Figures 20-38, it is also noted that the cracks do not open and close at the same strain levels. Hence, at high stress-strain levels where significant plstic strain is involved, the available analysis on closure/opening of fatigue cracks is insufficient.

# CHAPTER 4

## GENERAL DISCUSSION

Figure 41 illustrates the crack opening stresses normalized with respect to the maximum stress, as a function of the crack length at different strain levels. Since at each strain level, 3 or more crack length measurements were made, lines are fitted to the data points representing each strain level. It is observed that at higher strain levels, as the crack length increases, this relative opening level increases only slightly with the crack length. At lower strain levels, the relative opening level is higher for any given crack length and found to increase more with the crack length.

The corresponding strain level for crack opening, $\varepsilon_{op}$, normalized with respect to the maximum strain level, $\varepsilon_{max}$, as a function of the crack length is shown in Fig. 42 for different levels of strain amplitude. Here also it is observed that, at higher cyclic strain levels, the crack opens very early in its loading path, and the crack opening is delayed more for the lower cyclic strain levels. It is to be noticed that at low strain amplitude cycling, the crack opening level increases with crack length.

It is observed that the stress or the strain opening level is dependent upon the point along the crack length where the observations are made. The difference can be attributed to the irregular crack front, the measurement technique, and other microstructural

features. Stress and strain opening levels in this study are made considering points which are relatively near the crack tip, typically 0.004 in. Though it would be desirable to measure the crack opening displacements right at the crack tip, this is not feasible because of the limitations of the measuring techniques.

Figure 43 describes the variation of crack opening stress level as a function of $\Delta J$. $\Delta J$ has been calculated without considering closure effects, but considering plastic strain effects, using the formula obtained by Dowling [40]

$$\Delta J = (0.714)^2 a[\pi \frac{\Delta\sigma^2}{E} + 8.59\ \Delta\sigma\Delta\varepsilon_p] \qquad (35)$$

where 2a is the crack length, E is the elastic modulus, $\Delta\sigma$ is the stress range and $\Delta\varepsilon_p$ is the plastic strain range.

The data shown in Figure 43 do not indicate a clear correlation of the trends of the behavior with $\Delta J$. Thus no significant interpretations could be made from this figure. A larger number of tests covering the entire range would be helpful in describing the behavior with modifications to $\Delta J$ accounting for closure effects.

It is expected that, for an ideal rigid-plastic material, when the crack opens during the loading part of the cycle, the crack never closes unless a compressive strain is imposed which exceeds the tensile strain reached. This sets one limit and is shown by the solid line in Fig. 43. For cases where predominately elastic loading is

applied to the specimen, as is done in the usual fracture specimens under R > 0 loadings, there exists a crack opening level, obtained from different analyses [26,28] as illustrated in Fig. 43. All the earlier analyses on crack closure/opening have been done for the case of small scale yielding situations.

Extending the same small scale yielding analyses to R = -1 loading for smooth specimens, as done in our tests, where there are large scale deformations, the results seems to be not meaningful enough to describe the phenomenon observed.

Thus we observe that the analysis existing in the literature is limited to only special cases. We believe that cracks under large scale yielding conditions behave more similarly to an ideal crack with no wake effects and with no contact. Figure 45 illustrates the behavior of real (fatigue) crack behavior under large scale yielding conditions. Also shown in the figure is the behavior of an ideal linear elastic crack with no wake effect. As can be observed from Fig. 45, the closure level is lower than the opening level. Also it is to be noticed that the ideal crack closes and opens at $\sigma = 0$. This behavior of a ideal elastic crack sets one bound, while the other bound for large scale yielding situations is still to be analytically investigated.

It is also illustrated in the Fig. 45, in a manner qualitatively consistent with the present eperimental results, how the opening behavior of a real crack varies from large scale yielding to small

scale yielding conditions. This needs to be investigated and mathematical analysis and modelling done. Such an effort would aid in bridging the gap between the growth behavior of small microscopic flaws and that of long cracks.

It is observed that in the analysis [25,28] existing in the literature that the residual displacement, $\delta_R$, is assumed to be constant. But this may not be so, since the residual displacements near the tip of the crack may be different from that of the residual displacements behind the crack tip. This stems from the argument that, because the contact stress may exceed negative yield, the residual displacements are changed considerably as the crack front grows far beyond a given point.

Note that under compressive loading, the crack tip starts closing and the apparent crack tip recedes. This makes the crack tip singularity, such as of the type $\sqrt{r}$ in elastic analysis, to become weaker and vanish when the crack is fully closed. Considering the ideal rigid, perfectly plastic behavior of the material, it may be assumed that the apparent crack tip at any point during the compressive loading starts receding only when the contact stresses ahead, between the original crack surfaces, exceed the yield stress. Thus, a residual compressive deformation of the material exists along the original crack surface. Extending the same analogy to cyclic loading situations, it is believed that these contact stresses between the crack surfaces resulting in compressive residual deformation are

responsible for the observed 'no closure' effect in large scale deformations in R = -1 loading situations, as in our study. Since these residual deformations must be overcome during reloading, the crack opening is delayed and as observed takes place at a stress level $\sigma_{op} > \sigma_{min}$.

It is thus observed that linear residual displacements, as done in earlier analysis [25,26], holds if the maximum state fulfils small scale yielding conditions. This is the case if the monotonic plastic zone is small compared to the crack length. In the case of a real fatigue crack under large strains, the above analyses fails to predict the crack growth behavior accompanied by crack closure/opening.

Another aspect that is to be noted is the three dimensional nature of fatigue cracks. The 2-D analyses are only ideal and are only appropriate for thin sheets. Since the plastic zone ahead of the crack in a plane strain region is small compared to the plane stress zone, closure of cracks is less significant in plane strain situations. The crack closure measured by electric potential [38], ultrasonic [43], or compliance [44] methods reveal only an average obtained at the specimen surface and interior, with stress interaction effects being less significant in the interior. There exists in the literature [46] data from the measurement of closure behavior of cracks under pure plane strain conditions. But in that study also, the remote load level was gradually decreased as the crack propagated

to maintain the small scale yielding situations.

Other factors to be considered while studying crack closure/opening analysis are the effects of loading condition and specimen geometry. Dowling and Begley [14] applied the J-integral to elastic-plastic and general yield conditions and obtained a good correlation between the crack growth rate and the range of the J-integral, ($\Delta J$). The application of this J-integral to fatigue crack growth studies at high cyclic stresses and strains at different R ratios to observe the crack closure/opening phenomenon is planned to be investigated.

# CHAPTER 5

## CONCLUSIONS AND SCOPE FOR FURTHER STUDY

The observed closure/opening behavior of cracks reveals the limitations of the existing elastic-plastic fracture mechanics approach to the study of crack growth behavior. There exist no closed form solutions for the redistribution of stresses and displacements in a cracked body under any general elastic-plastic conditions. Assumptions made in several analyses just simplify the problem to a very special case of elastic-plastic fracture mechanics. The use of the Dugdale model is one such approximation. In this model, the size of the plastic zone ahead of the crack tip is completely ignored, and so is the elastic field surrounding it. The model can be applied to thin sheets under plane stress, where only the entire strip along the crack axis in front of the crack undergoes plastic deformation. In real crack situations, the Dugdale model fails to explain the observed behavior in totality, and in general cannot be extended to all cases.

An energy balance investigation (model) may be a suitable approach, thereby the plastic dissipative work within the plastic zone can be fully considered with the bounded elastic zone in a cyclic hardening or softening material. The early approach by Rice [7] to problems of fatigue cracks is to use deformation theory of plasticity, which is difficult to use for nonlinear cases such as

crack closure and an extending crack, even under small scale yielding situations.

Thus, the discrepancies observed between the experimental observations and the analytical models are because of both mechanics related factors and material related factors.

The mechanics related factors are:

(1) Re-distribution of stress and displacements in cracked bodies

(2) Material deformation behavior

(3) Local closure and contact stress effects

(4) Macroscopic closure due to residual stress and deformation

(5) Anisotropic effects and homogeneity

(6) Three dimensional nature of crack

Some of the material related factors are:

(1) Differences in cracking process

(2) Characteristic length comparisons, such as crack length versus the microstructural dimensions of the material

(3) Transient effects due to grain boundaries, inclusions, grain to grain non-orientations, etc.

Because of the complexities involved in fatigue crack growth, it is impossible to single out any one of the factors as a major controlling parameter. Thus, further research is needed in this area to critically analyze the most important parameter (material and/or geometric) related to plastic strains for the closure behavior of

cracks in fatigue.

Further research in this area includes conducting tests at different R ratios such as -0.5, 0 and 0.7, and examining the validity of existing analyses of the closure behavior of cracks in fatigue. This includes various parameters such as different strain levels, crack lengths, and different specimen geometries. Tests are being conducted, and the results are expected to provide a good understanding of this subject. Also, it is planned to carry out tests on different grain sizes, to expose the effects of grain size, thus checking the limitations of the continuum mechanics approach also.

We are at present conducting tests of 2-D cases on flat specimens to examine the effects of various parameters on the closure behavior of cracks. This is expected to bring results leading to differentiating among the actual mechanism of crack growth and its closure in fatigue in 2-D and 3-D situations. The variables that are being included in this study are the load ratio, maximum load, plastic strain level, and crack growth rate. The data will be analyzed based on J-integral, and new analysis of the closure of short cracks will be attempted.

Further work is also aimed at developing a model which describes the crack tip stresses and displacements, and hence redistributions of the stresses and displacements, under general elastic-plastic conditions, which are in turn expected to help in a better

understanding of the crack growth behavior over all strain ranges from gross plastic to elastic deformation.

## REFERENCES


1. Hoeppner, D. W., "Short Crack Fatigue Design Considerations: Modelling Characterization, Interpretation, Detection, Prediction of Behavior," Proc. of the 55th meeting of the AGARD Structures and Materials Panel, Toronto, Canada, Sept. 1982.

2. Ritchie, R. O., and Suresh, S., "Mechanics and Physics of the Growth of Small Cracks," AGARD report no. CP-328, 1983.

3. Potter, J. M., "Advances in Fastener Hole Quality through the Application of Solid Mechanics," Proc. of the Army Symposium on Solid Mechanics, Sept. 1978.

4. Hudak, S. J., "Small Crack Behavior and Prediction of Fatigue Life," J. of Engg. Matls and Technology, Transactions of ASME, vol. 103, 1981.

5. Schijve, J., "Differences Between the Growth of Small and Large Fatigue Cracks: The Relation to Threshold K Values," in Fatigue Thresholds eds., Backland, J., Blom, A., and Beevers, C. J., EMAS Ltd., Warley, U. K., vol. 2, 1981.

6. Lankford, J., "The Effect of Environment on the Growth of Small Fatigue Cracks," Fatigue of Engg. Matls. Structures, Vol. 5, 1982.

7. Rice, J. R., "Mechanics of Crack Tip Deformation and Extension by Fatigue," Fatigue Crack Propagation, ASTM, STP, 415, 1967.

8. Hult, J. A., and McClintock, F. A., "Elastic Plastic Stress Strain Distribution Around Sharp Notches under Repeated Shear," Proc. of the 9th International Congress of Applied Mechanics, Vol. 8, Brussels, 1956.

9. Irwin, G. R., and Wells, A. A., "A Continuum Mechanics View of Crack Propagation," Metallurgical Reviews, Vol. 10, no. 38, 1965.

10. Paris, P. C., and Sih, G. C., "Stress Analysis of Cracks," Symp. on Fracture Toughness Testing and its Application, ASTM, STP, 381, 1965.

11. Paris, P. C., "The Fracture Mechanics Approach to Fatigue," Fatigue- An Interdisciplinary Approach, Syracuse University Press, 1976.

12. Kanninen, M. F., Popellar, C. H., and Broek, D., "A Critical

Plastic Fracture to Nuclear Pressure Vessels and Piping," Nuclear Engg. and Design, vol. 67, 1981.

13. Dowling, N. E., "Crack Growth During Low Cycle Fatigue of Smooth Axial Specimens," Cyclic Stress-Strain and Plastic Deformation Aspects of Fatigue Crack Growth, ASTM, STP, 637, 1977.

14. Dowling, N. E., and Begley, J. A., "Fatigue Crack Growth During Gross Plasticity and the J-integral," Mechanics of Crack Growth, ASTM, STP, 590, 1976.

15. El Haddad, M. H., Smith, K. N., and Topper, T. H., "Fatigue Crack Propagation of Short Cracks," J. of Engg. Matls. and Technology, Transactions of ASME, vol. 101, no. 1, 1979.

16. Fuhring, H., "Calculation of Elastic Plastic Loading in Dugdale Cracks with Crack Closure on the Basis of Non-Linear Fracture Mechanics," Report of the Institut fur Statick and Stahlbam, Darmstadt, 1977.

17. Leis. B. N., "Fatigue Crack Propagation Through Inelastic Gradient Fields," Int. J. of Pressure Vessels and Piping, vol. 10, 1982.

18. Seeger, T., and Heuler, P., "Generalized Application of Neuber's Rule," J. of Testing and evaluation, ASTM, vol. 8, no. 4, 1980.

19. Ohuchida, H., Usami, S., and Nishioka, A. "Fatigue Limit of Steel with Cracks' bulletin of JSME, vol. 18, no. 125, 1975.

20. Elber, W., "Fatigue Crack Closure under Cyclic Tension," Engg. Fracture Mechanics, vol. 2, no. 1, 1970.

21. Elber, W., "The Significance of Fatigue Crack Closure," Damage Tolerance in Aircraft Structures, ASTM, STP, 590, 1976.

22. Katcher, M., and Kalpan, M., in Fracture Toughness and Slow Stable Cracking ASTM, STP, 559, 1974.

23. Bell, P. D., and Creager, M., in Crack Growth Analysis for Arbitrary Spectrum Loading, AFEDL-TR-74-129, 1974.

24. Satish Chand, and Garg, S.B.L., "Crack Closure Studies under Constant Amplitude Loading," Engg. Fracture Mechanics, vol. 18, no. 2, 1983.

25. Budiansky, B., and Hutchinson, J. W., "Analysis of Closure in Fatigue Crack Growth," J. of App. Mechanics, vol. 45, 1978.

26. Newman, J. C., Jr. "A Nonlinear Fracture Mechanics Approach to the Growth of Small Cracks," Proc. of the 55th meeting of the AGARD Structural and Materials Panel on Behavior of Short Cracks in Airframe Components, Toronto, Canada, Sept. 1982.

27. Sehitoglu, H., "Crack Opening and Closure in Fatigue," Report of the University of Illinois-Urbana, 1984.

28. Nakai, Y., Tanaka, and Yamashita, M., "Analysis of Closure Behavior of Small Fatigue Cracks," J. of Society of Materials Science, Japan, Jan. 1983.

29. Dill, H. D., and Saff, C. R., "Spectrum Crack Growth Prediction Method based on Crack Surface Displacements and Contact Analysis," Fatigue Crack Growth Under Spectrum Loads, ASTM, STP, 595, 1976.

30. Dill, H. D., and Saff, C. R., "Analysis of Crack Growth Following Compressive High Loads Based on Crack Surface Displacements and Contact Analysis," MCAIR-76-006, Report of McDonnel Aircraft Company, 1976.

31. Newmann, J. C. Jr., "Prediction of Fatigue Crack Growth under Variable Amplitude and Spectrum Loading Using a Closure Model," NASA Technical Memorandum, Jan. 1981.

32. Newman, J. C. Jr., "A Crack Closure Model Predicting Fatigue Crack Growth under Aircraft Spectrum Loading," NASA Technical Memorandum, Jan. 1981.

33. Ohji, K., Ogura, K., and Ohkubo, Y., "Cyclic Analysis of a Propagating Crack and its Correlation with Fatigue Crack Growth," Engg. Fracture Mechanics, vol. 7, 1975.

34. Ogura, K., and Kohji, K., "FEM Analysis of Crack Closure and Delay Effects in Fatigue Crack Growth Under Variable Amplitude Loading," Engg. Fracture Mechanics, vol. 9, 1977.

35. Suresh, S., and Ritchie, R. O, "A Geometric Model for Fatigue Crack Closure by Fracture Surface Roughness," Met. Trans. vol. 13A, 1982.

36. McCarver, J. F., and Ritchie, R. O., "Fatigue Crack Propagation Thresholds for Long and Short Cracks in Rene 95 Nickel Base Superalloy," Mater. Sci. Eng., vol. 55, 1982.

37. Morris, W. L., James, M. R., and Buck, O., "A Simple Model of

Stress Intensity Range Threshold and Crack Closure Stress," Engg. Fracture Mechanics, vol. 14, 1982.

38. Gangloff, R. P., "Electric Potential Monitoring of the Formation and Growth of Small fatigue Cracks in Embrittling Environments".

39. Murakami, Y., Harada, S. S., Endo, T., Taniishi, H., and Fukushima, Y., "Correlations Among Growth Law and Applicability of Miners Rule," Engg. Frcture Mechanics, vol. 18, no. 5, 1983.

40. Dowling, N. E., "Growth of Short Fatigue Cracks in an Alloy Steel," Paper for the ASME, 4th National Congress on Pressure Vessels and Piping Technology, June, 1983, Portland, Oregon, Also Scientific Paper no. 82-107-STINE-P2, Westinghouse R&D Center, Pittsburg, Pa., Dec. 1982.

41. Dowling, N. E., Private Communication

42. Dillner, C. W., "A Crack Closure Study of High Carbon Steel," Report of Dept. of Theoretical and Applied Mechanics, University of Illinois, Urbana, 1984.

43. Shih, T. T., and Wei, R. P., in Engineering fracture Mechanics, vol. 6, 1974.

44. Heubaum, F., and Fine, M. E., "Short Fatigue Crack Growth Behavior in a High Strength Low Alloy Steel," Scripta Metallurgica, vol. 18, 1984.

45. Kikukawa, M., Jano, M., and Hora, H., "Fatigue Crack Propagation and Closure Behavior Under Plane Strain Condition," Report of the Dept. of Mechanical Engg., Osaka University, Japan.

46. Gray, G. T., III, and Luetjering, G., "The Influence of Crack Closure on the Fatigue Crack Propagation of Ti-6Al-4V and Ti-8-6Al", Fatigue, 1984.

47. Macha, D. E., Corbly, D. M., and Jones, J. W., "On the Variation of Fatigue crack Opening Load with Measurement Location," Experimental Mechanics, vol. 19, 1979.

TABLE 1

CHEMICAL COMPOSITION

AISI 4340 Steel

| Ni | C | S | P | Si | Mn | Mo | Cr |
|---|---|---|---|---|---|---|---|
| 1.89 | 0.38 | 0.052 | 0.012 | 0.29 | 0.77 | 0.21 | 0.83 |

Heat Treatment:

1. Austenitize at 1560°F, 5 hours to temperature; hold 3 hours; oil quench.
2. Temper at 1225°F, 4 hours to temperature; hold 8 hours; air cool.

TABLE 2

MECHANICAL PROPERTIES

| Heat No: | Ultimate (Ksi) | 0.2% yield (Ksi) | % Red. Area | True Fr. Strength |
|---|---|---|---|---|
| 61738 | 114 | 94 | 68 | 225 |

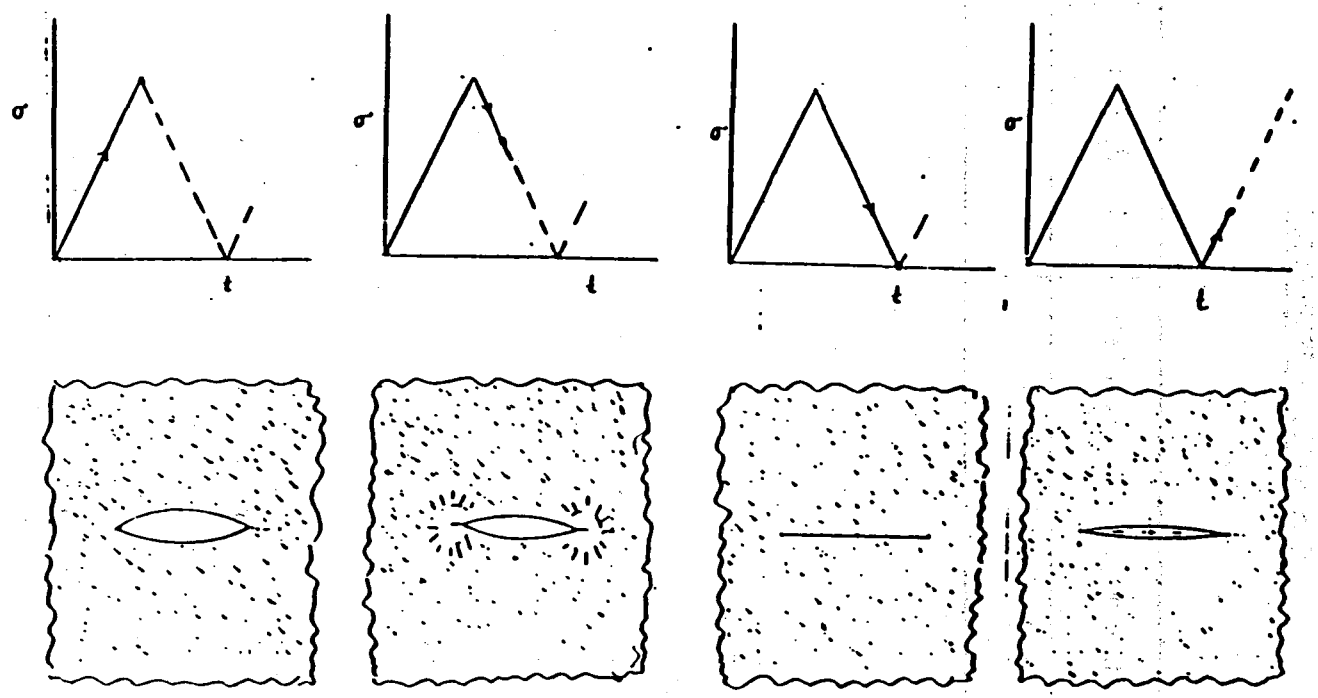


Fig. 1: Schematic diagram of plasticity induced closure

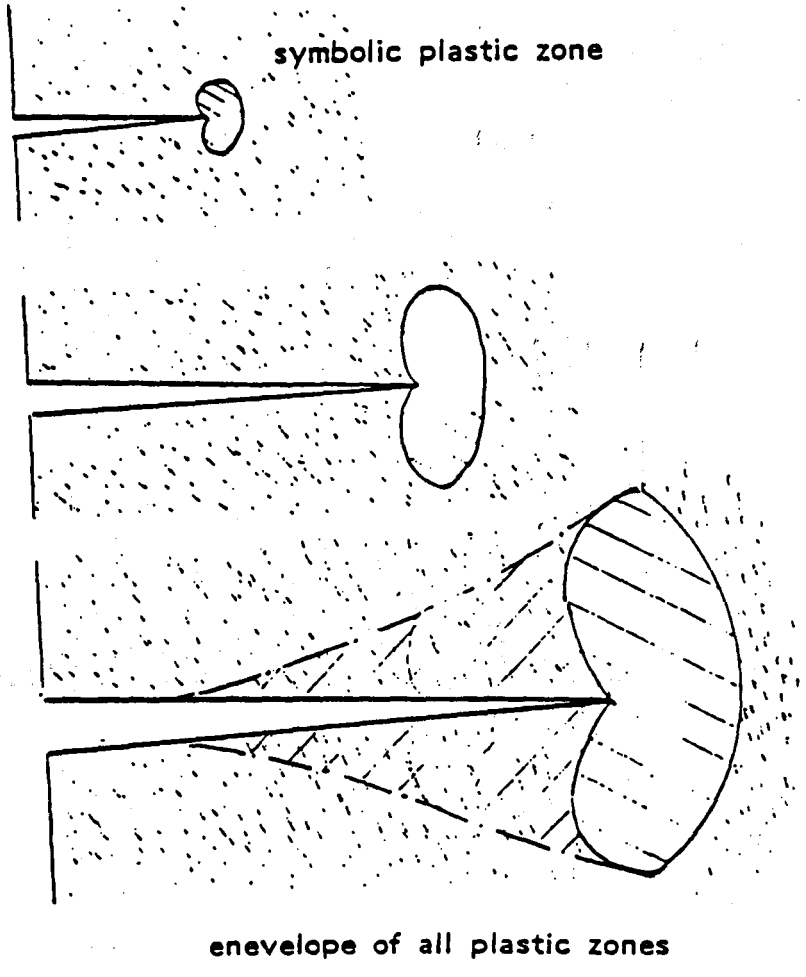


Fig. 2: Schematic diagram showing the wake effects

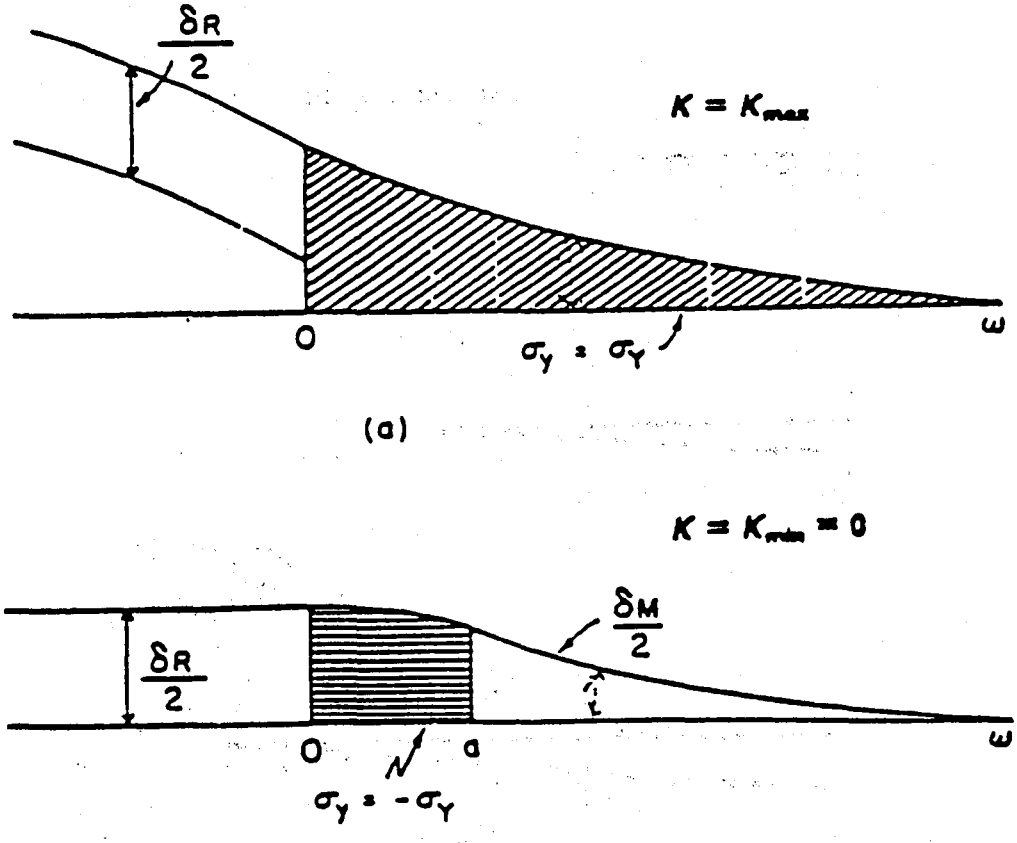


Fig. 3: Crack tip parameters

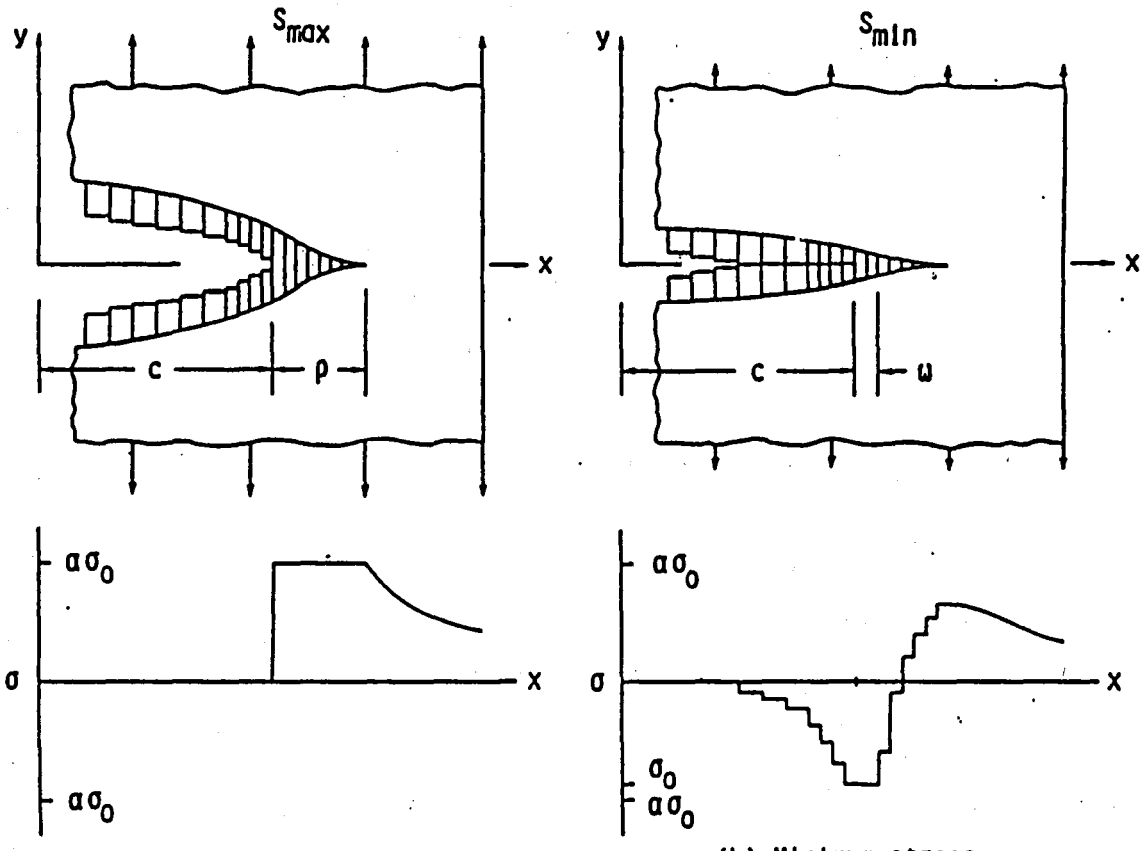


Fig. 4: Crack surface displacements and stress distributions (26)

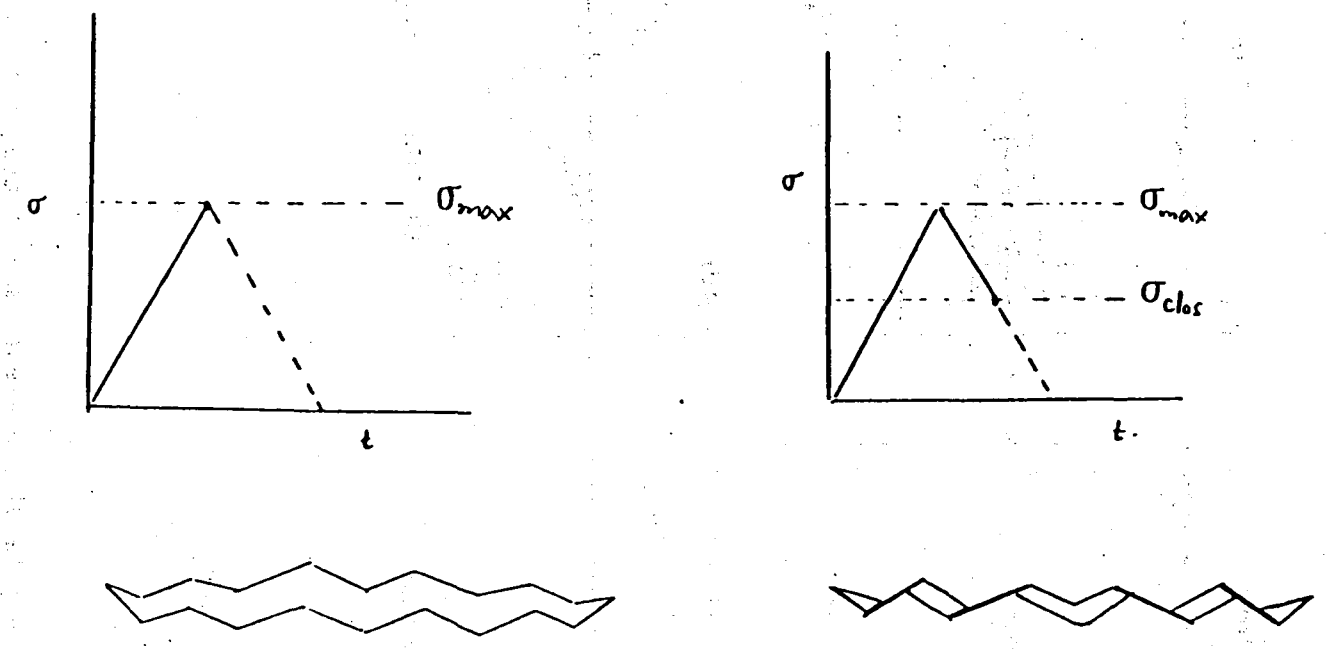


Fig. 5: Schematic diagram of roughness induced closure

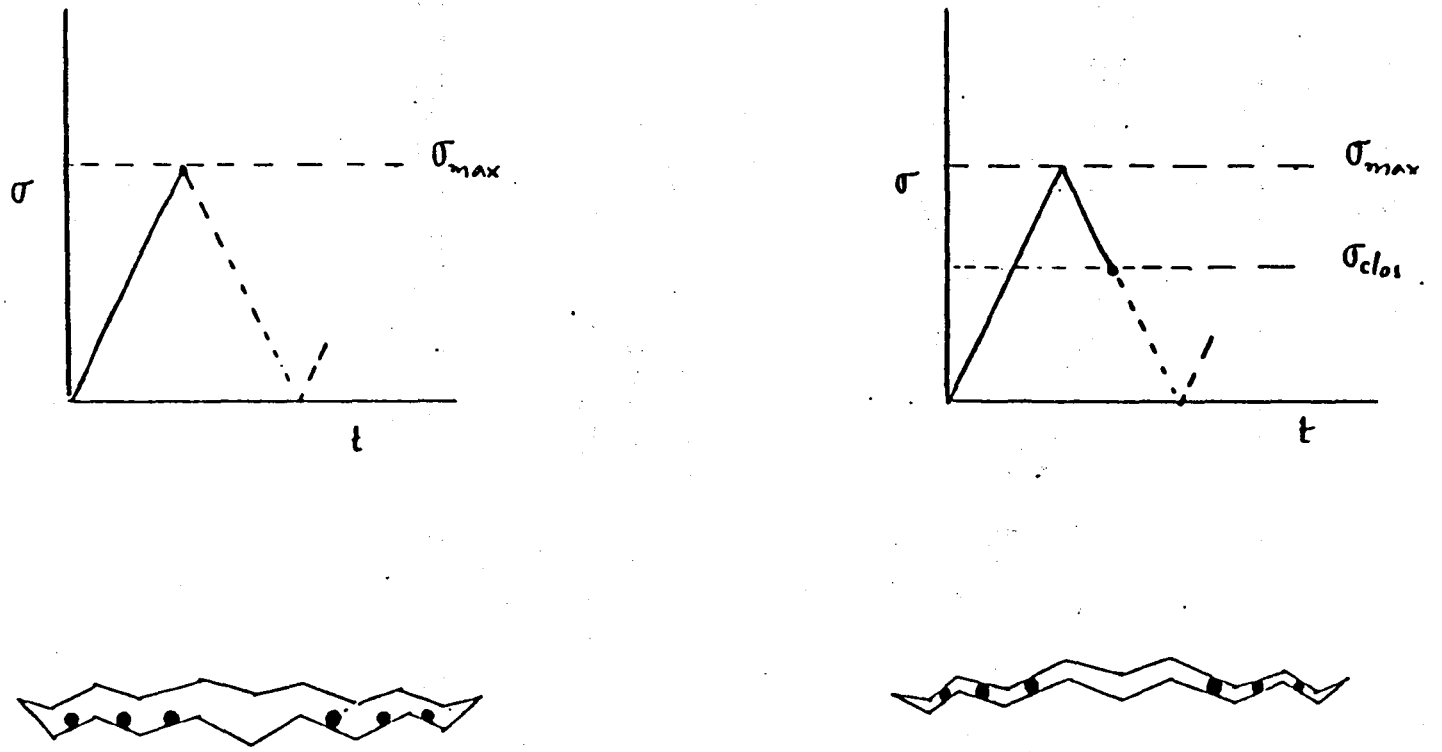


Fig. 6: Schematic diagram of oxide induced closure

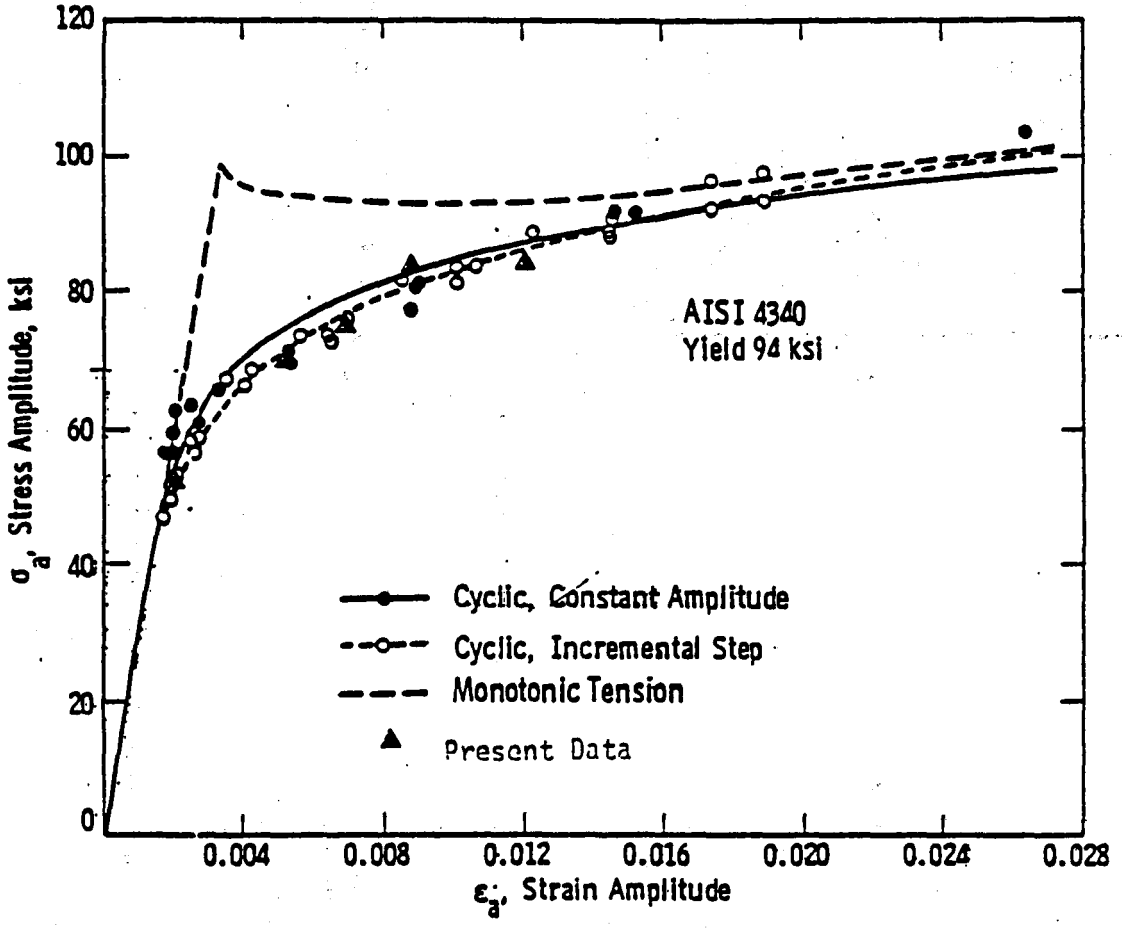


Fig. 7: Monotonic and cyclic stress-strain curve for AISI 4340 steel [41]

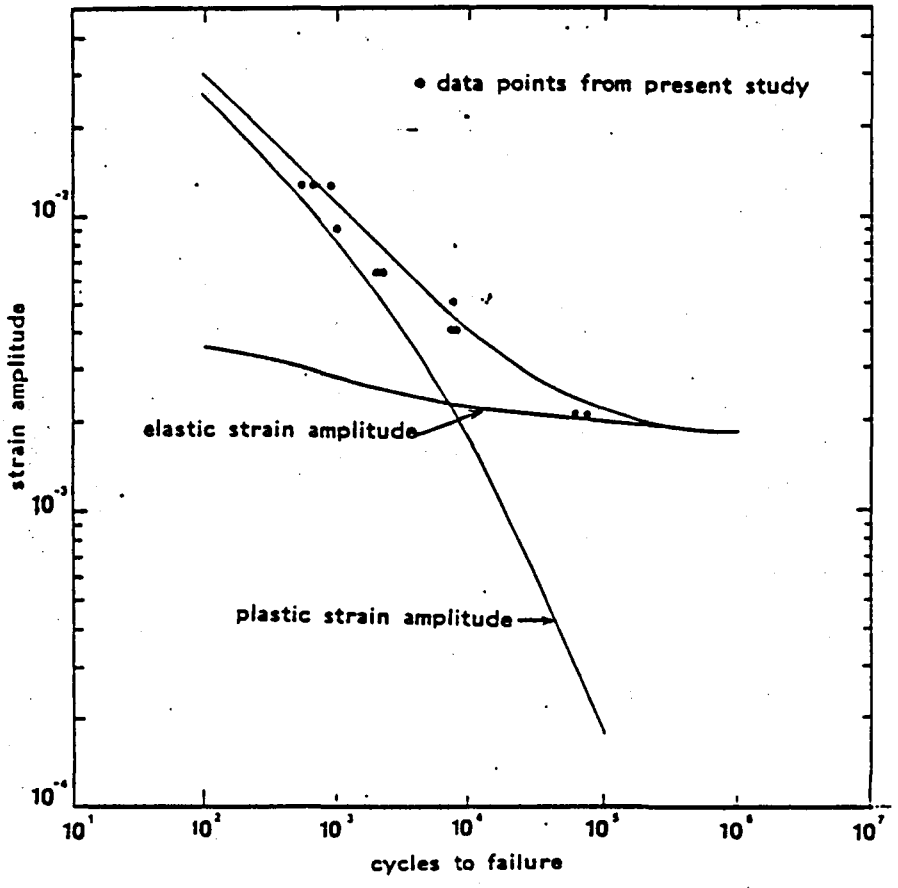


Fig. 8: Strain life curve for AISI 4340 steel (40)

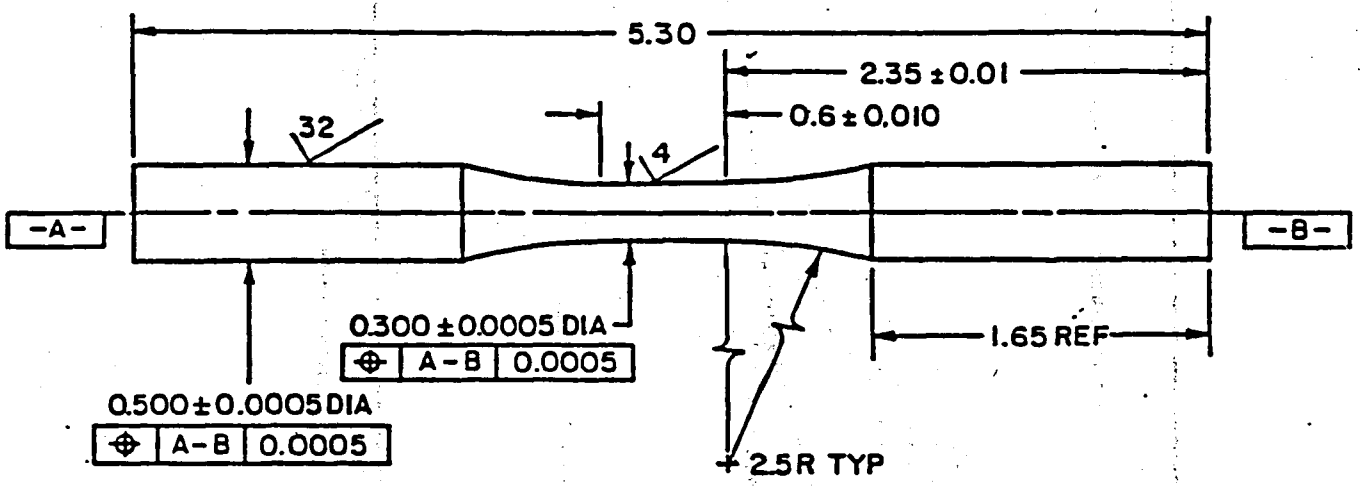


Fig. 9: Specimen geometry

All dimensions in inches

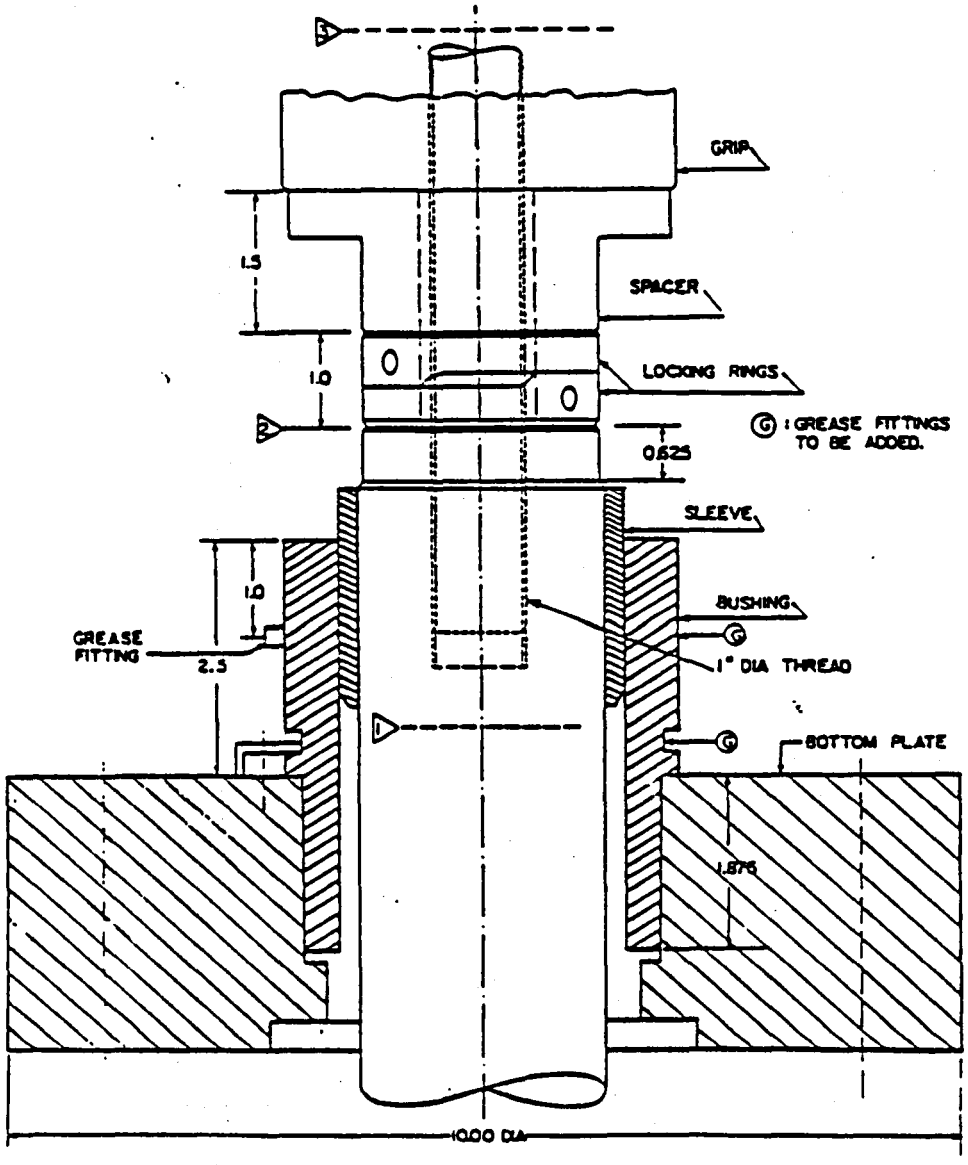


Fig. 10: Hydraulic actuator with the stiffener

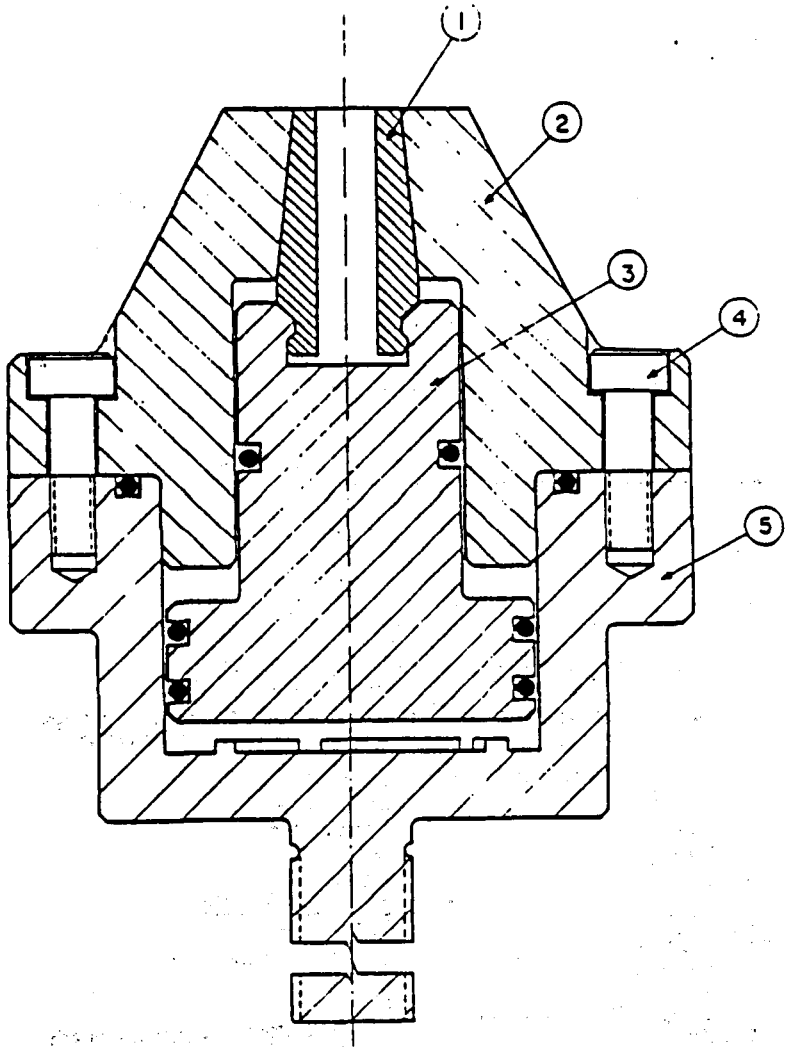


| Part No. | Part Name | No. Reqd. | Material | Hardness |
|---|---|---|---|---|
| 1 | Universal AF-123 Collet | 2 | (supplied) | ——— |
| 2 | Cover | 2 | CC 450SS | $R_c$ 42 |
| 3 | Collet Holder | 2 | CC 450SS | $R_c$ 42 |
| 4 | 3/8-16 Sock Hd Cap Screws SAE Grade 8, 1.25 in. long | 16 | (std. bolting) | ——— |
| 5 | Housing | 2 | CC 450SS | $R_c$ 42 |

Fig. 11: Assembled view of the grip

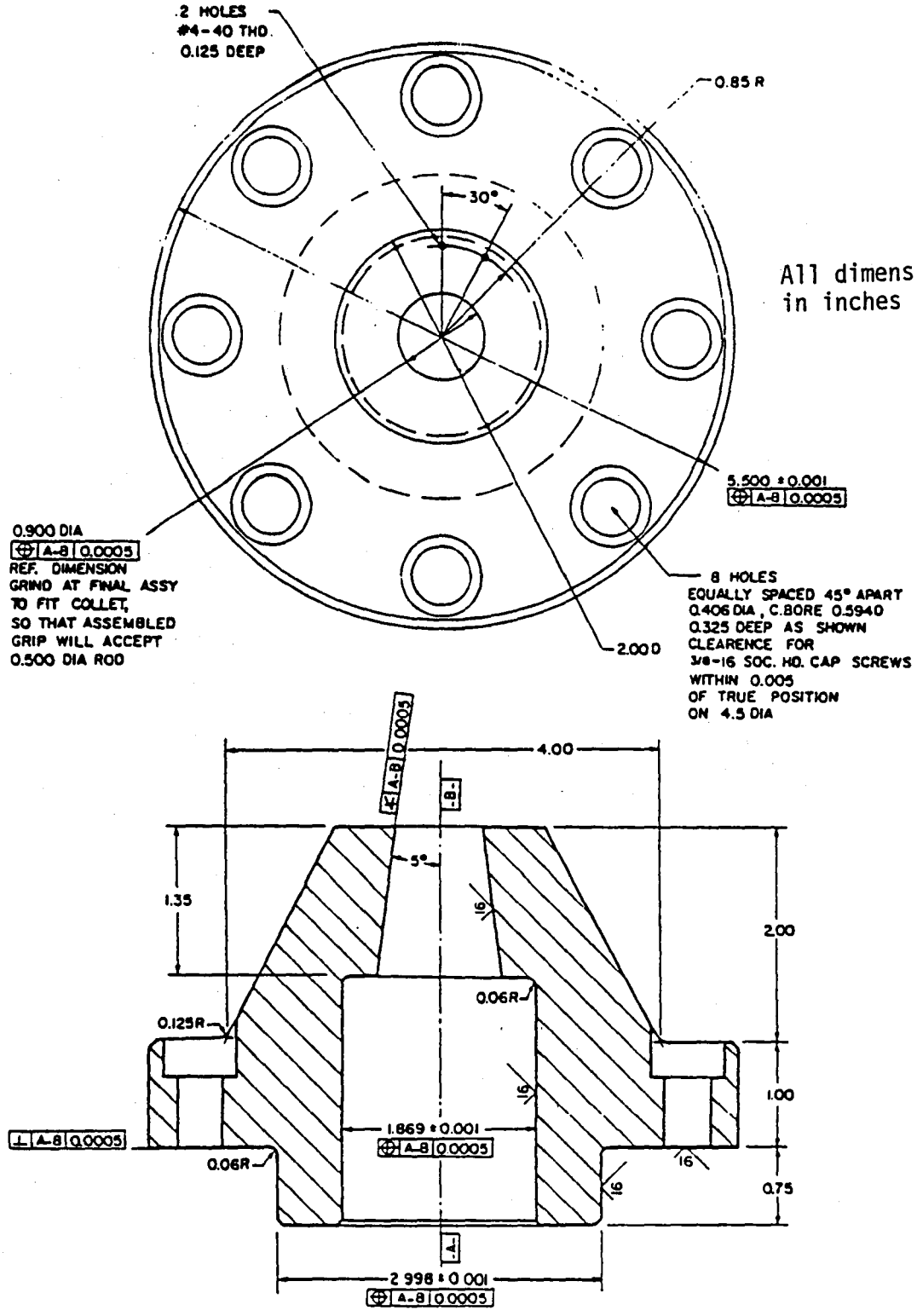


Fig. 12 (a) Details of the grip - Cover

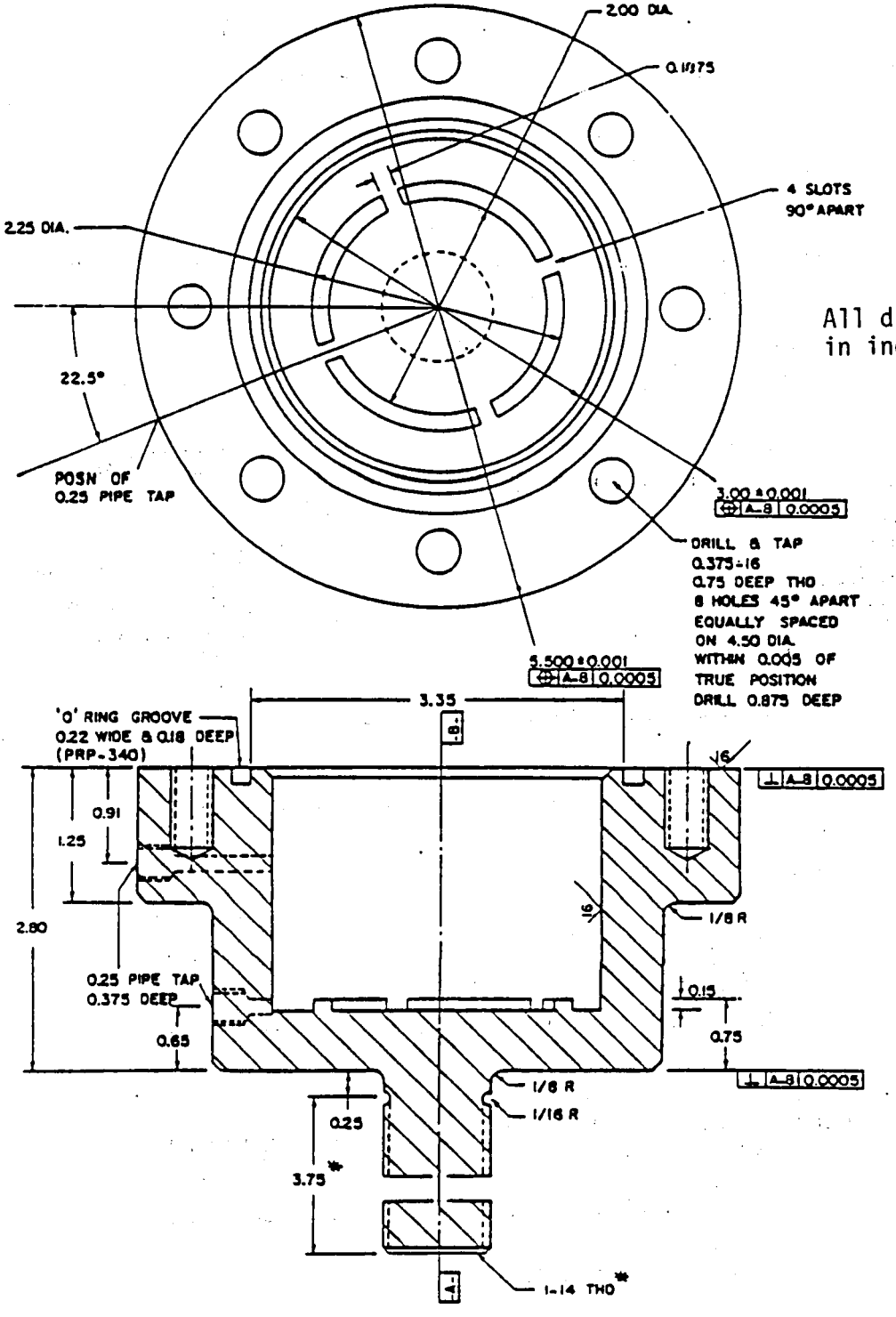


Fig. 12 (b) Details of the grip - Housing

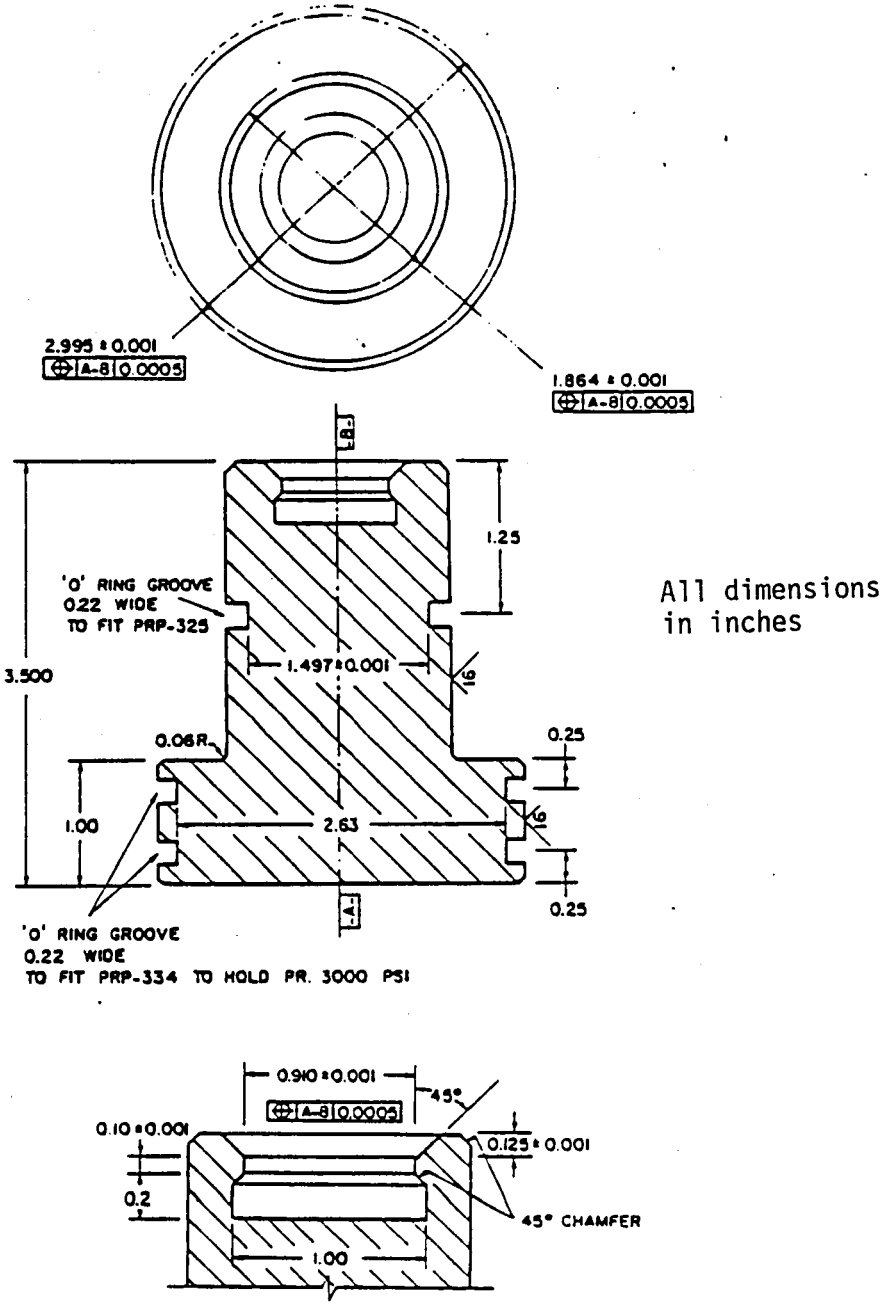


Fig. 12 (c) Details of the grip - Collet Holder

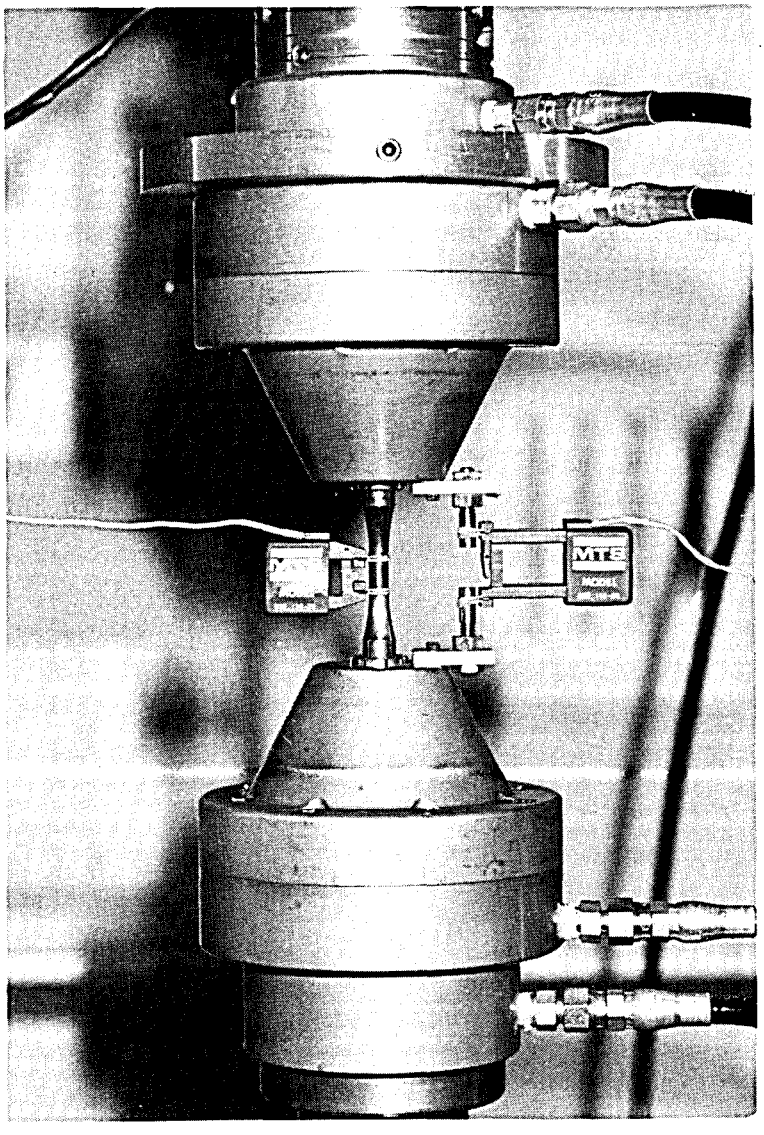


Fig. 13: Deflection control testing with two clip gauges

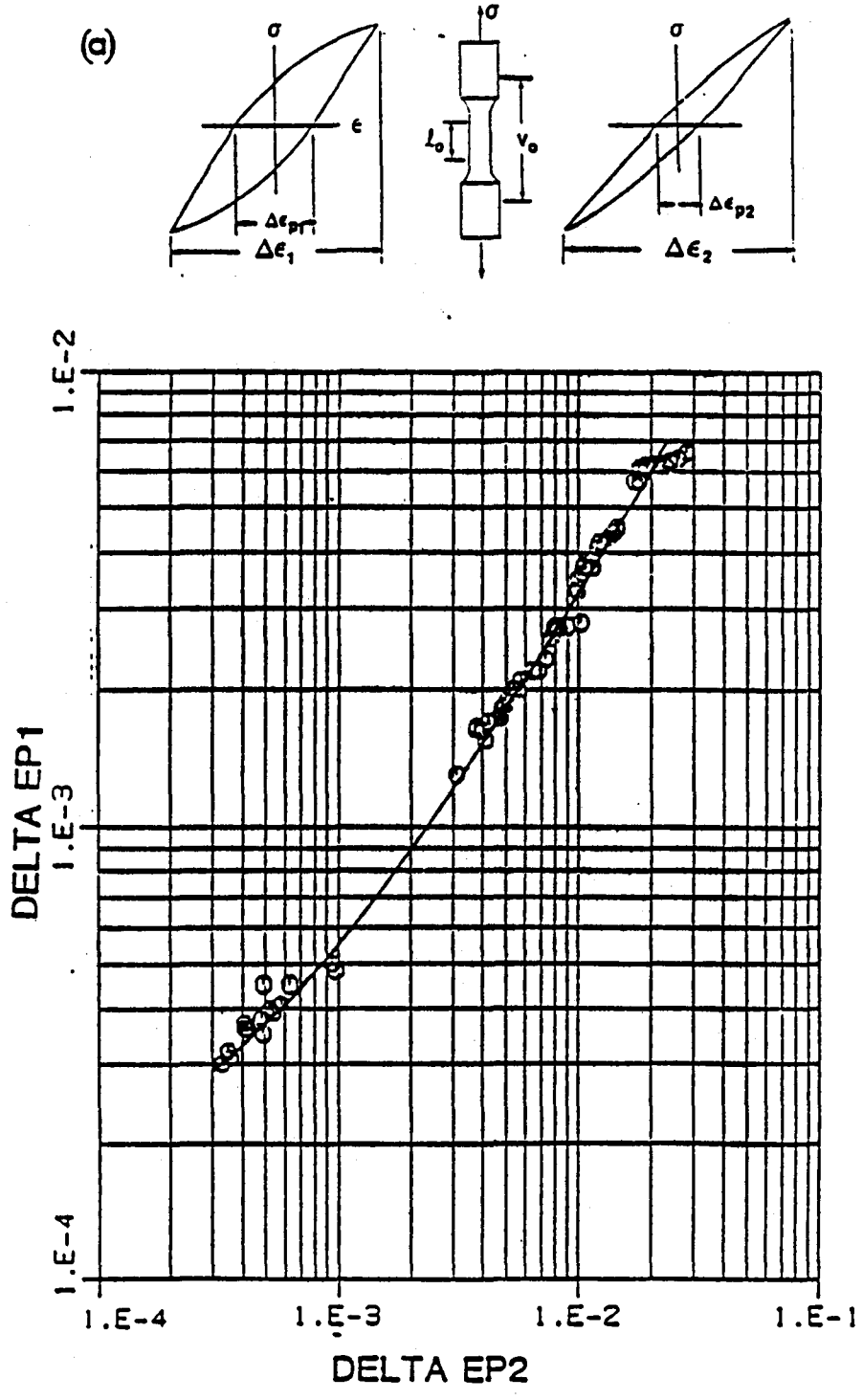


Fig. 14: (a) Schematic diagram of strain measurements
(b) Correlation between plastic strains

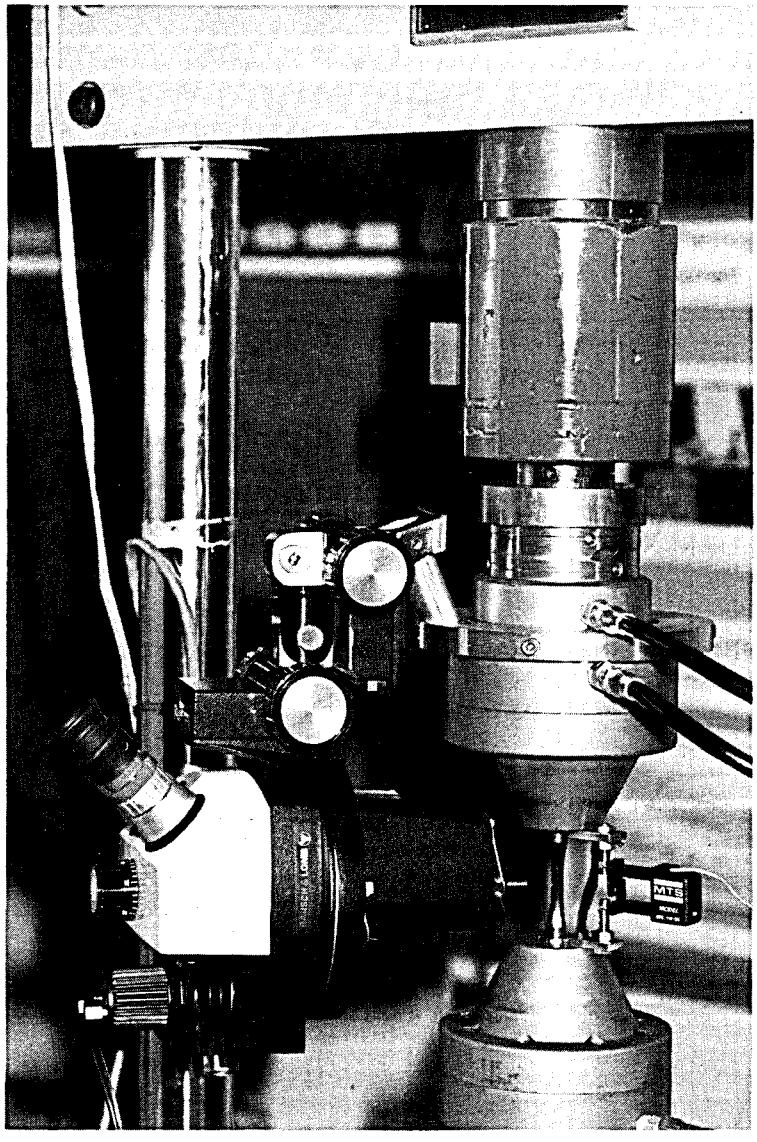


Fig. 15: Strain control testing with the clip gauge mounted across the grip ends.

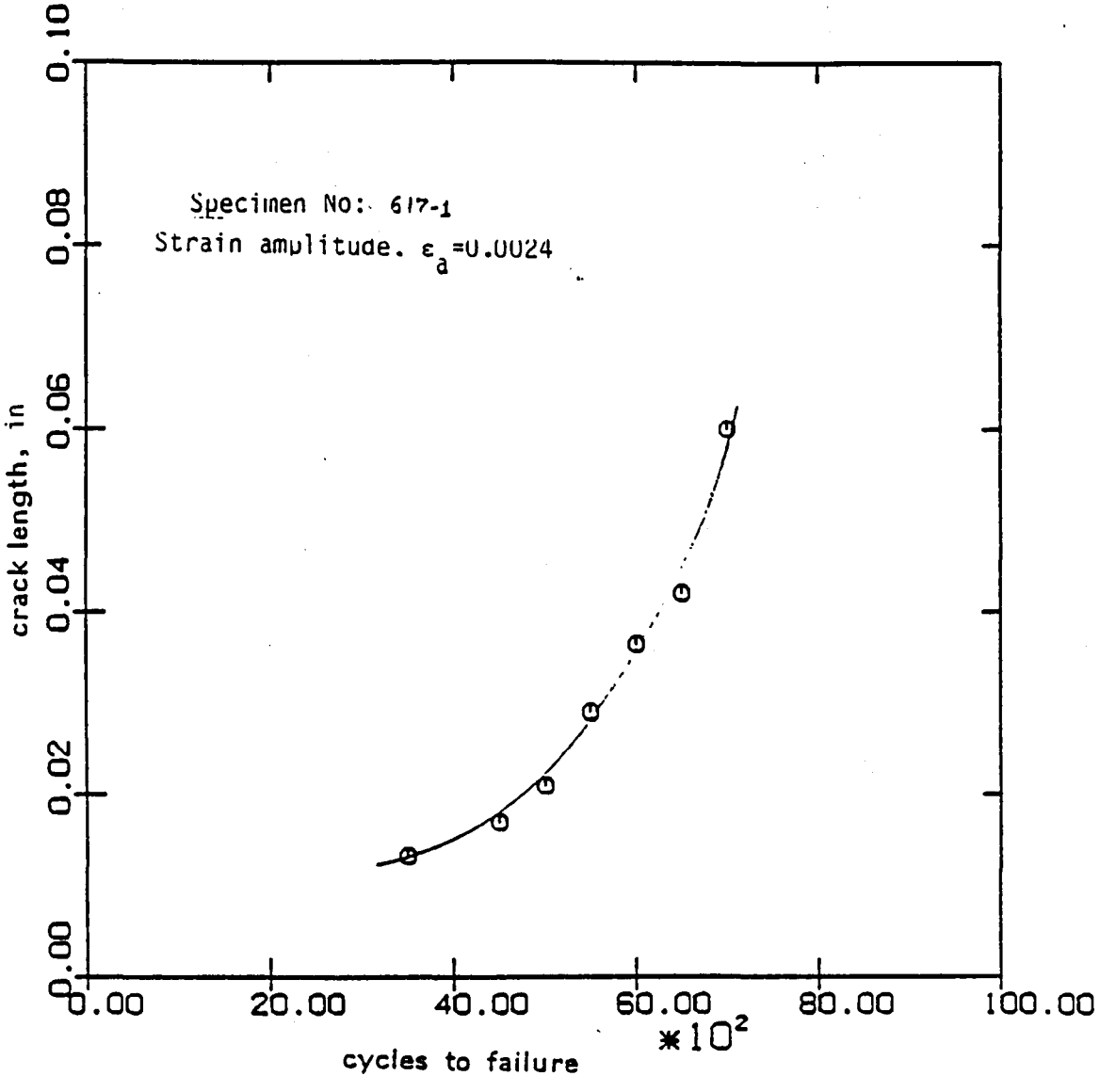


Fig. 16: A typical measurement of cack length vs cycles

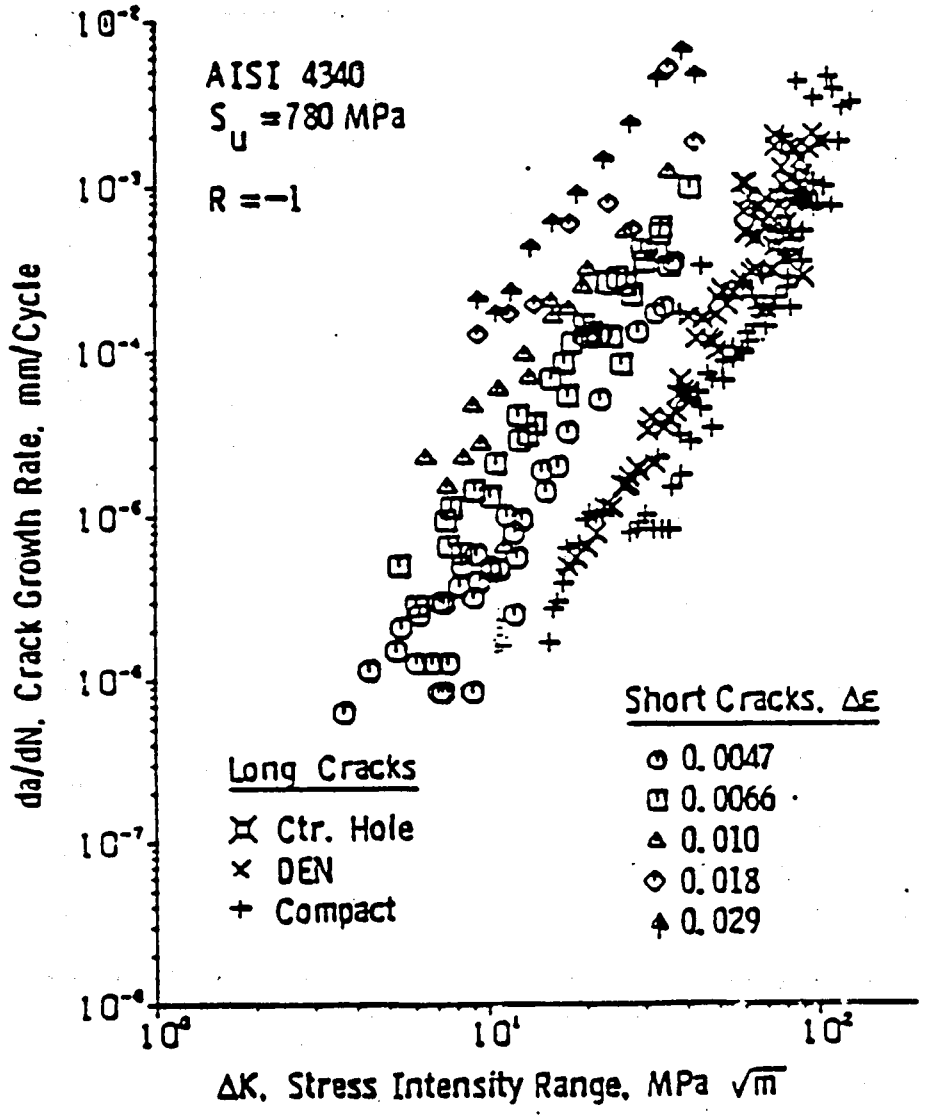


Fig. 17: da/dn vs ΔK for AISI 4340 steel (40)

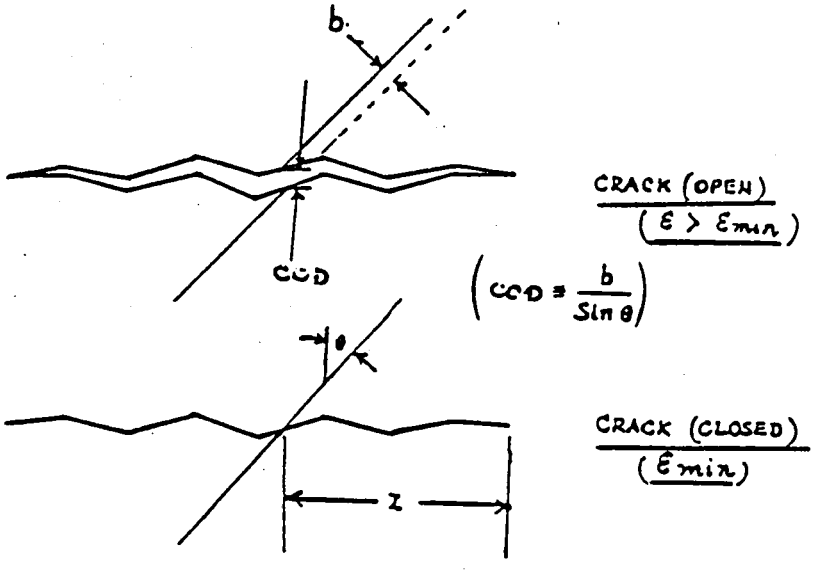


Fig. 18: Schematic diagram of closure measurement

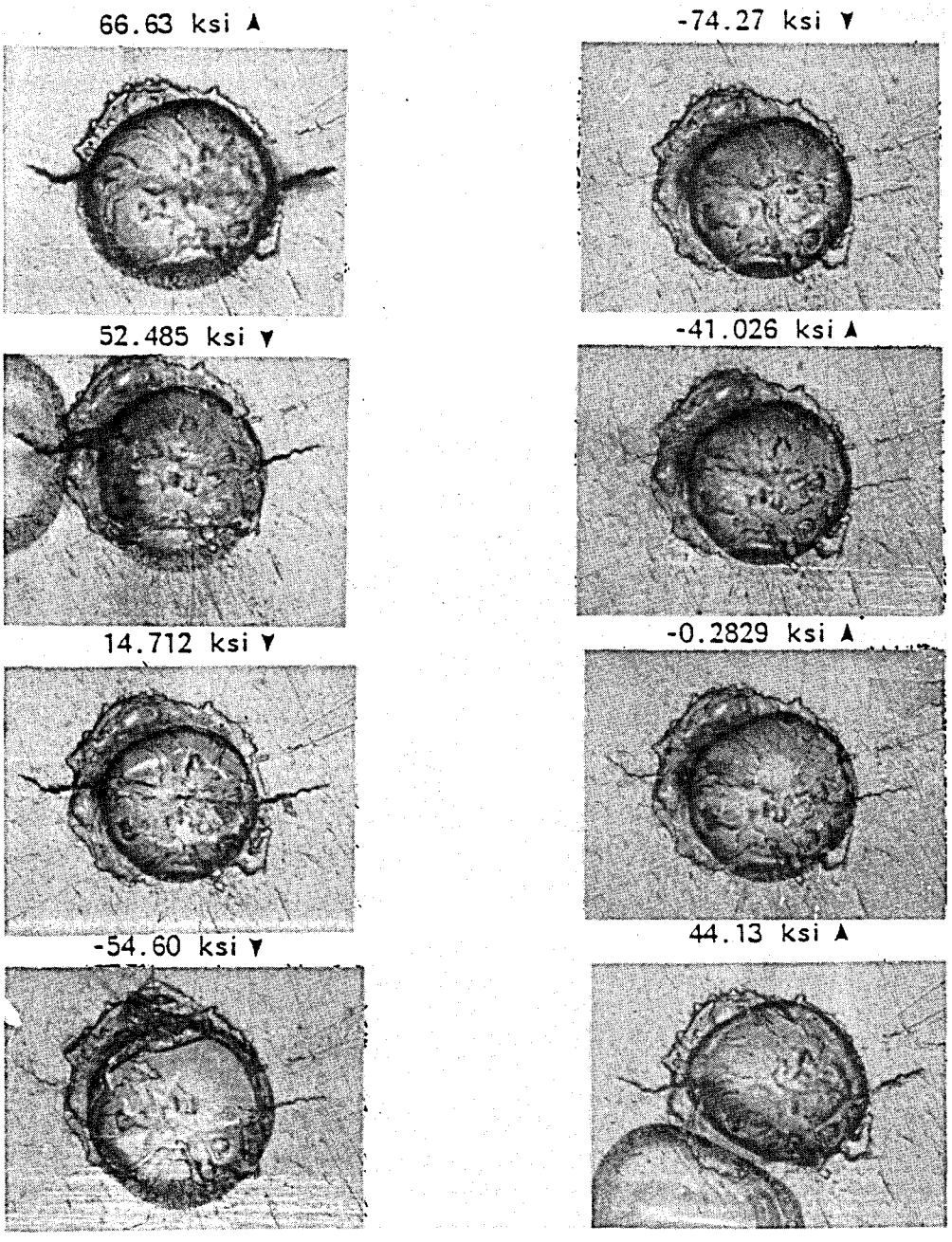


$\sigma_{max}$ = 74.8 ksi
specimen no. 617-5
strain amplitude= 0.0066
N1200R
2a=0.0171 in

Fig. 19: Typical crack at various stress levels in one complete cycle

(X100)

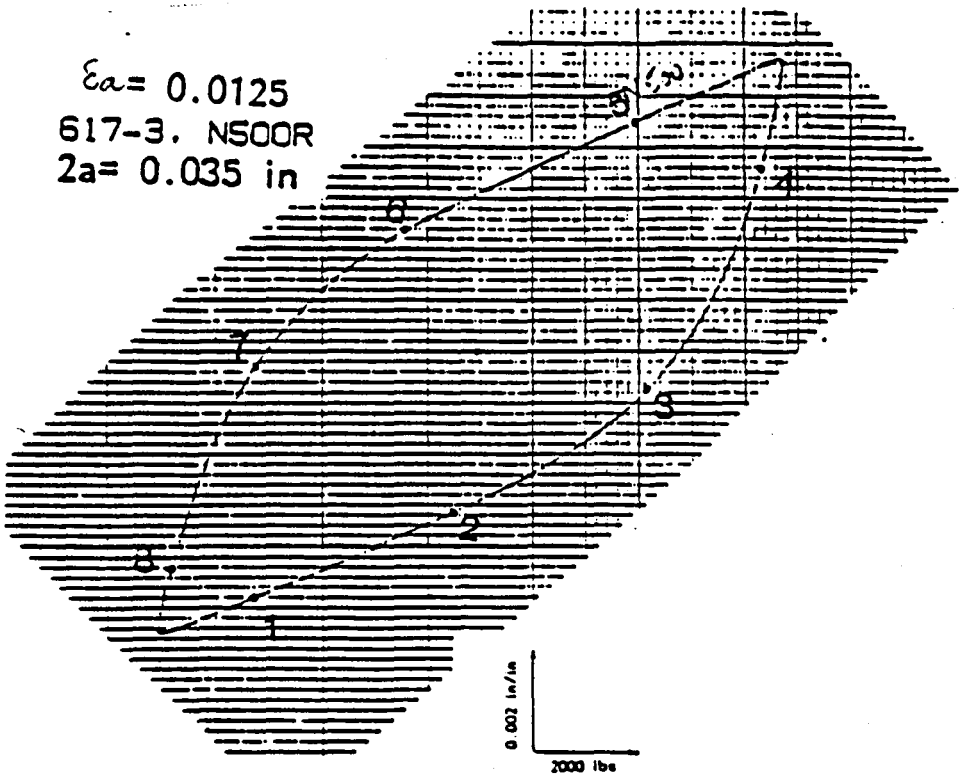


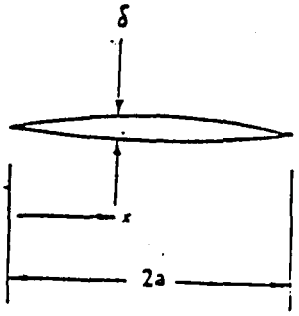


| | Stress (ksi) | Strain |
|---|---|---|
| 1 | -59.13 | -0.0115 |
| 2 | - 7.07 | -0.0095 |
| 3 | 44.98 | -0.0055 |
| 4 | 75.97 | 0.00435 |
| 5 | 42.44 | 0.0105 |
| 6 | -21.22 | 0.007 |
| 7 | -59.27 | 0.0013 |
| 8 | -81.34 | -0.0089 |

Fig. 20: Crack opening displacements measured in one complete cycle
(a) Load displacement loop as obtained from clip gauge mounted across the grip ends and the points (corresponding stress and strain levels shown in table) where closure observations were made.

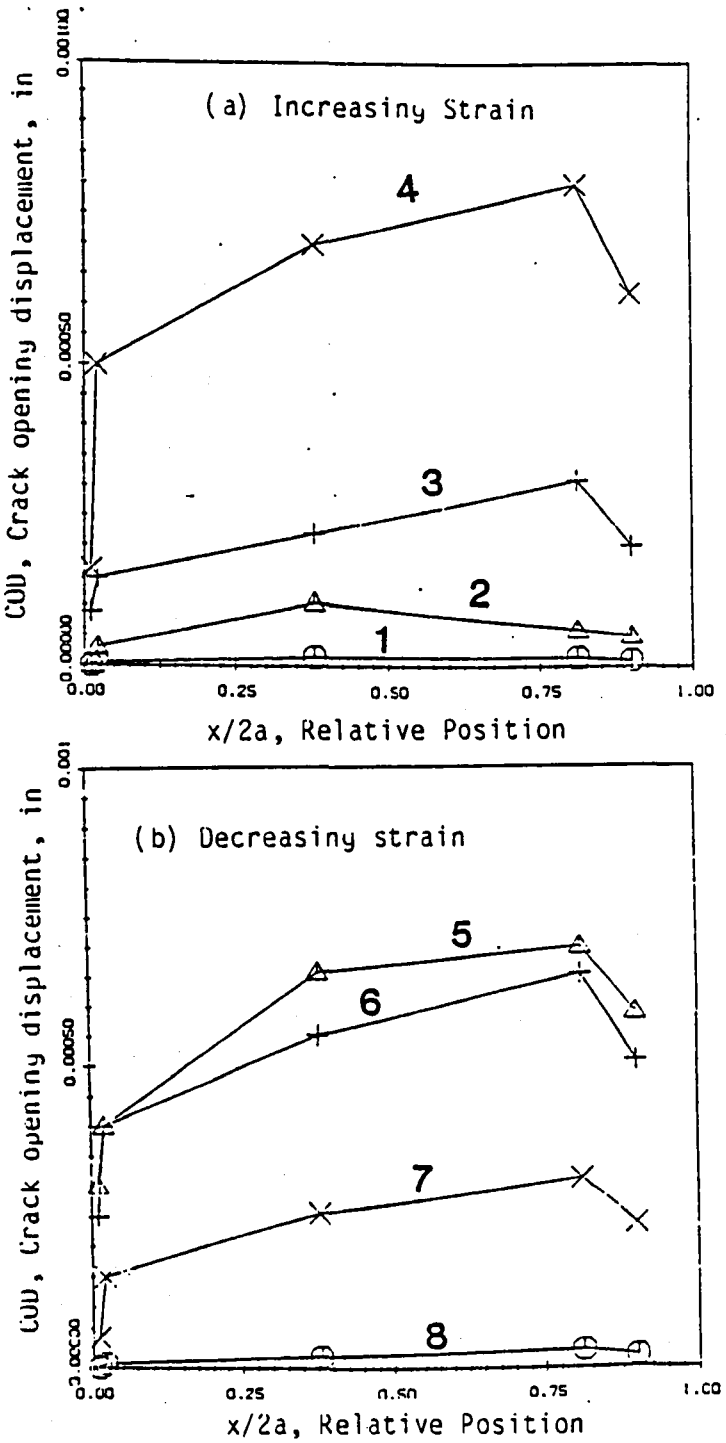


(b) Crack opening displacement during increasing (loading) and decreasing strain (unloading) at different points along the crack length. Different stress (strain) levels correspond to the points shown in load displacement loop.

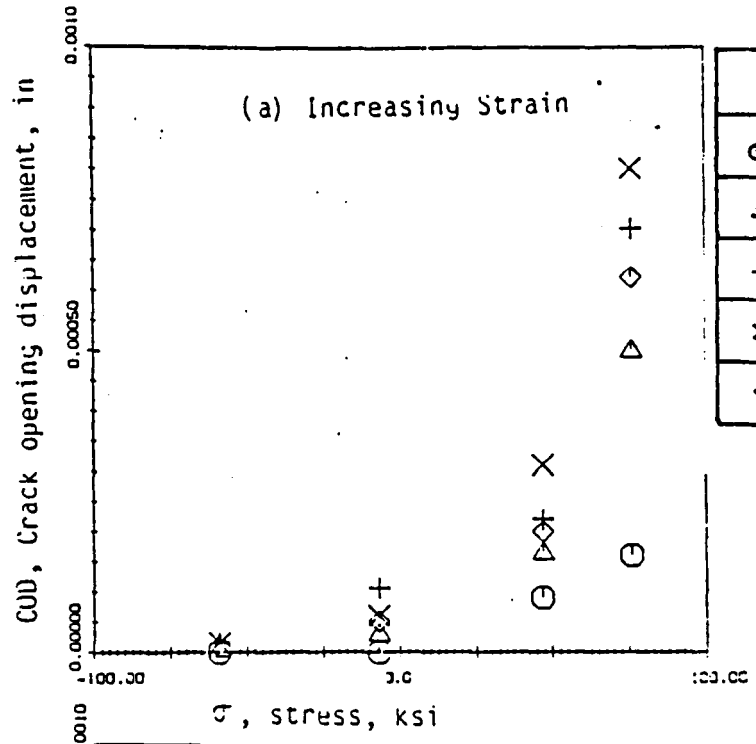


| | x(in) | x/2a |
|---|---|---|
| ○ | 0.0039 | 0.01114 |
| △ | 0.0076 | 0.02171 |
| + | 0.0133 | 0.380 |
| × | 0.0284 | 0.8114 |
| ◇ | 0.0315 | 0.9 |

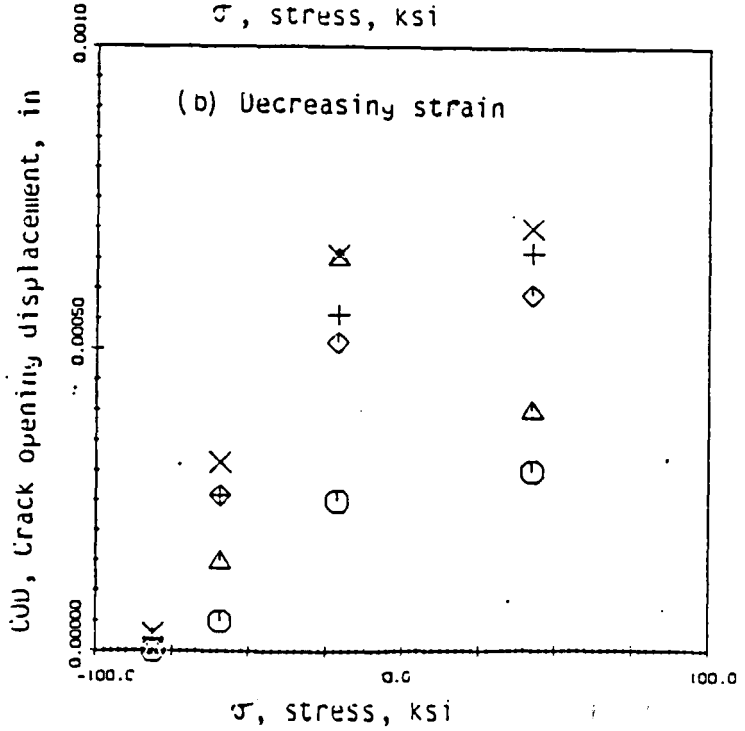


(c) Crack opening displacement as a function of stress at different points along the crack length during increasing and decreasing strain.

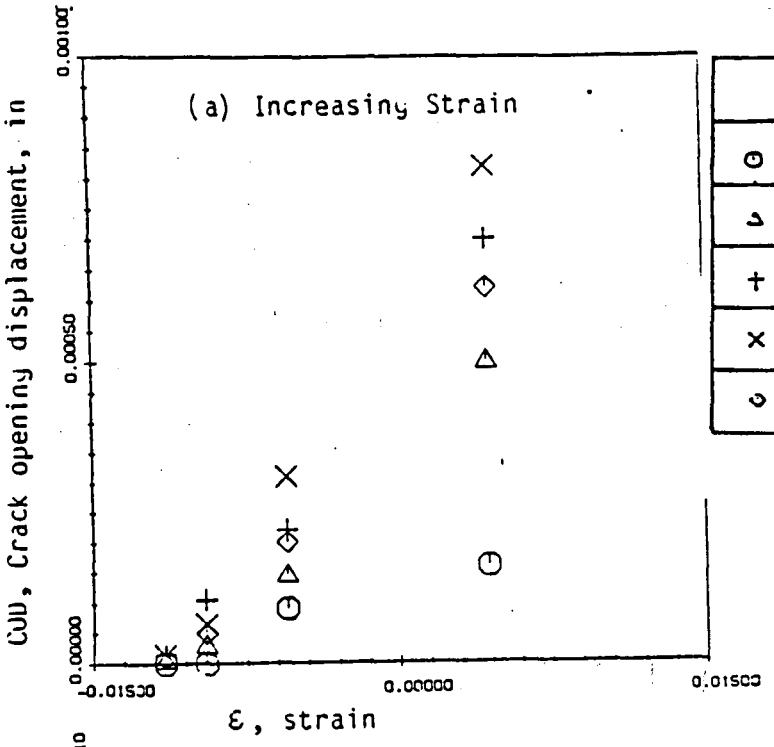


| | x(in) | x/2a |
|---|---|---|
| ○ | 0.0039 | 0.01114 |
| △ | 0.0076 | 0.02171 |
| + | 0.0133 | 0.380 |
| × | 0.0284 | 0.8114 |
| ◇ | 0.0315 | 0.9 |

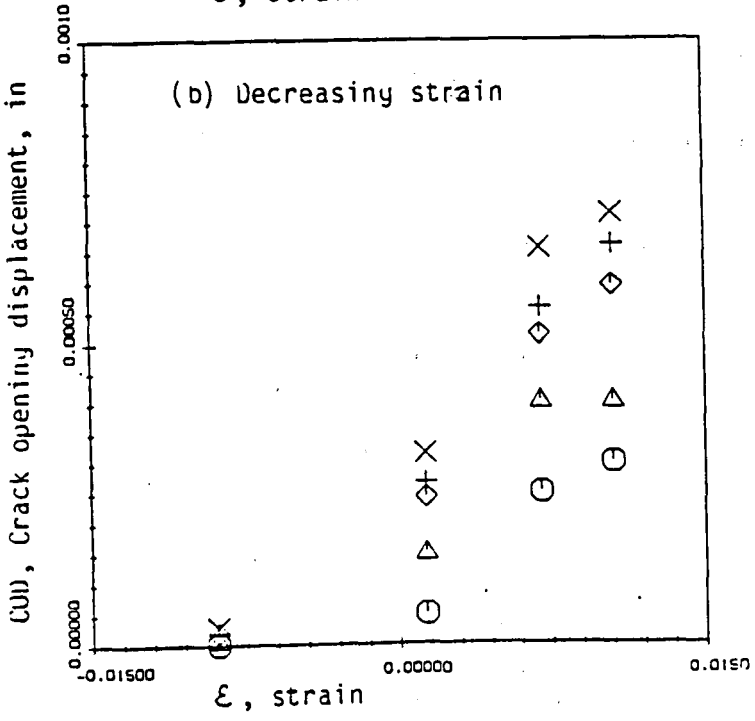


(d) Crack opening displacement as a function of strain at different points along the crack length during increasing and decreasing strain.

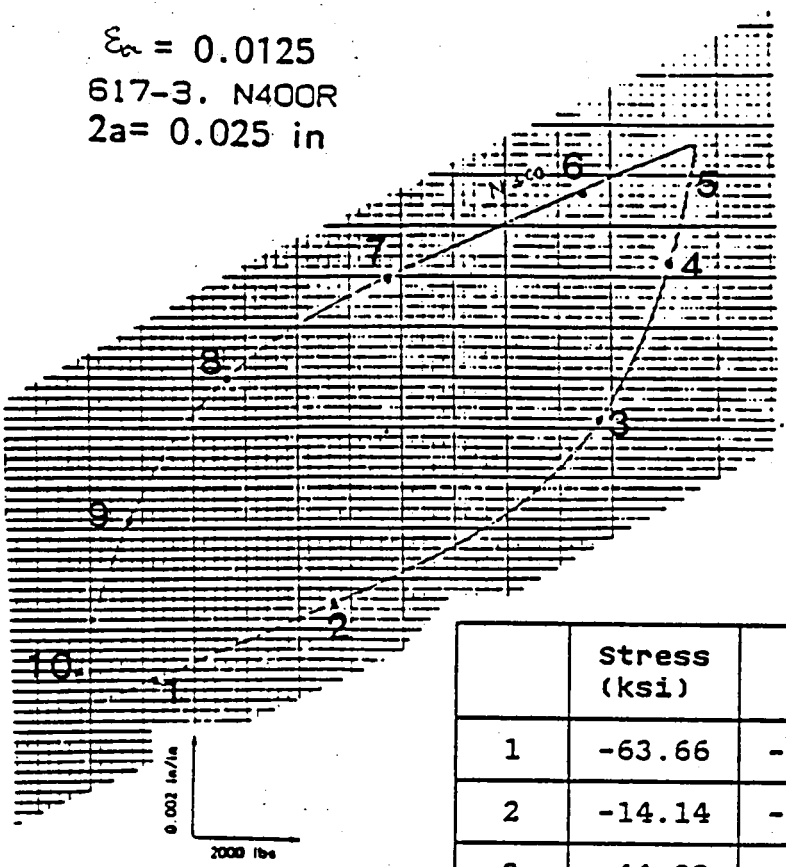


| | Stress (ksi) | Strain |
|---|---|---|
| 1 | -63.66 | -0.01105 |
| 2 | -14.14 | -0.00925 |
| 3 | 44.09 | -0.0045 |
| 4 | 56.59 | -0.00225 |
| 5 | 74.67 | 0.0057 |
| 6 | 52.77 | 0.01215 |
| 7 | 0.00 | 0.0096 |
| 8 | -42.44 | -0.00615 |
| 9 | -70.73 | - 0.0025 |
| 10 | -82.76 | - 0.0104 |

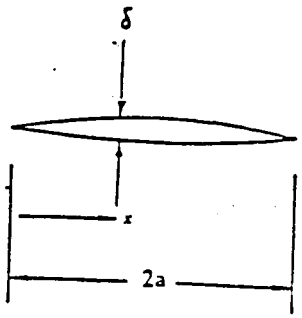


Fig. 21: Crack opening displacements measured in one complete cycle
(a) Load displacement loop as obtained from clip gauge mounted across the grip ends and the points (corresponding stress and strain levels shown in table) where closure observations were made.

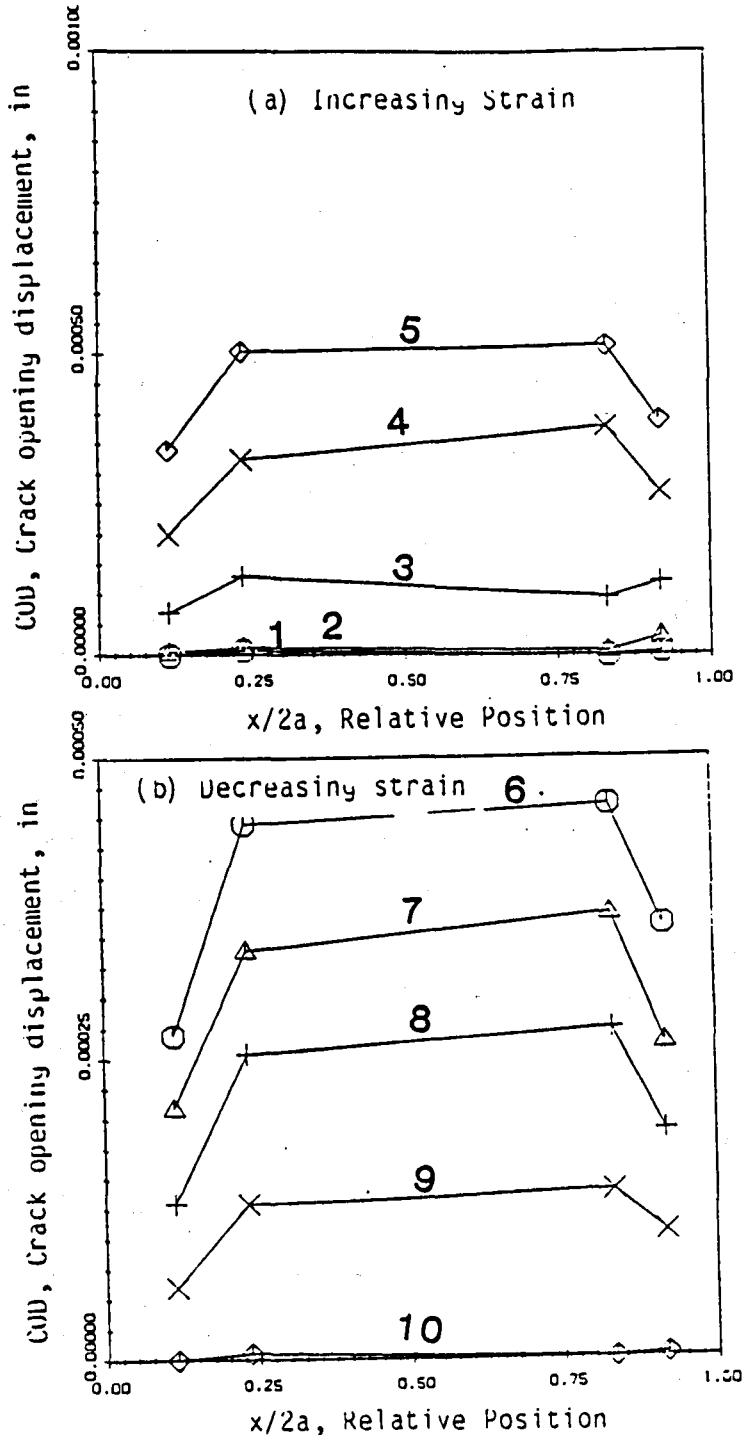


(b) Crack opening displacement during increasing (loading) and decreasing strain (unloading) at different points along the crack length. Different stress (strain) levels correspond to the points shown in load displacement loop.

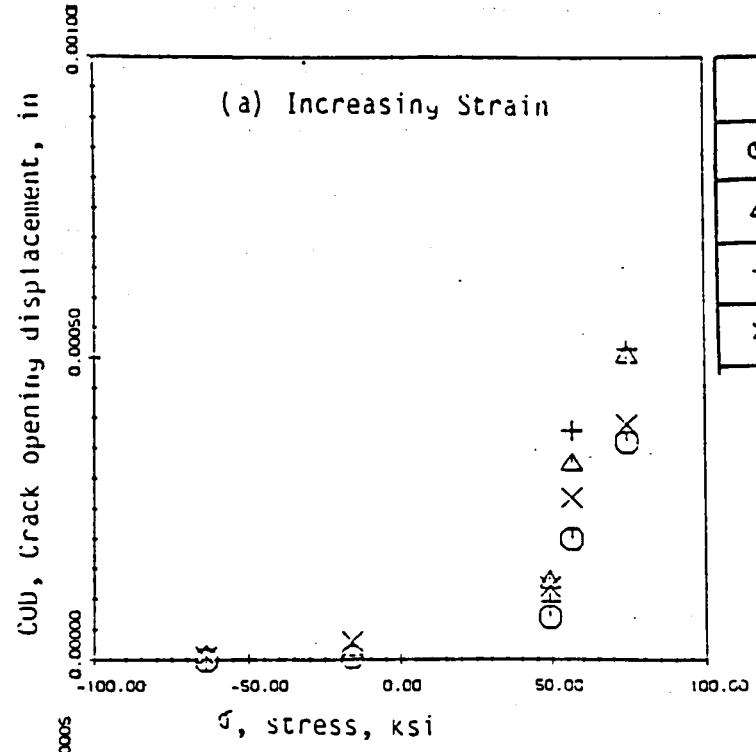


| | x(in) | x/2a |
|---|---|---|
| ⊙ | 0.0028 | 0.01143 |
| △ | 0.00575 | 0.2347 |
| + | 0.0204 | 0.8327 |
| × | 0.0225 | 0.9183 |

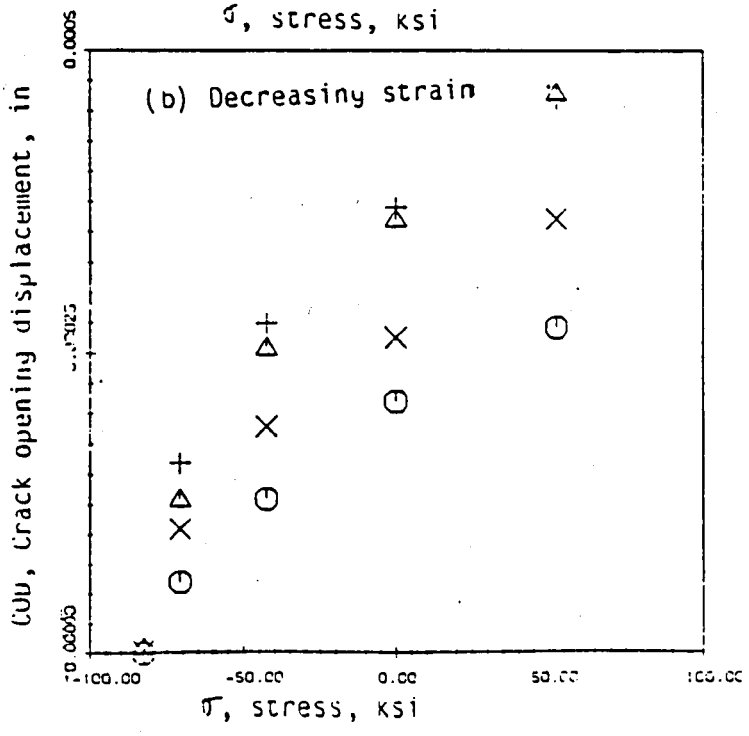


(c) Crack opening displacement as a function of stress at different points along the crack length during increasing and decreasing strain.

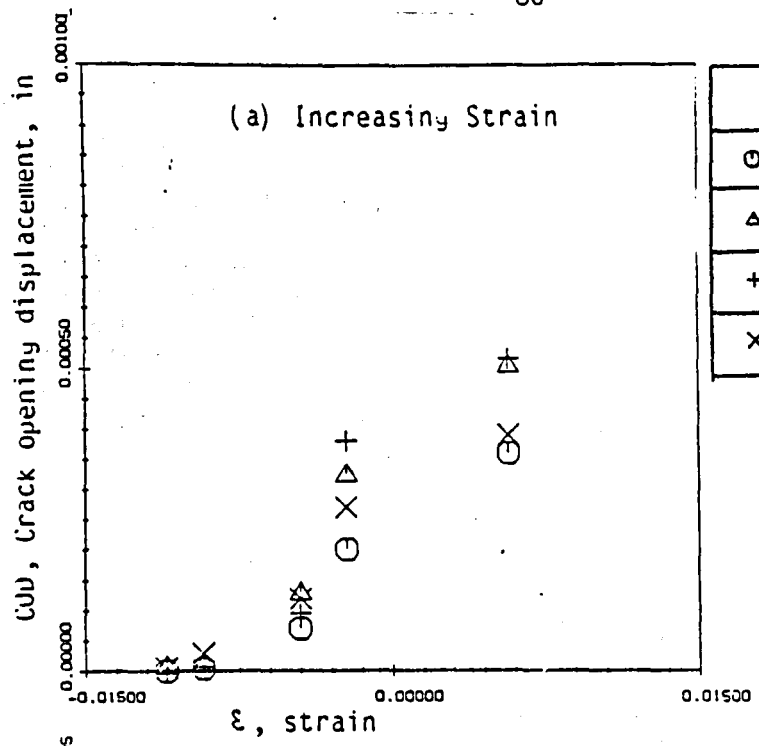


| | x(in) | x/2a |
|---|---|---|
| ⊙ | 0.0028 | 0.01143 |
| △ | 0.00575 | 0.2347 |
| + | 0.0204 | 0.8327 |
| × | 0.0225 | 0.9183 |

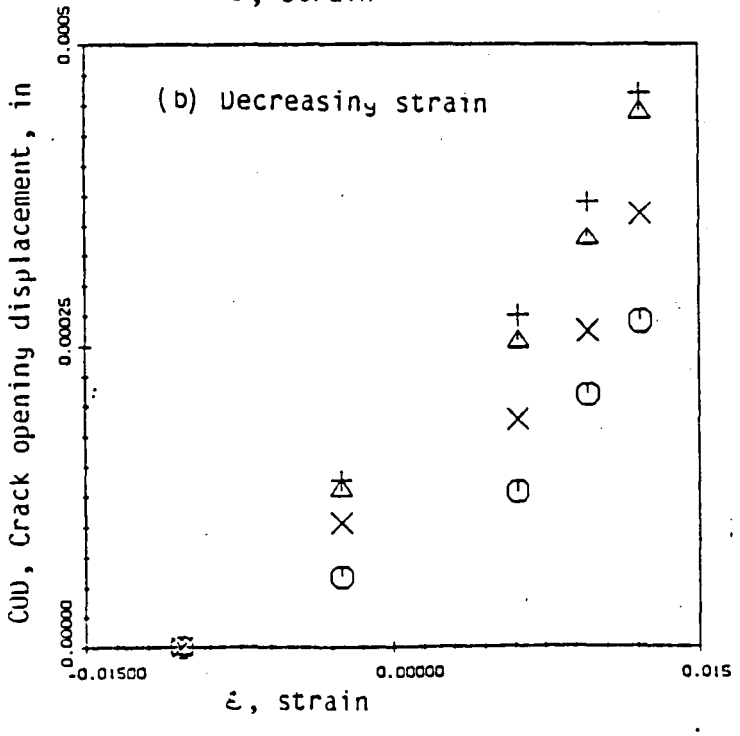


(a) Crack opening displacement as a function of strain at different points along the crack length during increasing and decreasing strain.

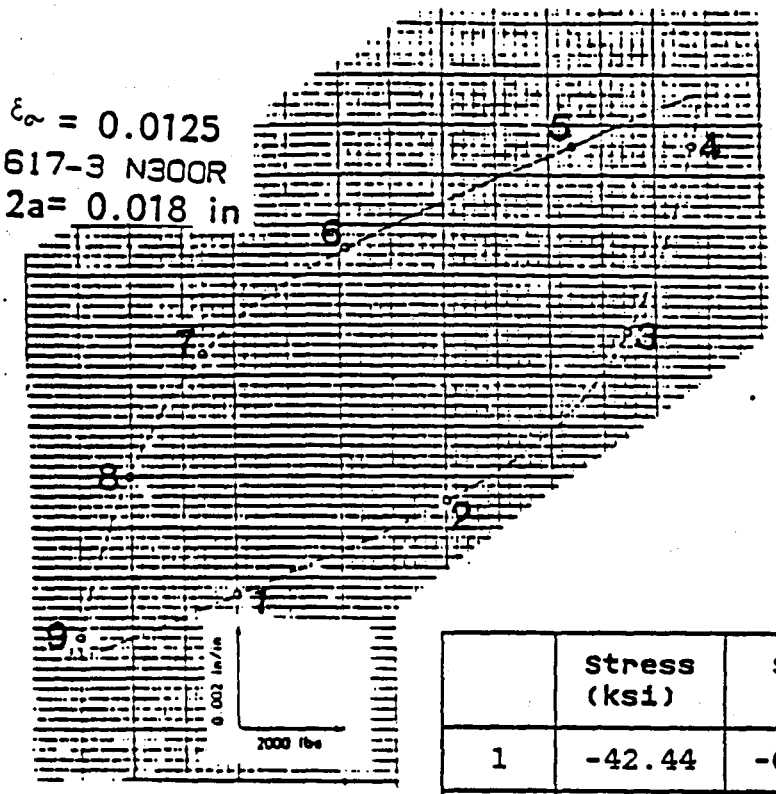


| | Stress (ksi) | Strain |
|---|---|---|
| 1 | -42.44 | -0.0105 |
| 2 | -14.14 | -0.0071 |
| 3 | 63.37 | -0.0046 |
| 4 | 81.06 | 0.0081 |
| 5 | 49.57 | 0.01125 |
| 6 | -11.88 | 0.0085 |
| 7 | -44.56 | 0.00545 |
| 8 | -71.58 | -0.00490 |
| 9 | -81.34 | -0.0115 |

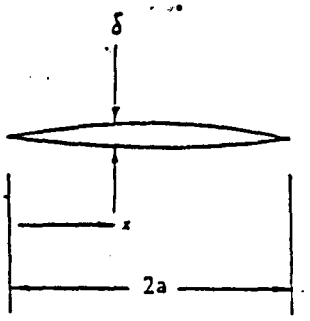


Fig. 22: Crack opening displacements measured in one complete cycle
(a) Load displacement loop as obtained from clip gauge mounted across the grip ends and the points (corresponding stress and strain levels shown in table) where closure observations were made.

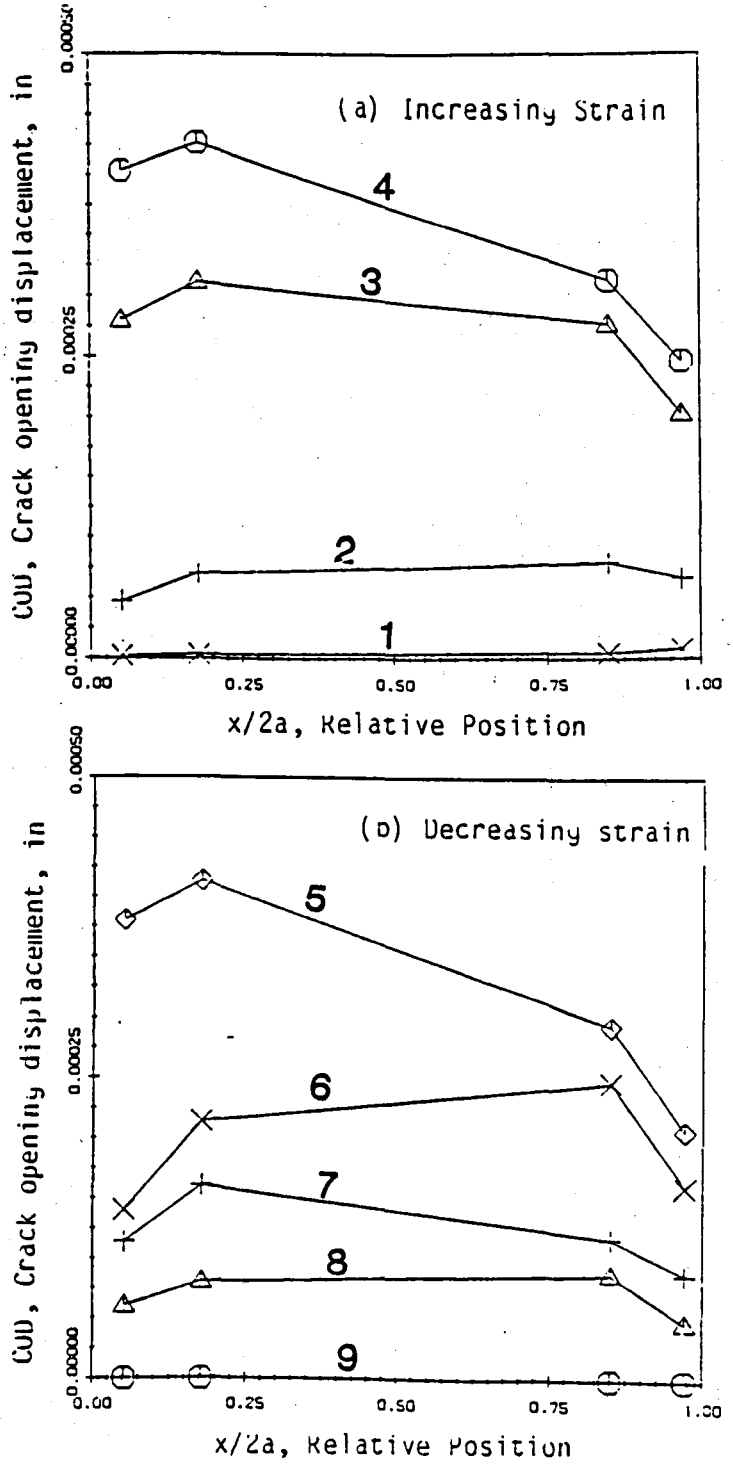


(b) Crack opening displacement during increasing (loading) and decreasing strain (unloading) at different points along the crack length. Different stress (strain) levels correspond to the points shown in load displacement loop.

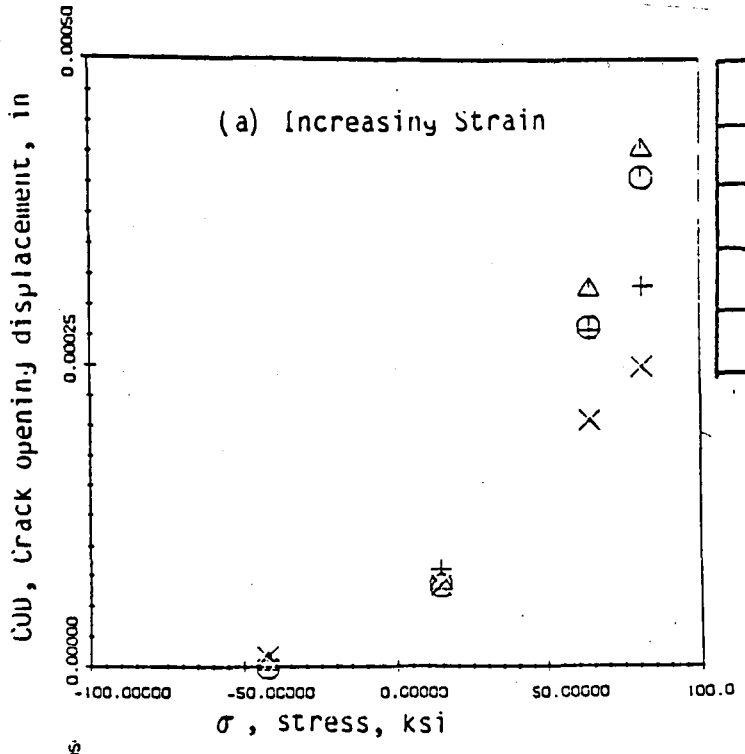


| | x(in) | x/2a |
|---|---|---|
| ⊙ | 0.00093 | 0.05123 |
| △ | 0.0032 | 0.1778 |
| + | 0.0153 | 0.85 |
| × | 0.01746 | 0.97 |

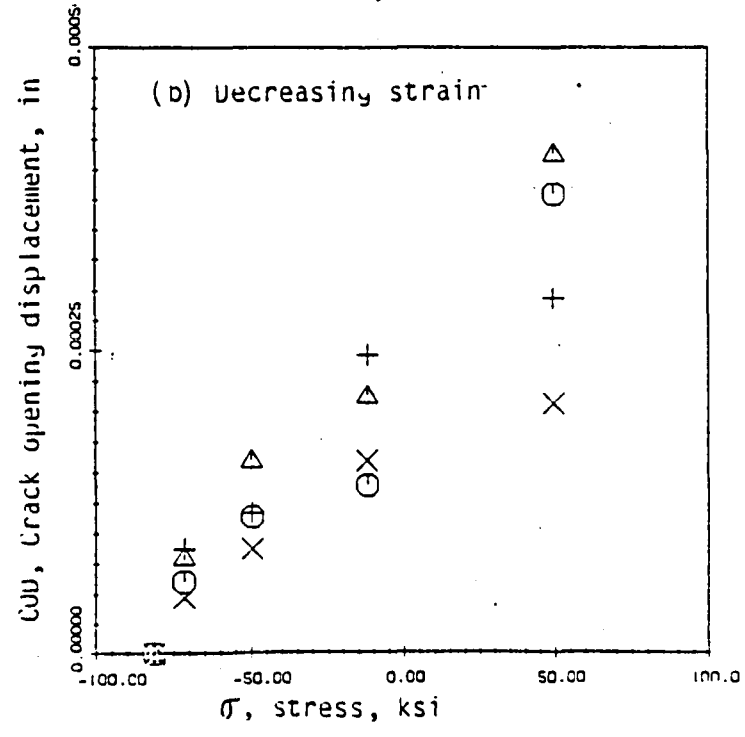


(c) Crack opening displacement as a function of stress at different points along the crack length during increasing and decreasing strain.

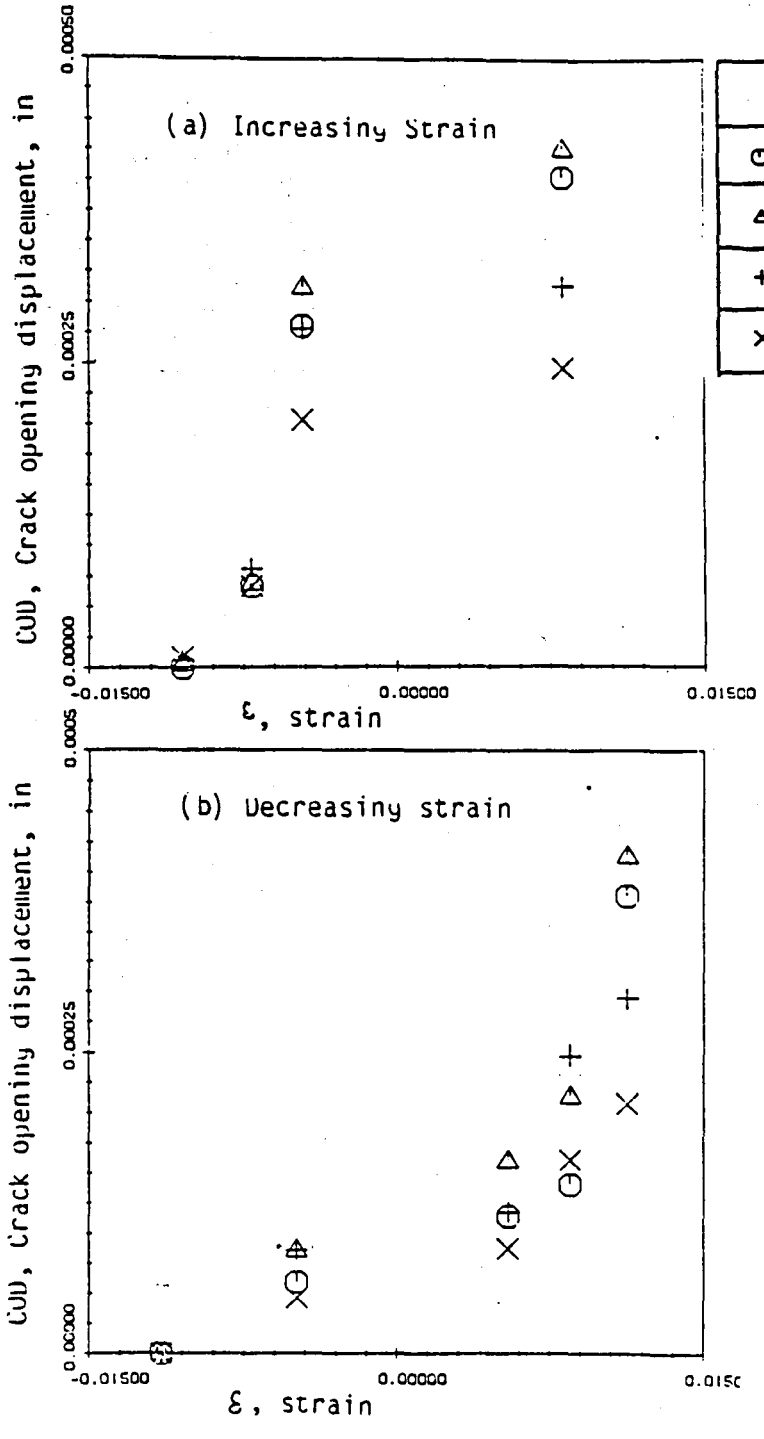


| | x(in) | x/2a |
|---|---|---|
| ⊙ | 0.00093 | 0.05123 |
| △ | 0.0032 | 0.1778 |
| + | 0.0153 | 0.85 |
| × | 0.01746 | 0.97 |

(d) Crack opening displacement as a function of strain at different points along the crack length during increasing and decreasing strain.

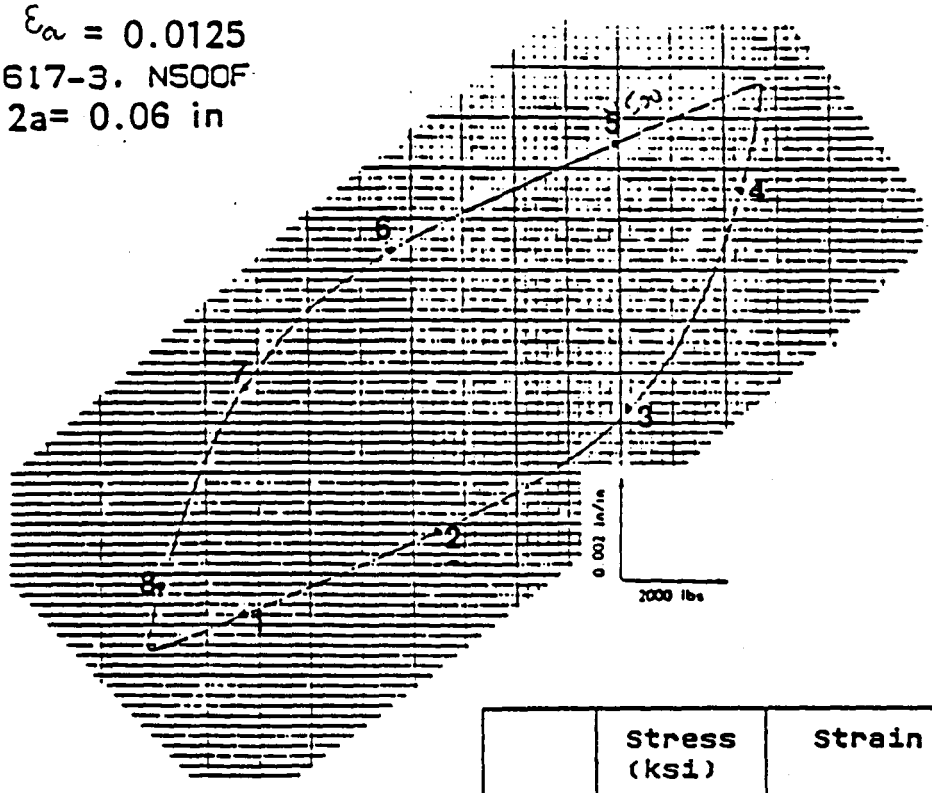


| | Stress (ksi) | Strain |
|---|---|---|
| 1 | -59.27 | -0.0115 |
| 2 | - 7.07 | -0.0095 |
| 3 | 44.98 | -0.0055 |
| 4 | 75.97 | 0.00435 |
| 5 | 42.44 | 0.0105 |
| 6 | -21.22 | 0.007 |
| 7 | -59.27 | 0.0013 |
| 8 | -81.34 | -0.0089 |

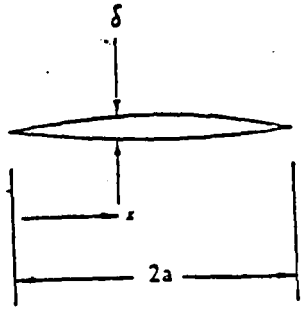


Fig. 23: Crack opening displacements measured in one complete cycle
(a) Load displacement loop as obtained from clip gauge mounted across the grip ends and the points (corresponding stress and strain levels shown in table) where closure observations were made.

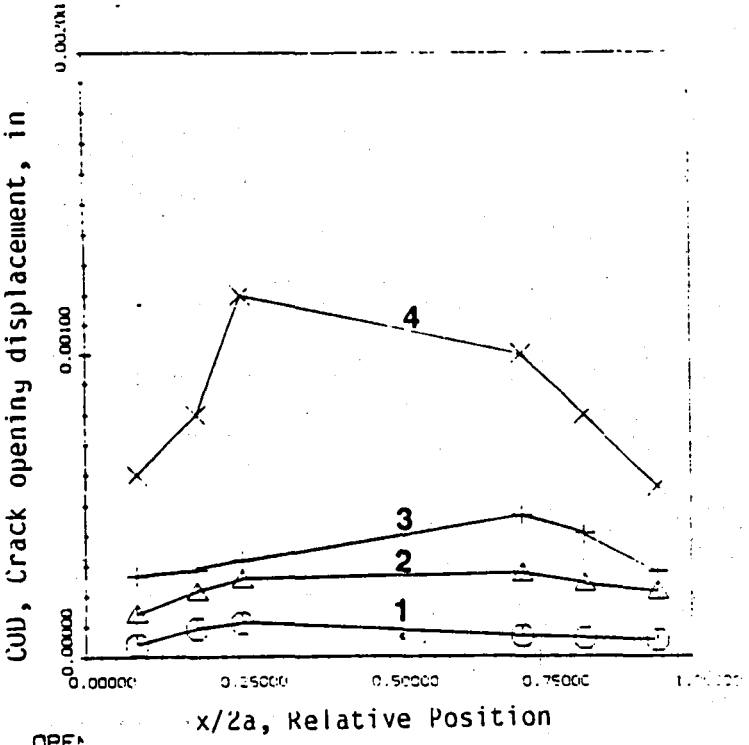


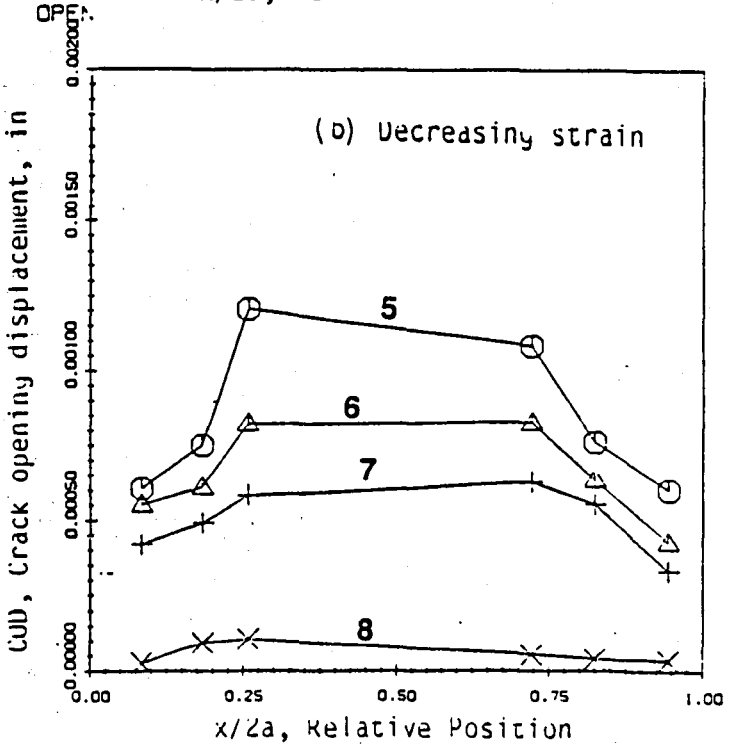


(b) Crack opening displacement during increasing (loading) and decreasing strain (unloading) at different points along the crack length. Different stress (strain) levels correspond to the points shown in load displacement loop.

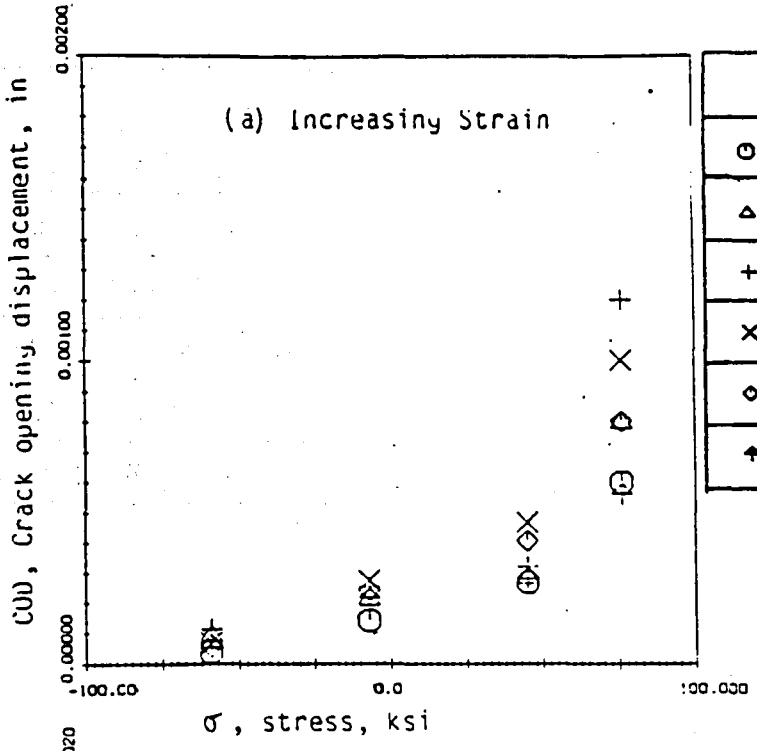


| | x(in) | x/2a |
|---|---|---|
| ○ | 0.00506 | 0.0844 |
| △ | 0.01133 | 0.1888 |
| + | 0.01546 | 0.2577 |
| × | 0.0433 | 0.7217 |
| ◇ | 0.04946 | 0.8243 |
| ✦ | 0.05667 | 0.9445 |

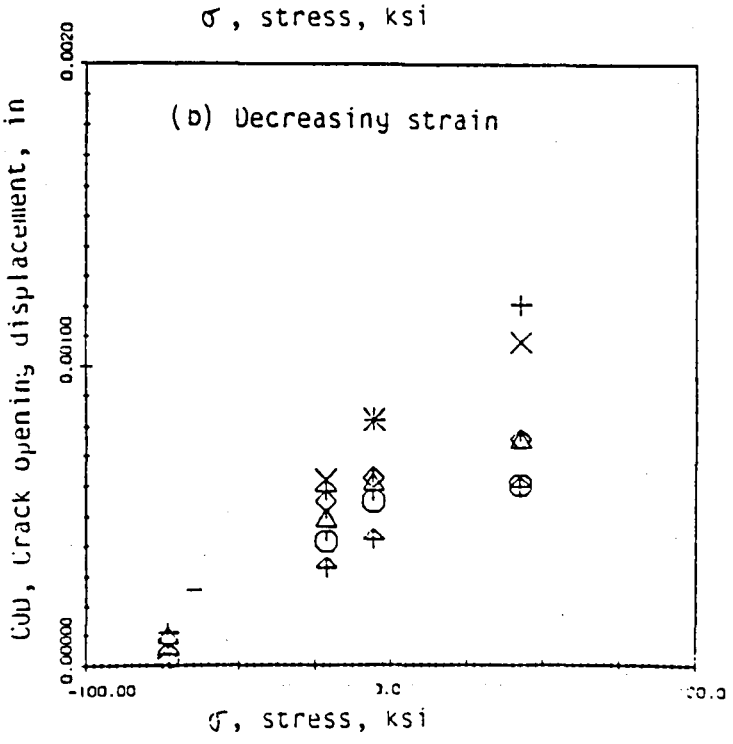


(c) Crack opening displacement as a function of stress at different points along the crack length during increasing and decreasing strain.

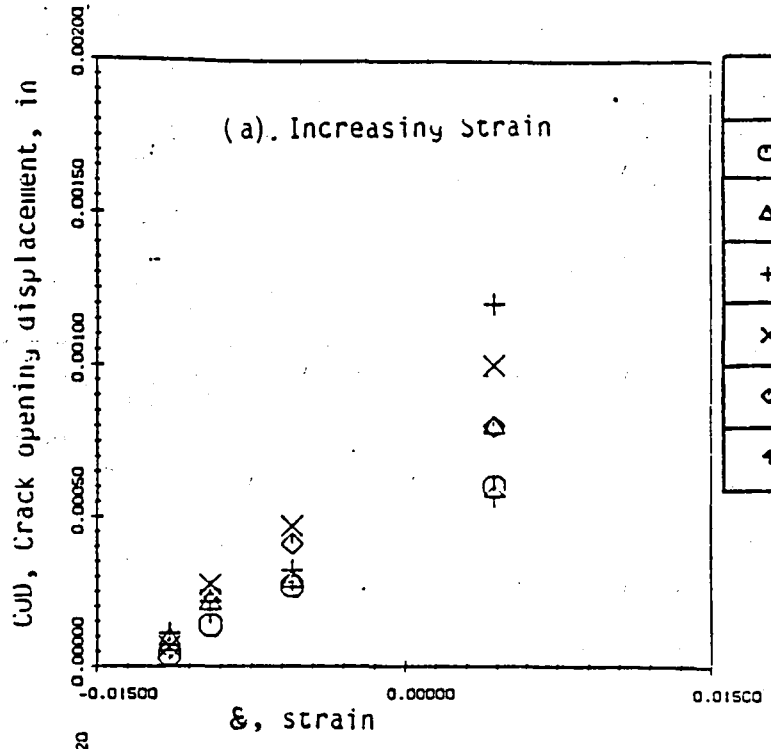


| | x(in) | x/2a |
|---|---|---|
| ⊙ | 0.00506 | 0.0844 |
| △ | 0.01133 | 0.1888 |
| + | 0.01546 | 0.2577 |
| × | 0.0433 | 0.7217 |
| ◇ | 0.04946 | 0.8243 |
| ↑ | 0.05667 | 0.9445 |

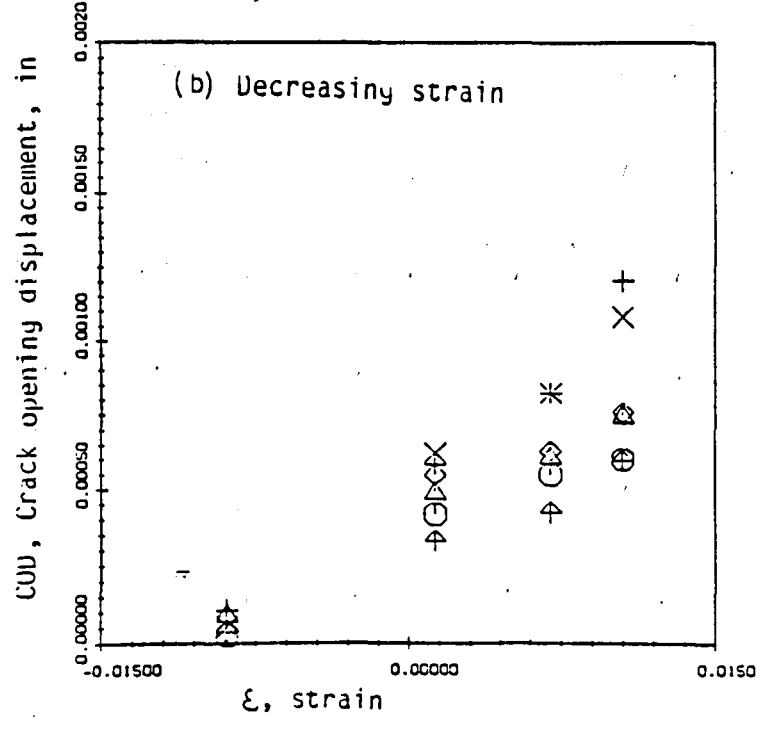


(d) Crack opening displacement as a function of strain at different points along the crack length during increasing and decreasing strain.

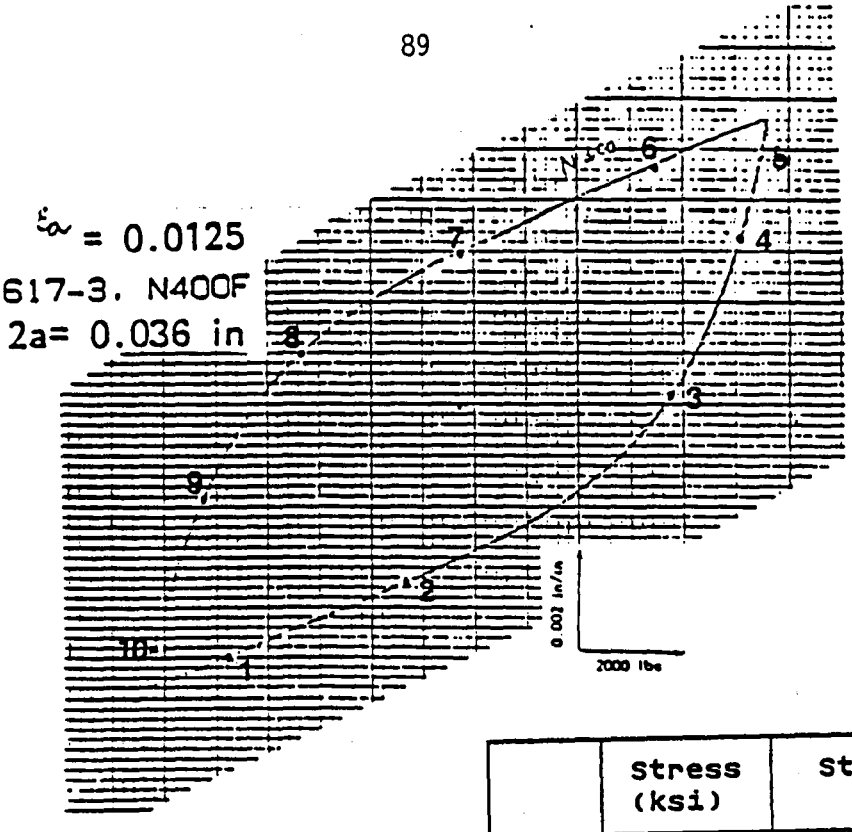


| | Stress (ksi) | Strain |
|---|---|---|
| 1 | -63.66 | -0.01105 |
| 2 | -14.14 | -0.00925 |
| 3 | 44.09 | -0.0045 |
| 4 | 56.59 | -0.00225 |
| 5 | 74.67 | 0.0057 |
| 6 | 52.77 | 0.01215 |
| 7 | 0.00 | 0.0096 |
| 8 | -42.44 | -0.00615 |
| 9 | -70.73 | - 0.0025 |
| 10 | -82.76 | - 0.0104 |

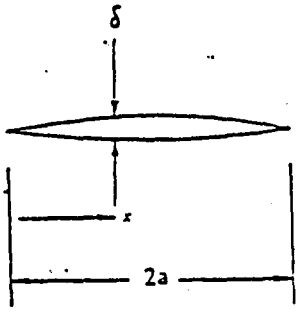


Fig. 24: Crack opening displacements measured in one complete cycle
(a) Load displacement loop as obtained from clip gauge mounted across the grip ends and the points (corresponding stress and strain levels shown in table) where closure observations were made.

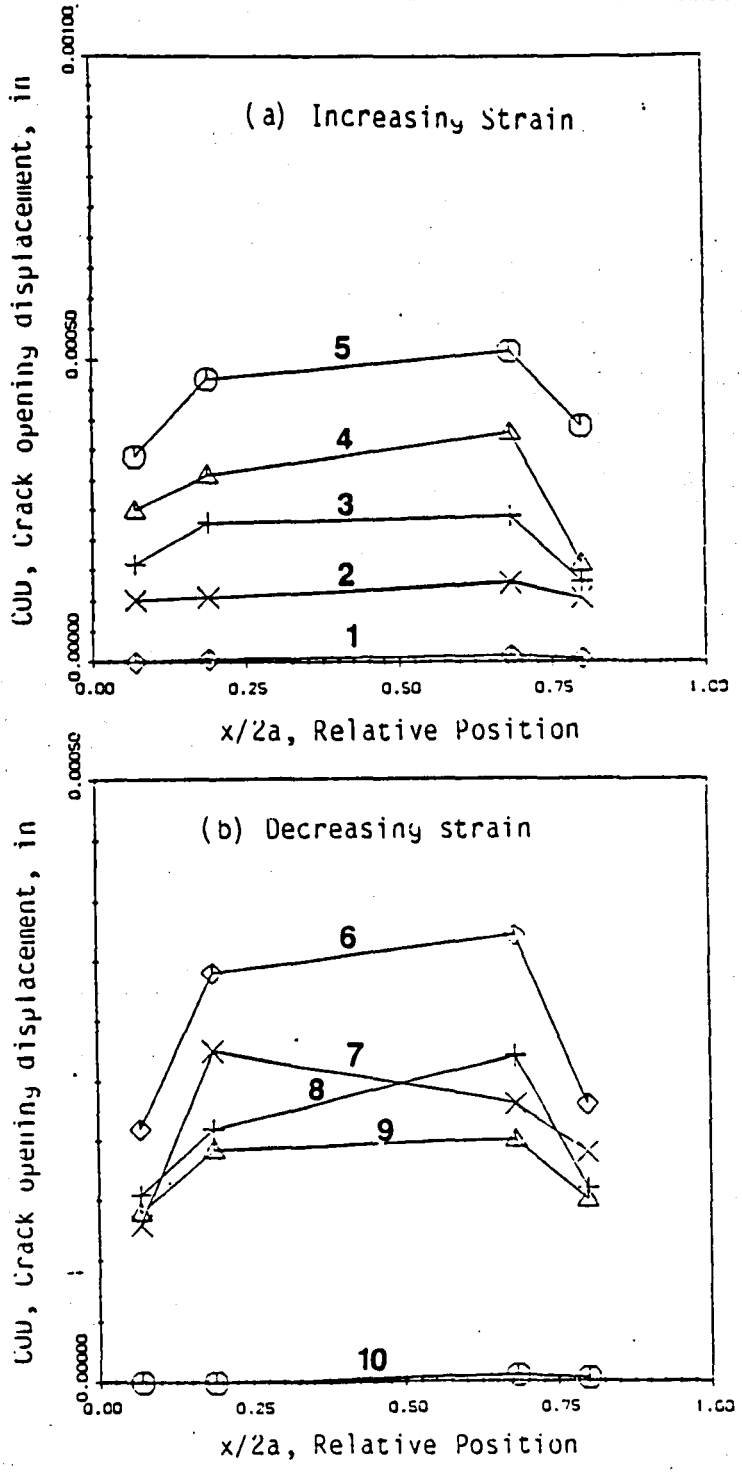


(b) Crack opening displacement during increasing (loading) and decreasing strain (unloading) at different points along the crack length. Different stress (strain) levels correspond to the points shown in load displacement loop.

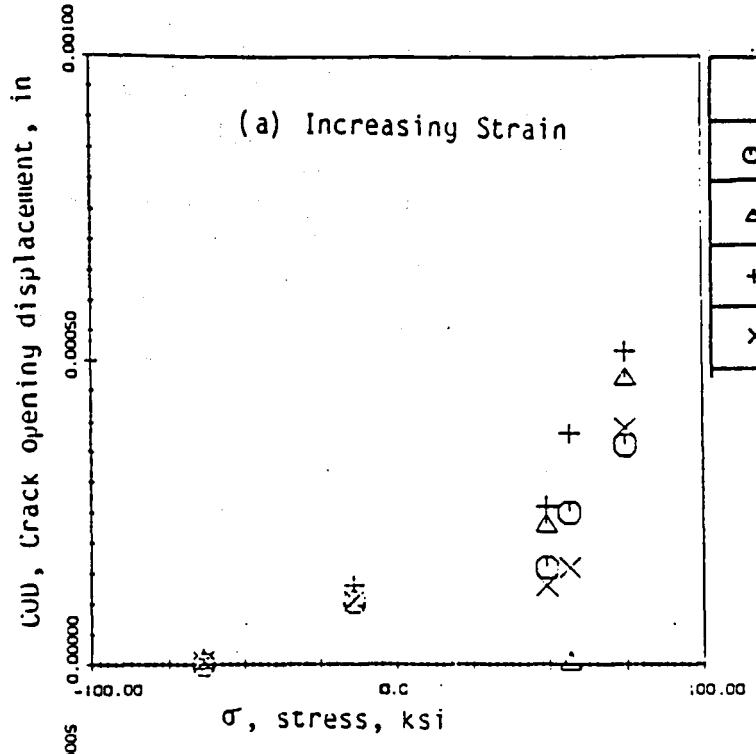


| | x(in) | x/2a |
|---|---|---|
| ⊙ | 0.0025 | 0.0694 |
| △ | 0.0062 | 0.1889 |
| + | 0.0246 | 0.6833 |
| × | 0.0288 | 0.8 |

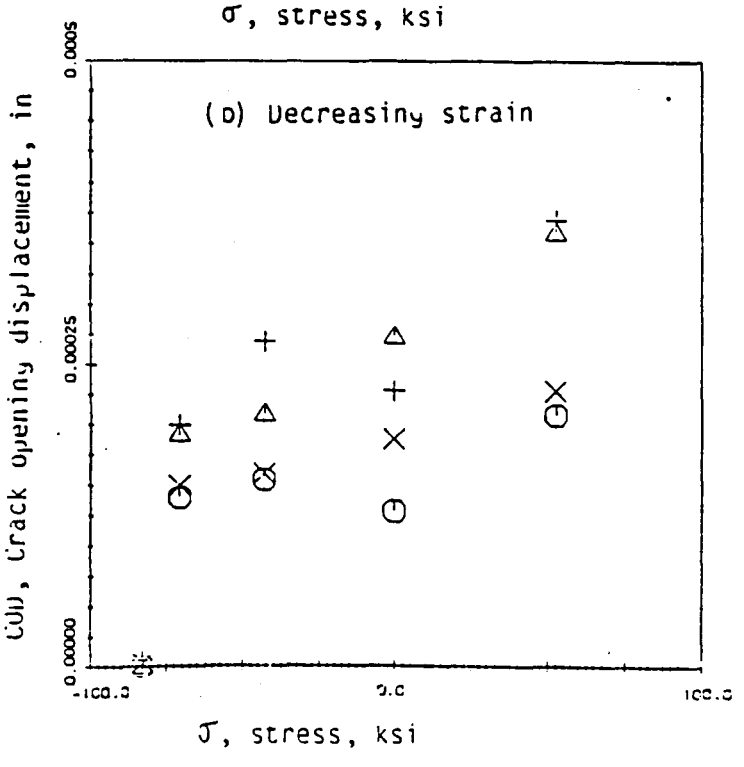


(c) Crack opening displacement as a function of stress at different points along the crack length during increasing and decreasing strain.

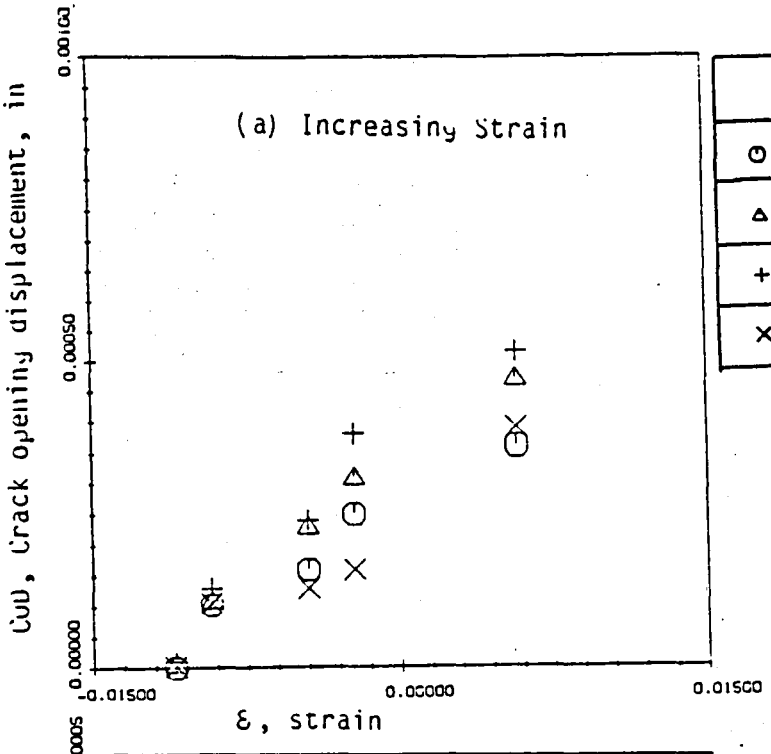


| | x(in) | x/2a |
|---|---|---|
| ○ | 0.0025 | 0.0694 |
| △ | 0.0062 | 0.1889 |
| + | 0.0246 | 0.6833 |
| × | 0.0288 | 0.8 |

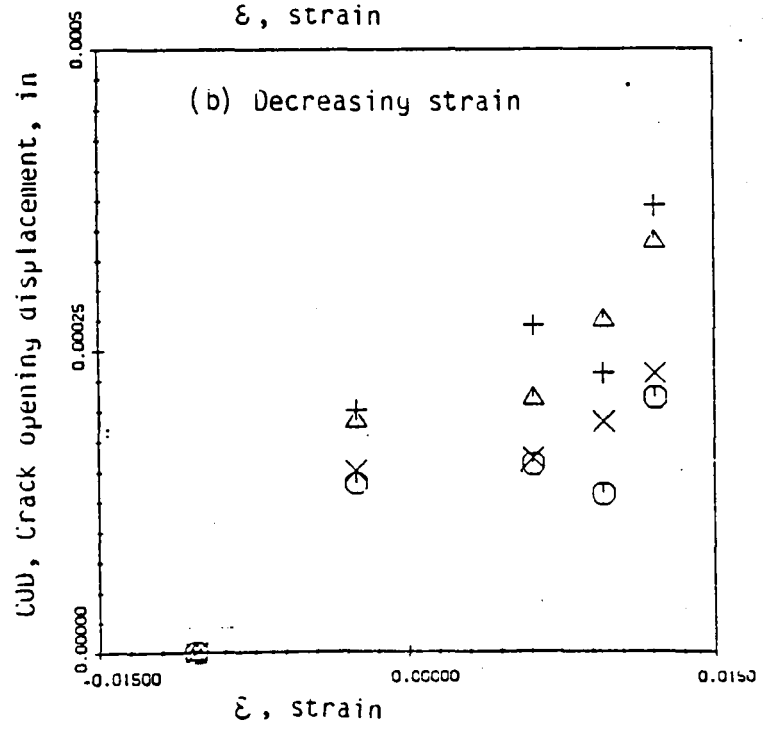


(a) Crack opening displacement as a function of strain at different points along the crack length during increasing and decreasing strain.

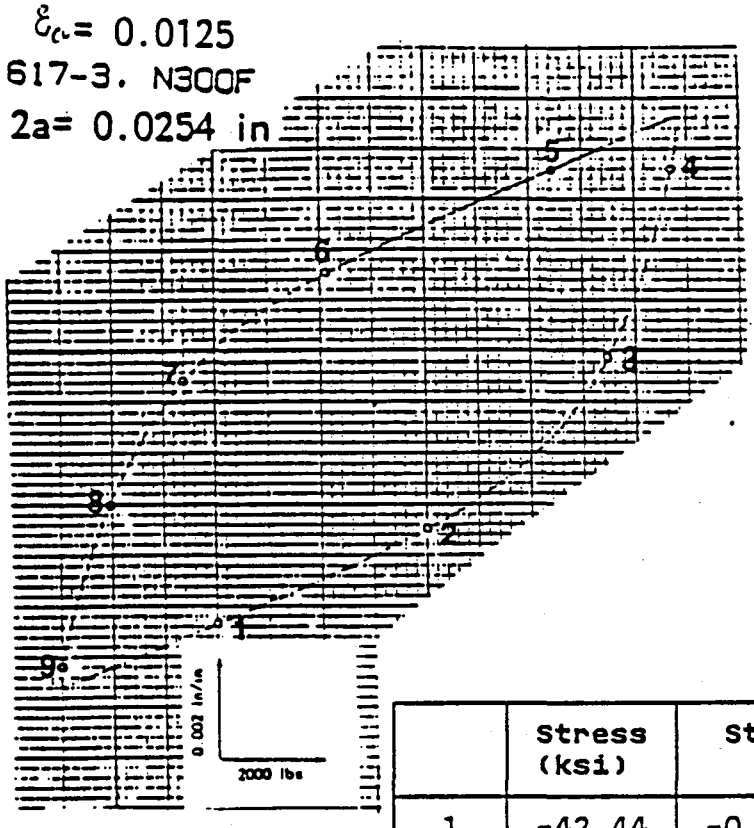


| | Stress (ksi) | Strain |
|---|---|---|
| 1 | -42.44 | -0.0105 |
| 2 | -14.14 | -0.0071 |
| 3 | 63.37 | -0.0046 |
| 4 | 81.06 | 0.0081 |
| 5 | 49.57 | 0.01125 |
| 6 | -11.88 | 0.0085 |
| 7 | -44.56 | 0.00545 |
| 8 | -71.58 | -0.00490 |
| 9 | -81.34 | -0.0115 |

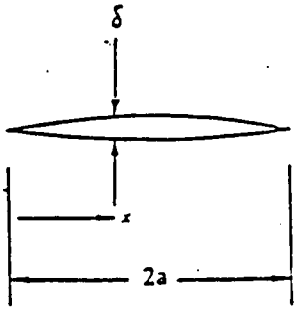


Fig. 25: Crack opening displacements measured in one complete cycle
(a) Load displacement loop as obtained from clip gauge mounted across the grip ends and the points (corresponding stress and strain levels shown in table) where closure observations were made.

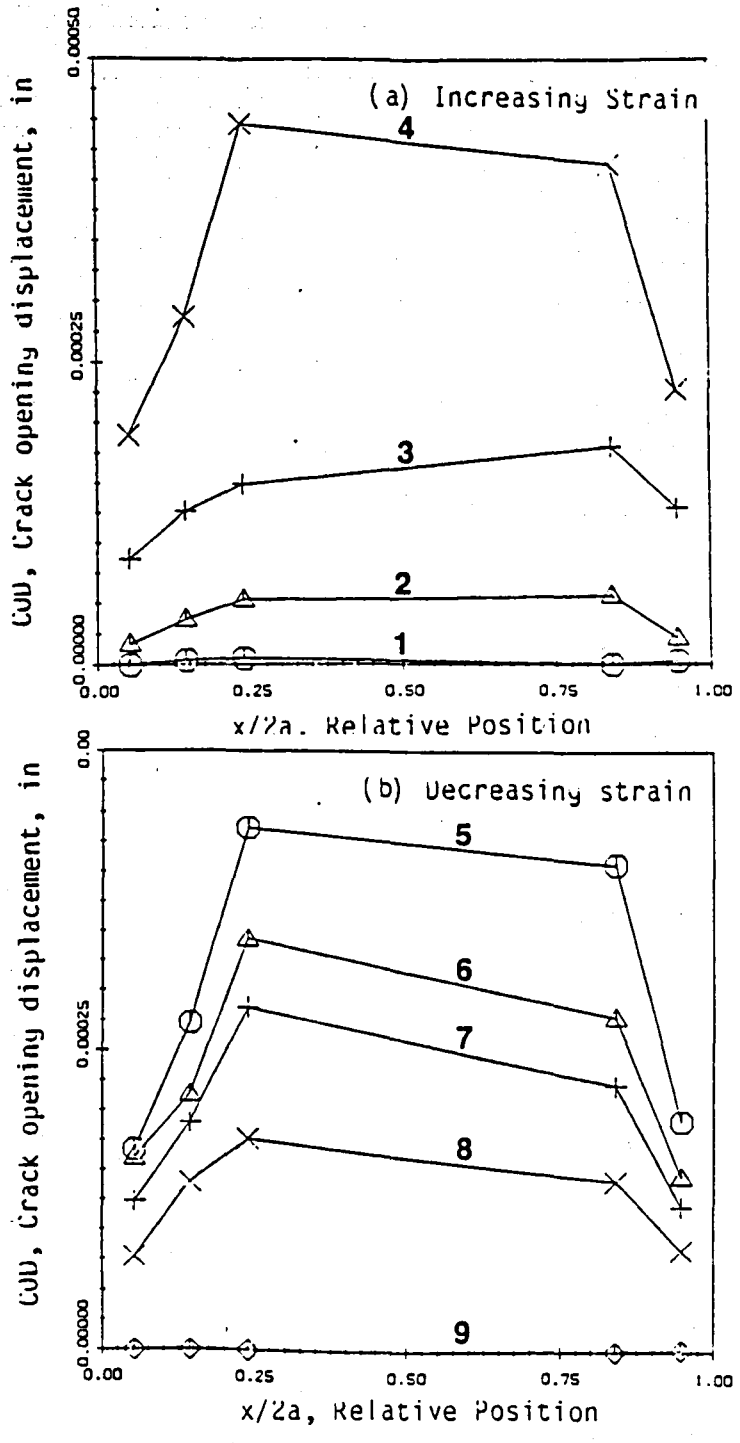


(b) Crack opening displacement during increasing (loading) and decreasing strain (unloading) at different points along the crack length. Different stress (strain) levels correspond to the points shown in load displacement loop.

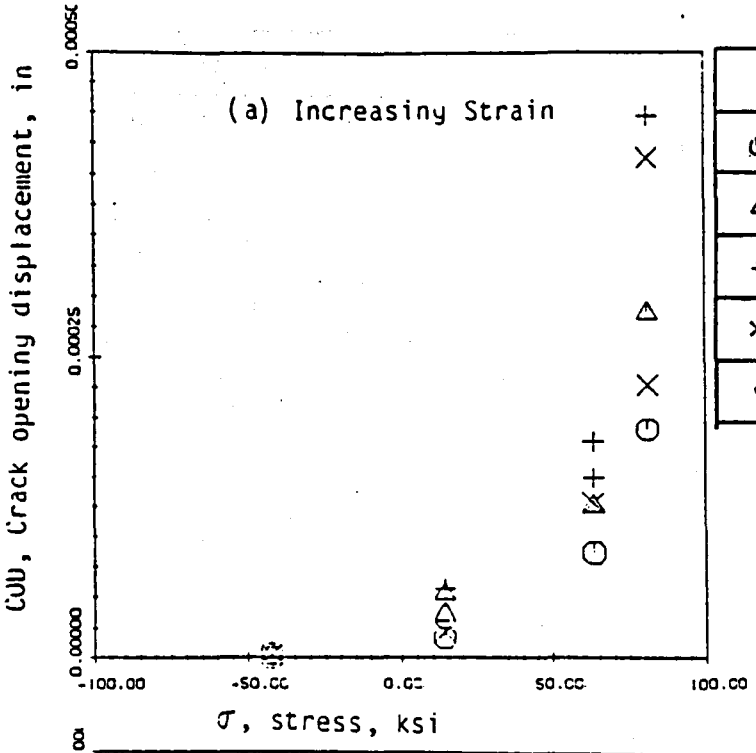


| | x(in) | x/2a |
|---|---|---|
| ⊙ | 0.00133 | 0.0523 |
| △ | 0.00366 | 0.1444 |
| + | 0.00606 | 0.2386 |
| × | 0.02133 | 0.8398 |
| ◇ | 0.02406 | 0.9472 |

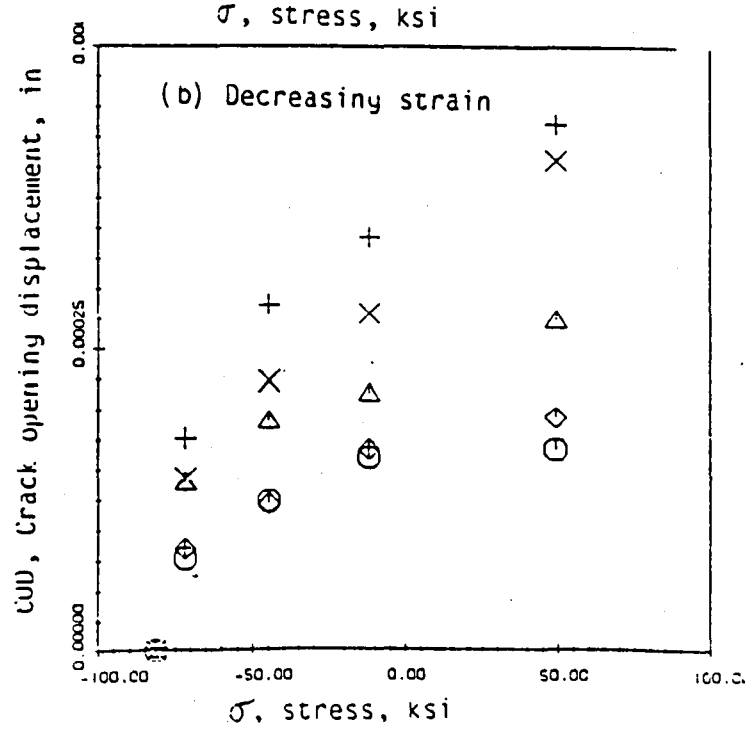


(c) Crack opening displacement as a function of stress at different points along the crack length during increasing and decreasing strain.

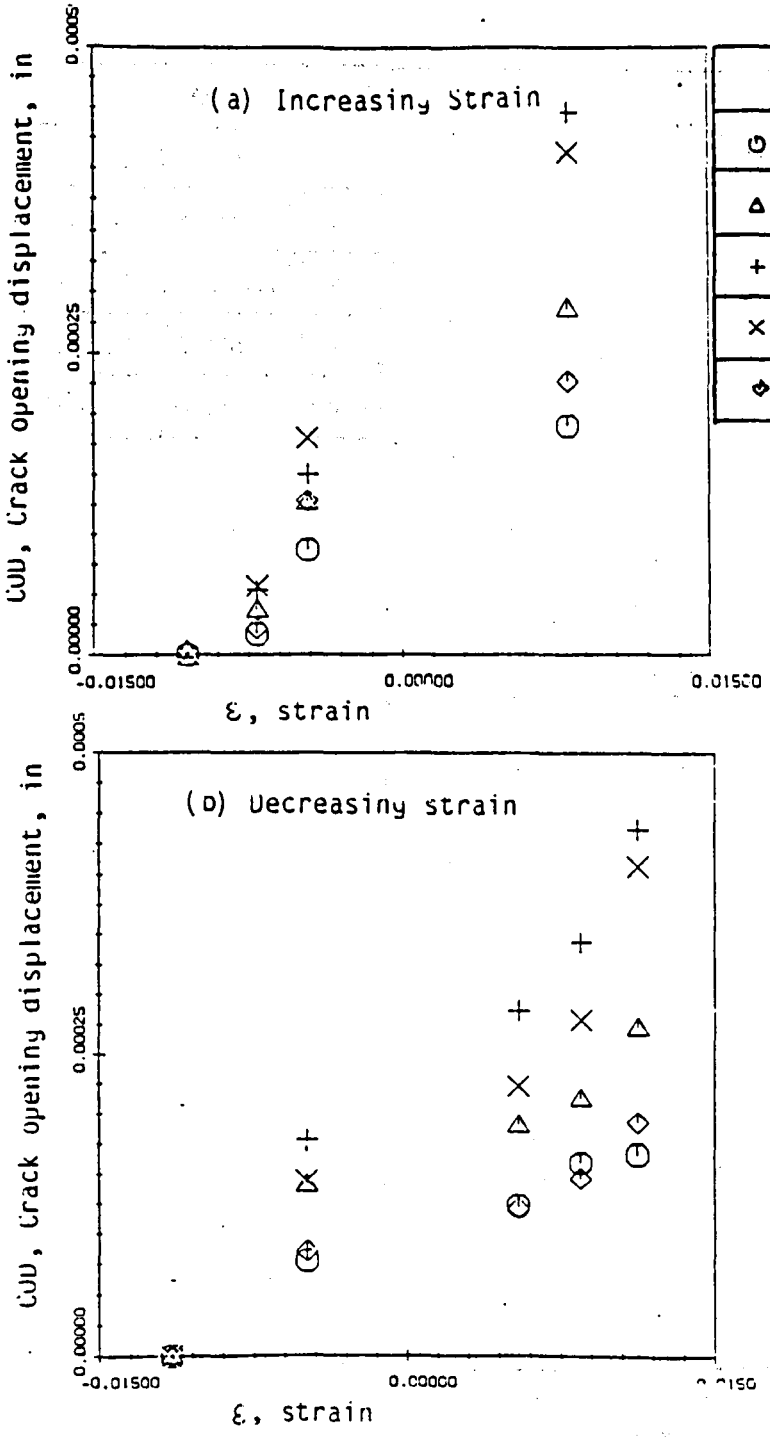


| | x(in) | x/2a |
|---|---|---|
| ⊙ | 0.00133 | 0.0523 |
| △ | 0.00366 | 0.1444 |
| + | 0.00606 | 0.2386 |
| × | 0.02133 | 0.8398 |
| ◇ | 0.02406 | 0.9472 |

(d) Crack opening displacement as a function of strain at different points along the crack length during increasing and decreasing strain.

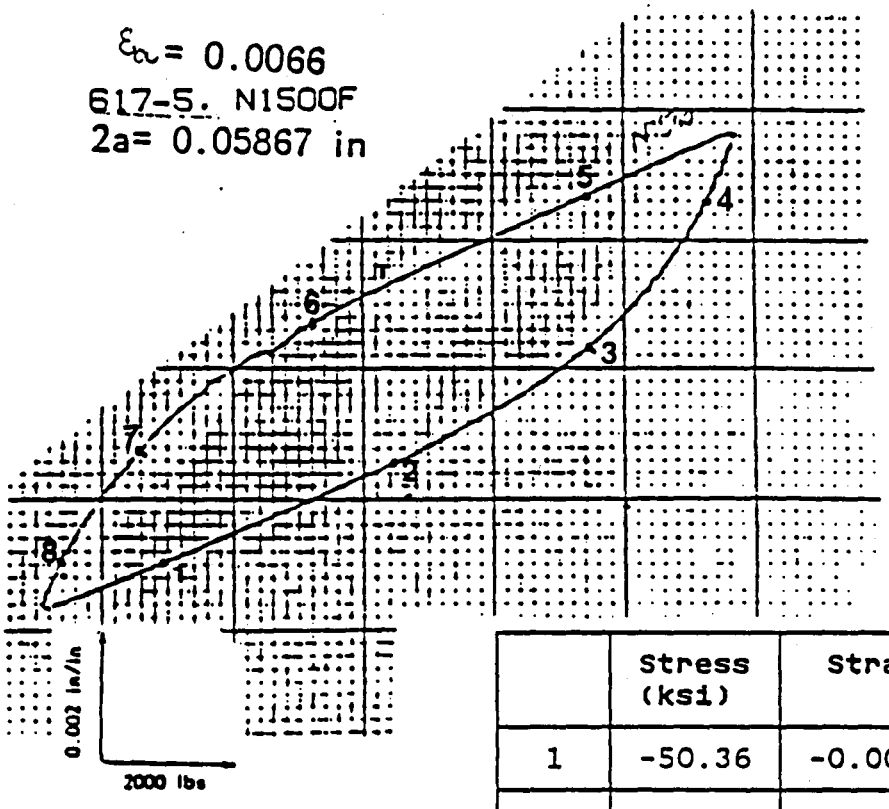


| | Stress (ksi) | Strain |
|---|---|---|
| 1 | -50.36 | -0.006 |
| 2 | 0.00 | -0.0043 |
| 3 | -42.58 | 0.0014 |
| 4 | 68.33 | 0.0038 |
| 5 | 42.44 | 0.006 |
| 6 | -17.40 | 0.0032 |
| 7 | -53.90 | -0.0009 |
| 8 | -71.02 | -0.0050 |

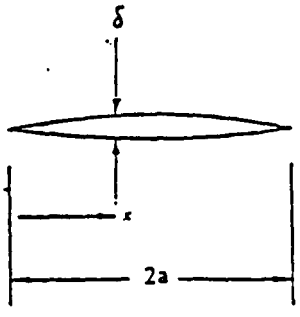


Fig. 26: Crack opening displacements measured in one complete cycle
(a) Load displacement loop as obtained from clip gauge mounted across the grip ends and the points (corresponding stress and strain levels shown in table) where closure observations were made.

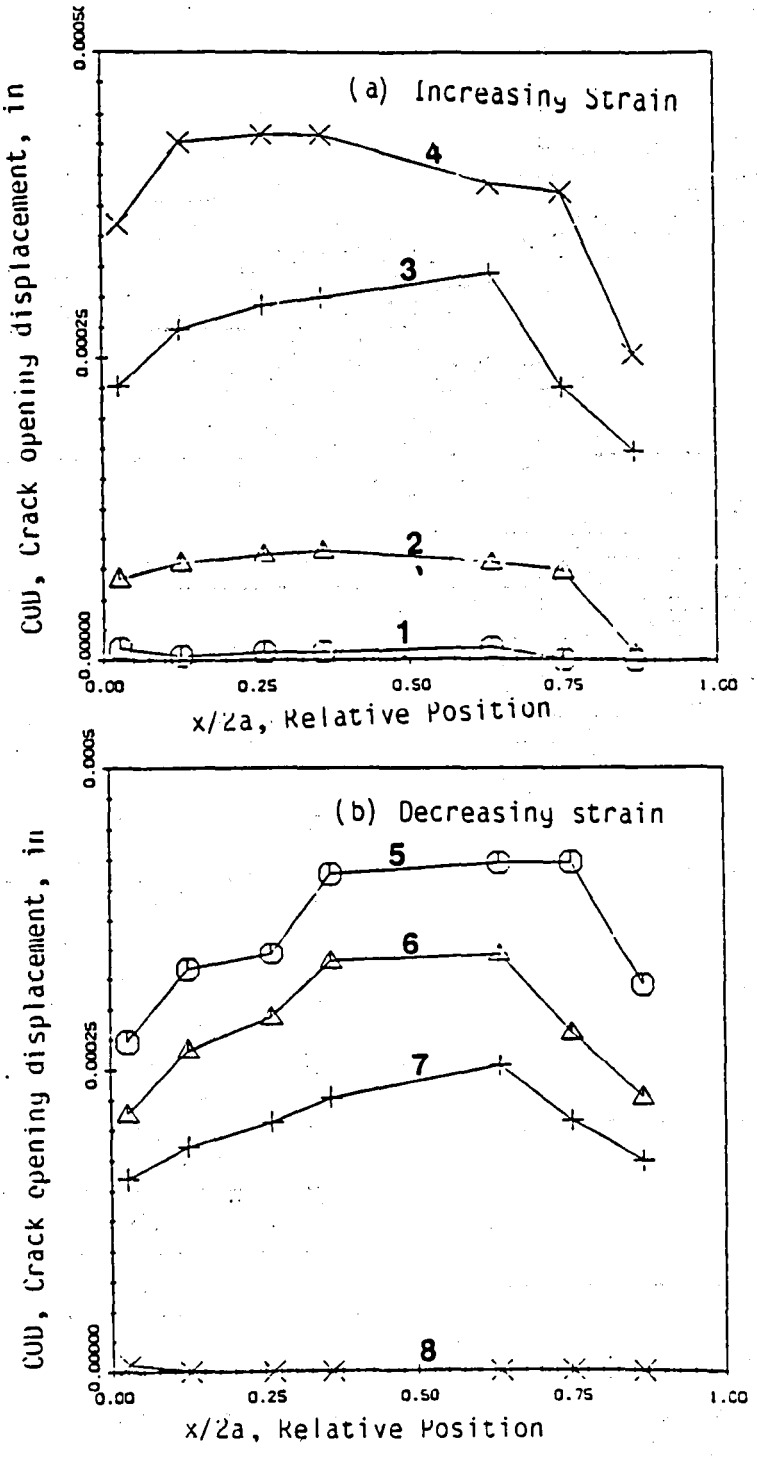


(b) Crack opening displacement during increasing (loading) and decreasing strain (unloading) at different points along the crack length. Different stress (strain) levels correspond to the points shown in load displacement loop.

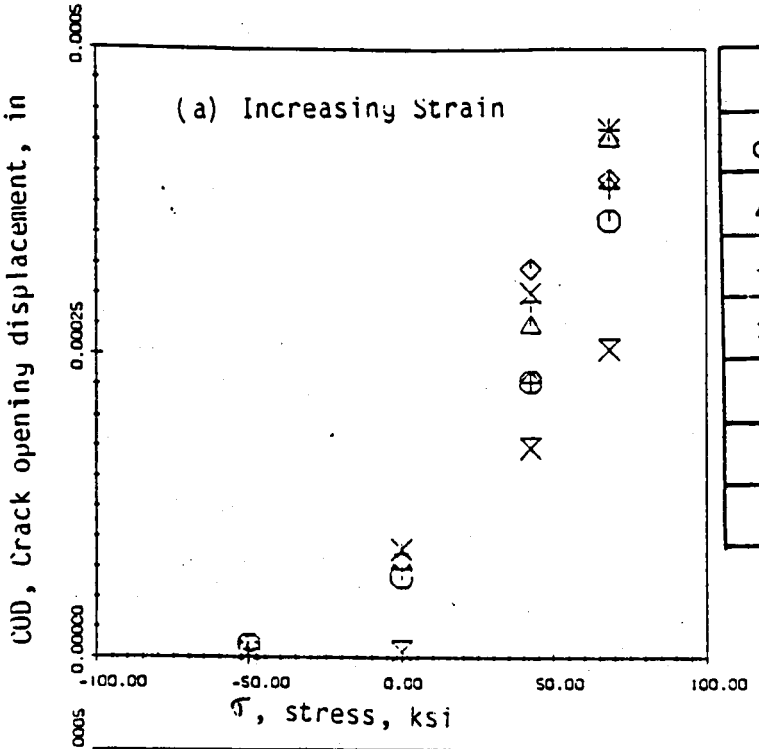


| | x(in) | x/2a |
|---|---|---|
| ⊙ | 0.0016 | 0.0272 |
| △ | 0.00746 | 0.1271 |
| + | 0.01546 | 0.2635 |
| × | 0.02106 | 0.3590 |
| ◇ | 0.0273 | 0.6357 |
| ✦ | 0.04413 | 0.7521 |
| ⧖ | 0.05093 | 0.8680 |

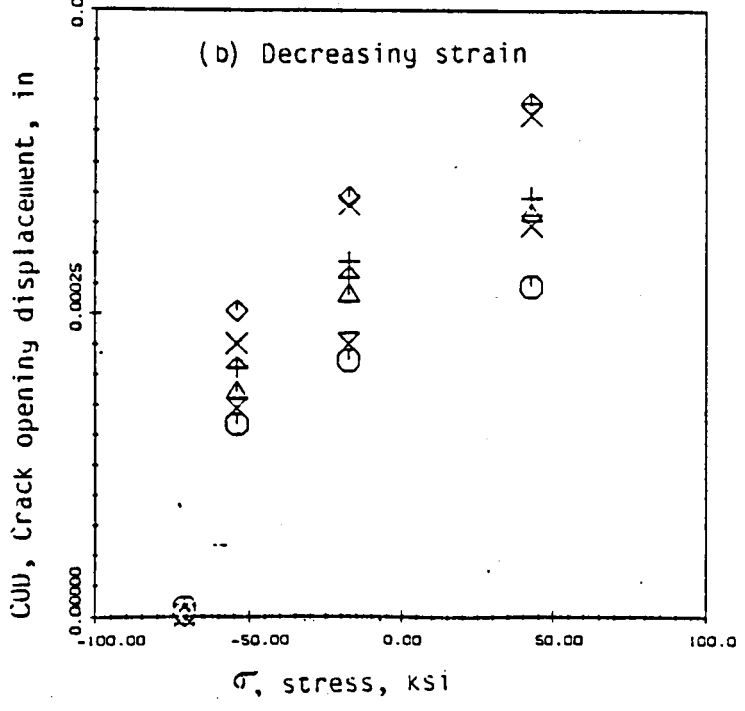


(c) Crack opening displacement as a function of stress at different points along the crack length during increasing and decreasing strain.

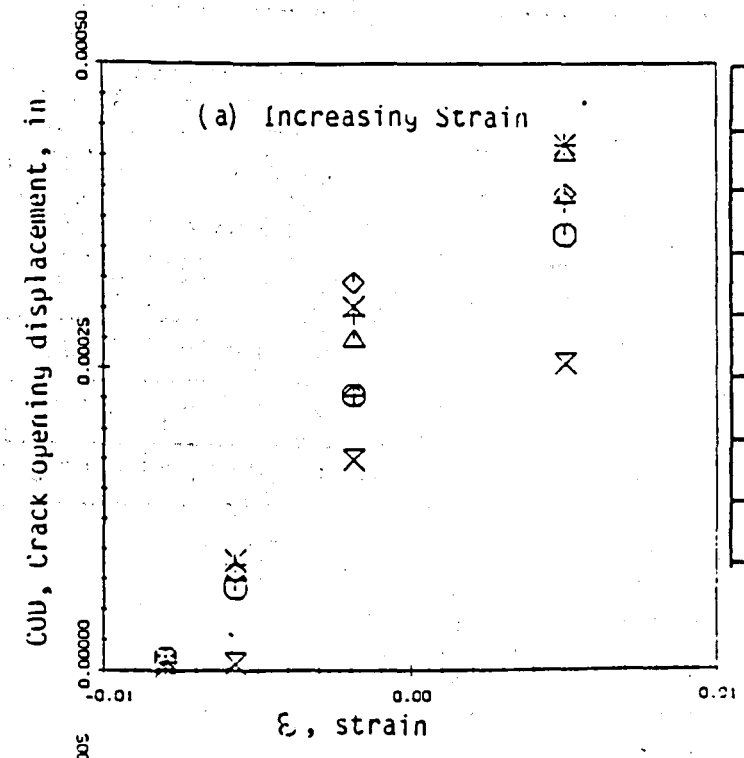


| | x(in) | x/2a |
|---|---|---|
| ○ | 0.0016 | 0.0272 |
| △ | 0.00746 | 0.1271 |
| + | 0.01546 | 0.2635 |
| × | 0.02106 | 0.3590 |
| ◇ | 0.0273 | 0.6357 |
| ✦ | 0.04413 | 0.7521 |
| ⧖ | 0.05093 | 0.8680 |

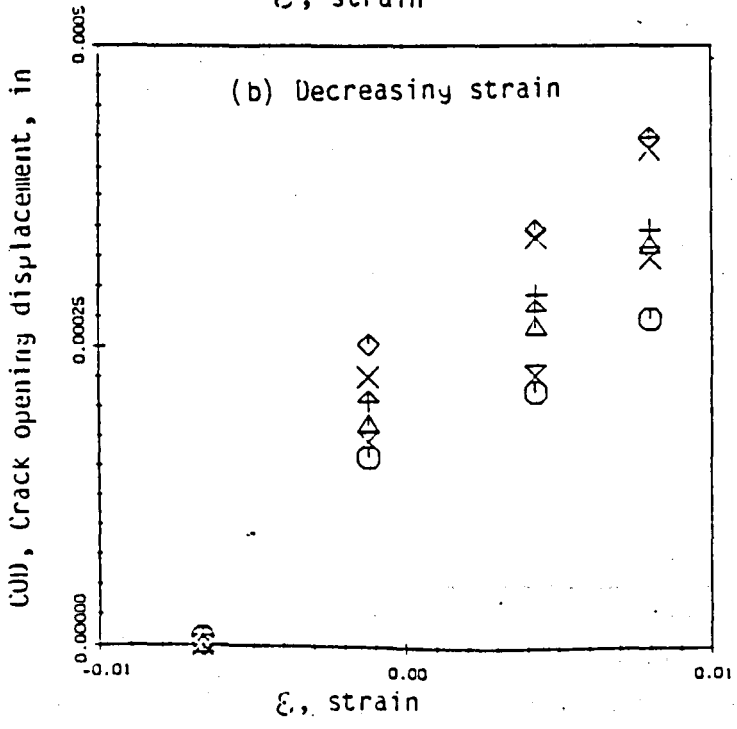


(d) Crack opening displacement as a function of strain at different points along the crack length during increasing and decreasing strain.

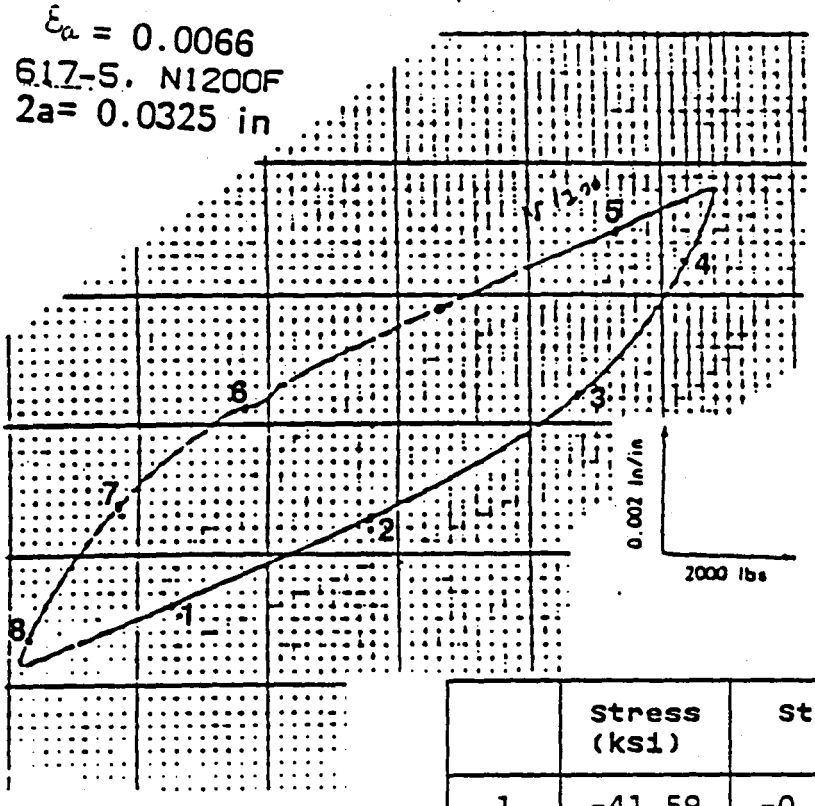


| | Stress (ksi) | Strain |
|---|---|---|
| 1 | -41.59 | -0.0058 |
| 2 | - 0.28 | -0.004 |
| 3 | 44.13 | -0.0011 |
| 4 | 66.33 | 0.0037 |
| 5 | 54.06 | 0.0061 |
| 6 | -27.30 | 0.00246 |
| 7 | -54.60 | -0.00052 |
| 8 | -74.27 | -0.005 |

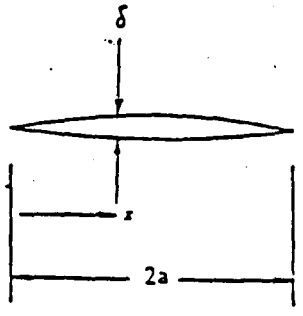


Fig. 27: Crack opening displacements measured in one complete cycle
(a) Load displacement loop as obtained from clip gauge mounted across the grip ends and the points (corresponding stress and strain levels shown in table) where closure observations were made.

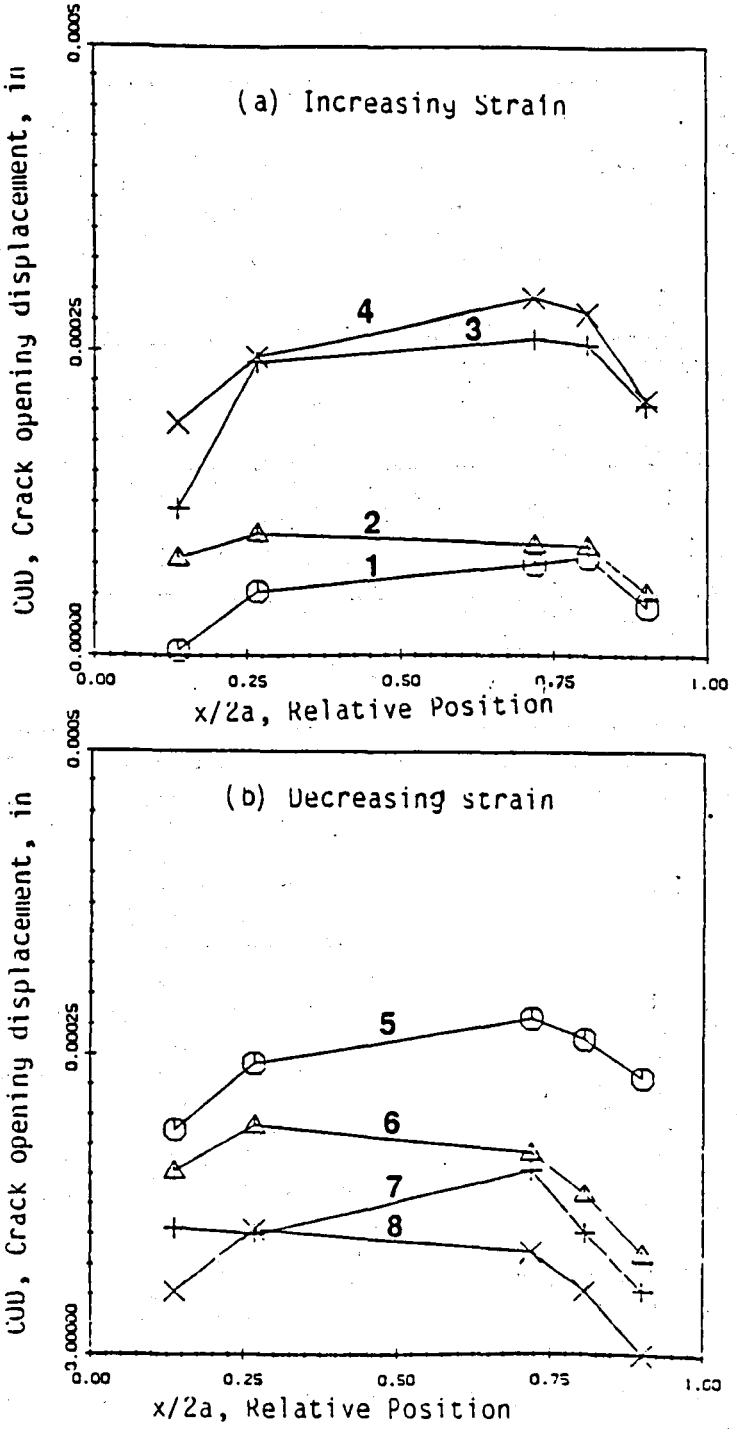


(b) Crack opening displacement during increasing (loading) and decreasing strain (unloading) at different points along the crack length. Different stress (strain) levels correspond to the points shown in load displacement loop.

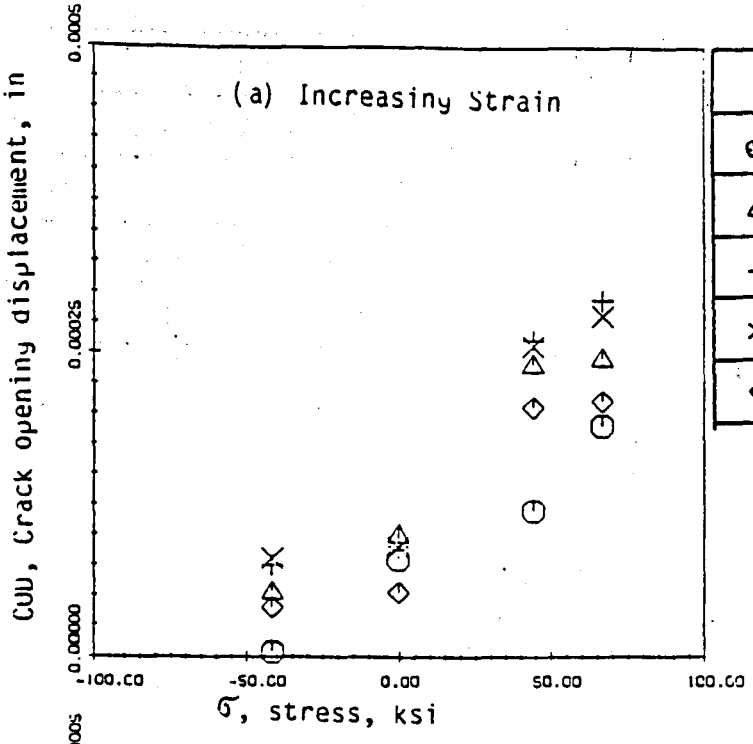


| | x(in) | x/2a |
|---|---|---|
| ⊙ | 0.0045 | 0.1384 |
| △ | 0.0087 | 0.2673 |
| + | 0.0234 | 0.72 |
| × | 0.0262 | 0.806 |
| ◇ | 0.02935 | 0.9015 |

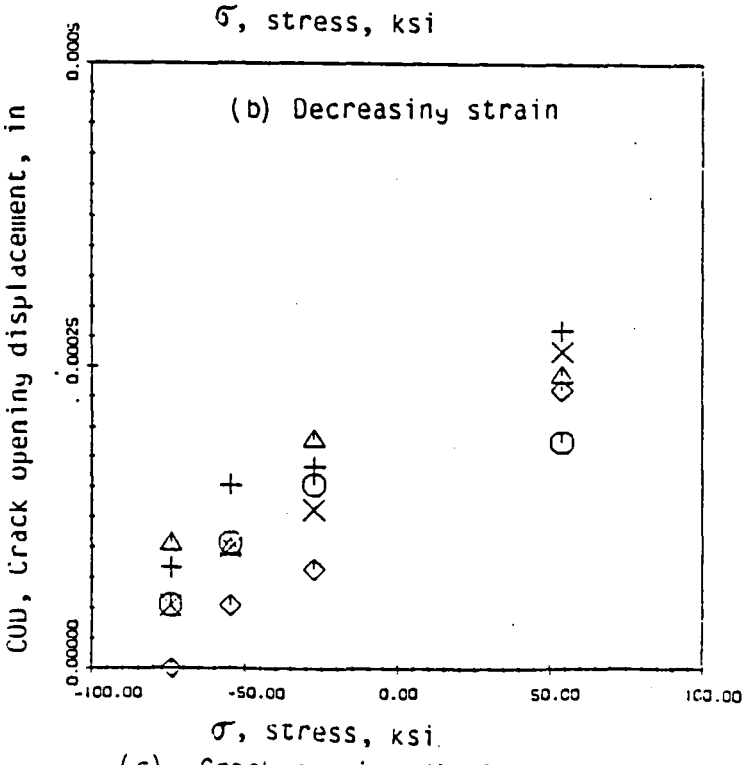


(c) Crack opening displacement as a function of stress at different points along the crack length during increasing and decreasing strain.

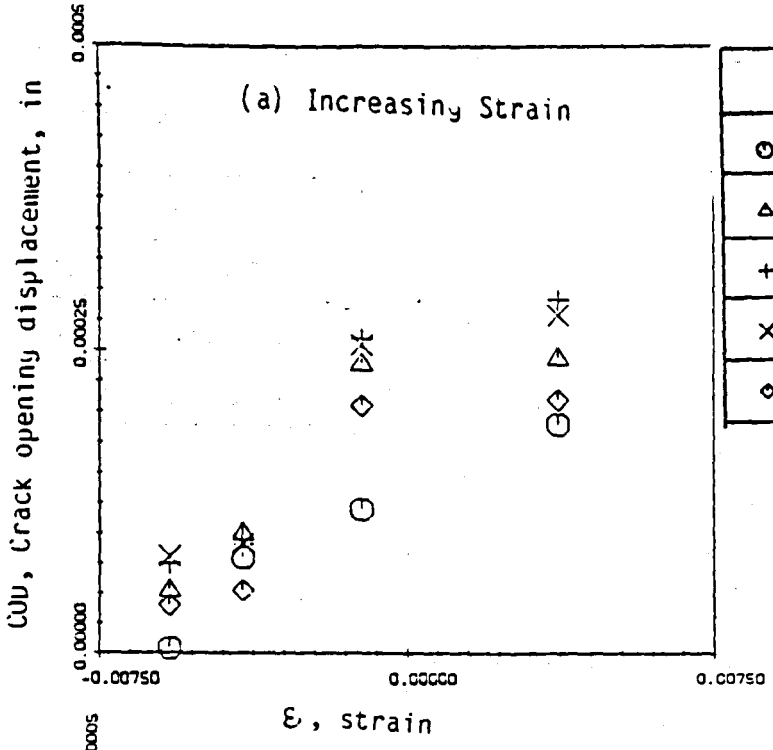


| | x(in) | x/2a |
|---|---|---|
| ⊙ | 0.0045 | 0.1384 |
| △ | 0.0087 | 0.2673 |
| + | 0.0234 | 0.72 |
| × | 0.0262 | 0.806 |
| ◇ | 0.02935 | 0.9015 |

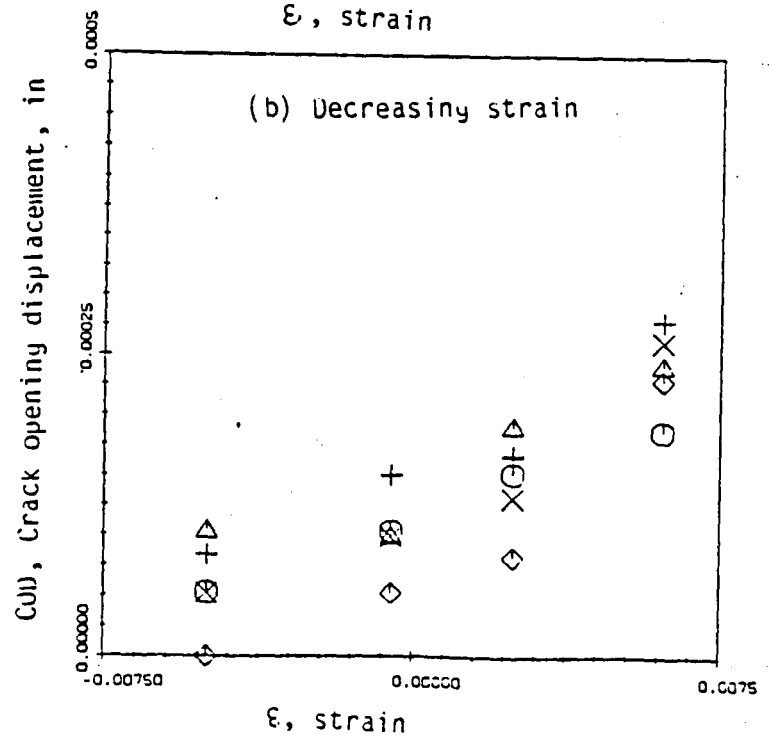


(d) Crack opening displacement as a function of strain at different points along the crack length during increasing and decreasing strain.

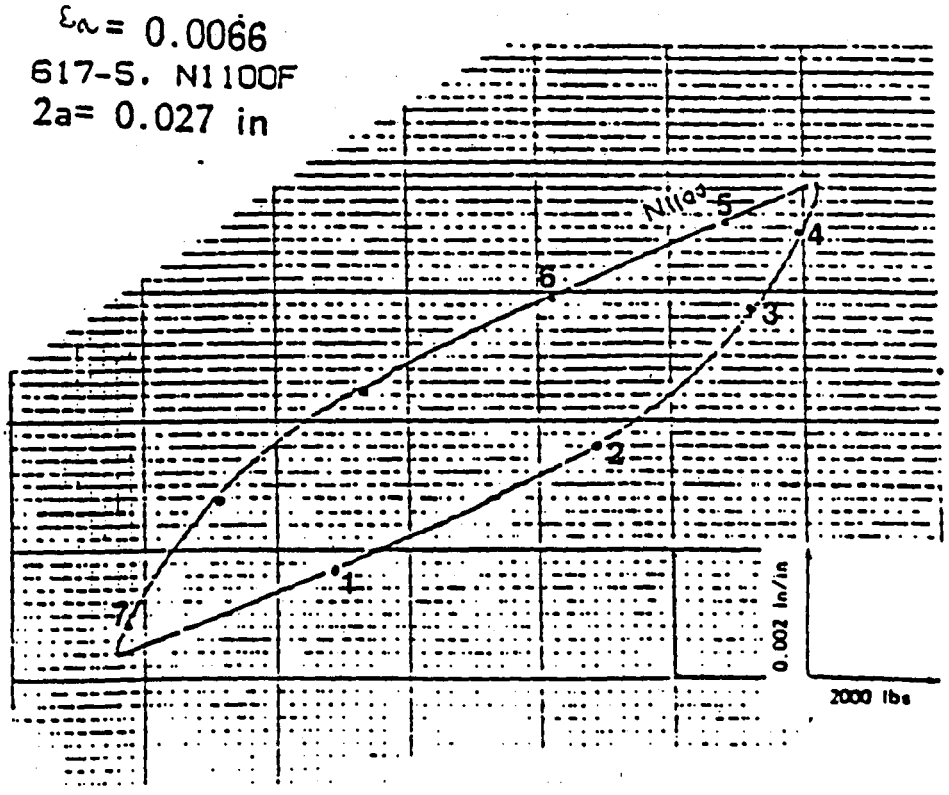


| | Stress (ksi) | Strain |
|---|---|---|
| 1 | -29.42 | -0.0052 |
| 2 | 26.59 | -0.0027 |
| 3 | 58.71 | 0.0009 |
| 4 | 69.03 | 0.0036 |
| 5 | 55.17 | 0.006 |
| 6 | 17.83 | 0.0032 |
| 7 | -72.85 | -0.0047 |

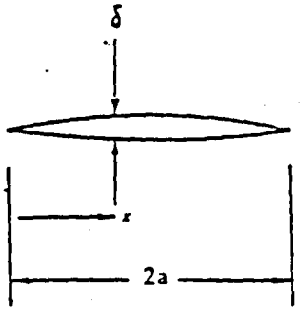


Fig. 28: Crack opening displacements measured in one complete cycle
(a) Load displacement loop as obtained from clip gauge mounted across the grip ends and the points (corresponding stress and strain levels shown in table) where closure observations were made.

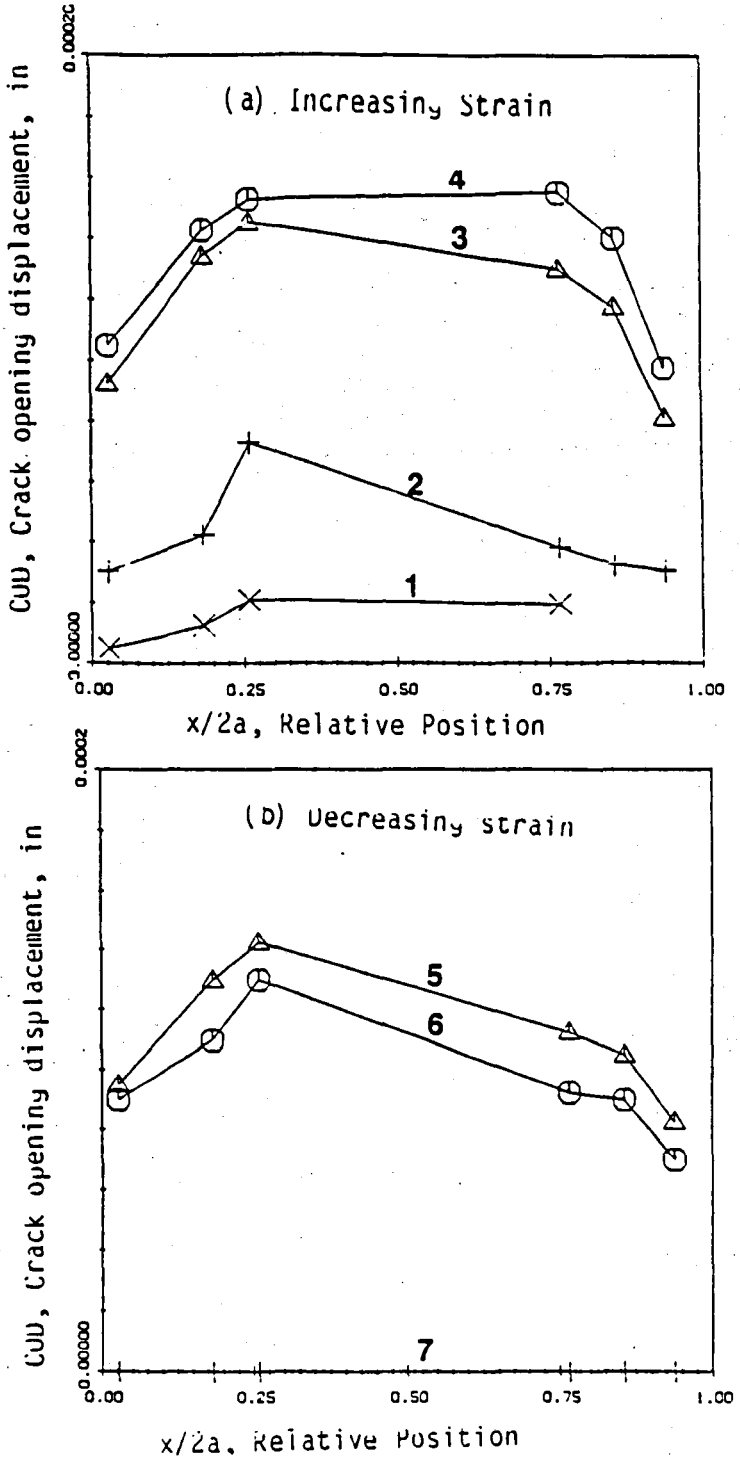


(b) Crack opening displacement during increasing (loading) and decreasing strain (unloading) at different points along the crack length. Different stress (strain) levels correspond to the points shown in load displacement loop.

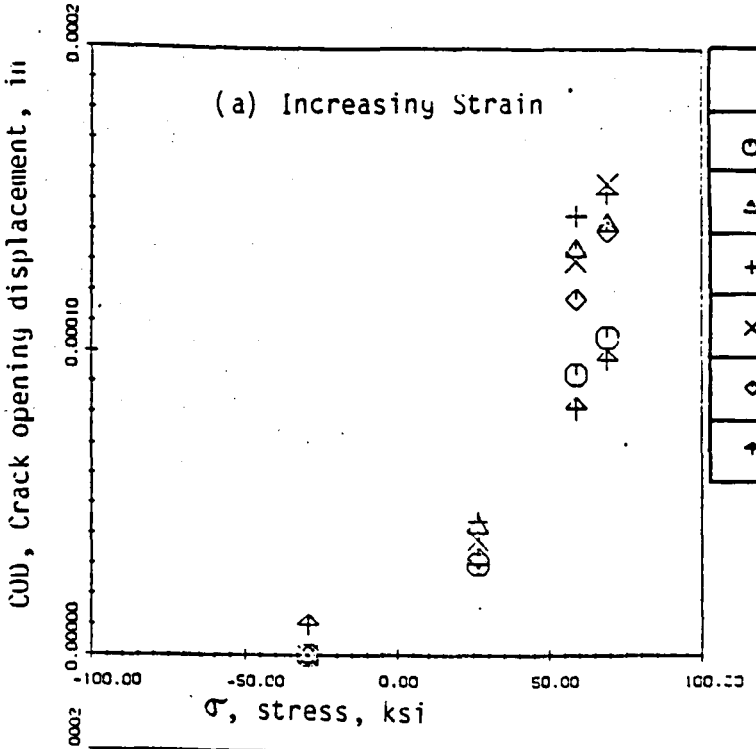


| | x(in) | x/2a |
|---|---|---|
| ⊖ | 0.002 | 0.0278 |
| △ | 0.0051 | 0.1834 |
| + | 0.0072 | 0.2589 |
| × | 0.0213 | 0.7661 |
| ◇ | 0.0238 | 0.8581 |
| ↑ | 0.0261 | 0.9382 |

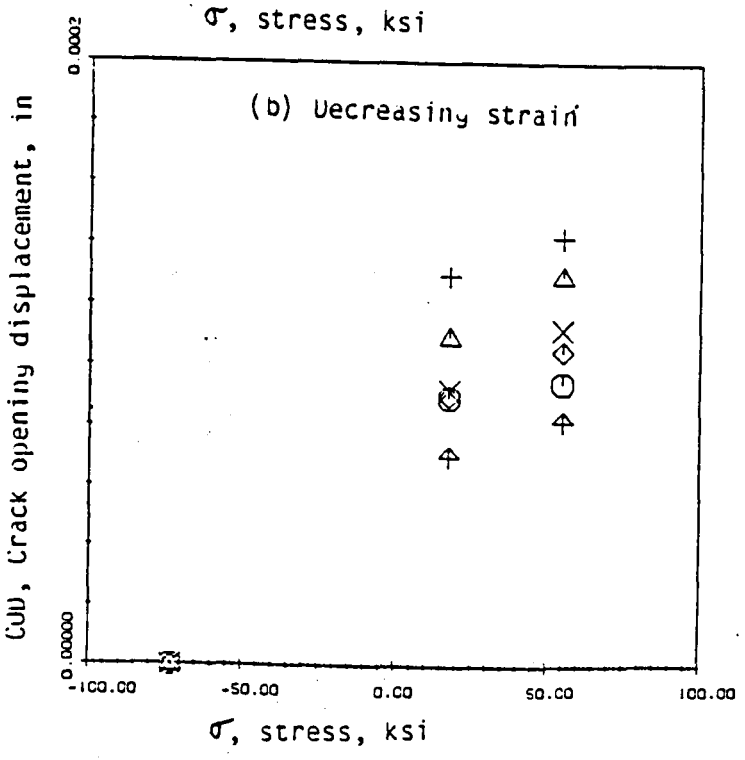


(c) Crack opening displacement as a function of stress at different points along the crack length during increasing and decreasing strain.

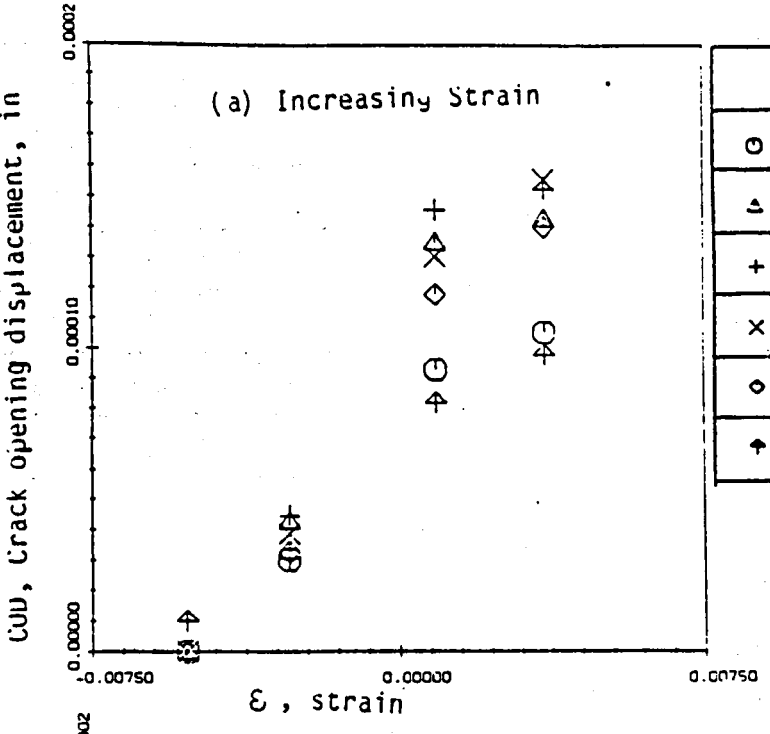


| | x(in) | x/2a |
|---|---|---|
| ○ | 0.002 | 0.0278 |
| △ | 0.0051 | 0.1834 |
| + | 0.0072 | 0.2589 |
| × | 0.0213 | 0.7661 |
| ◇ | 0.0238 | 0.8581 |
| ↑ | 0.0261 | 0.9382 |

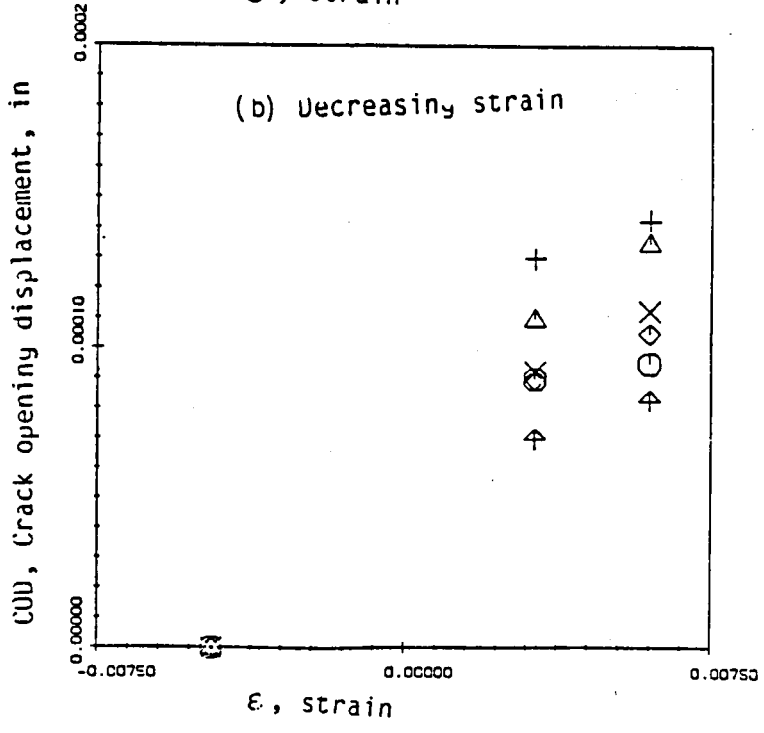


(a) Crack opening displacement as a function of strain at different points along the crack length during increasing and decreasing strain.

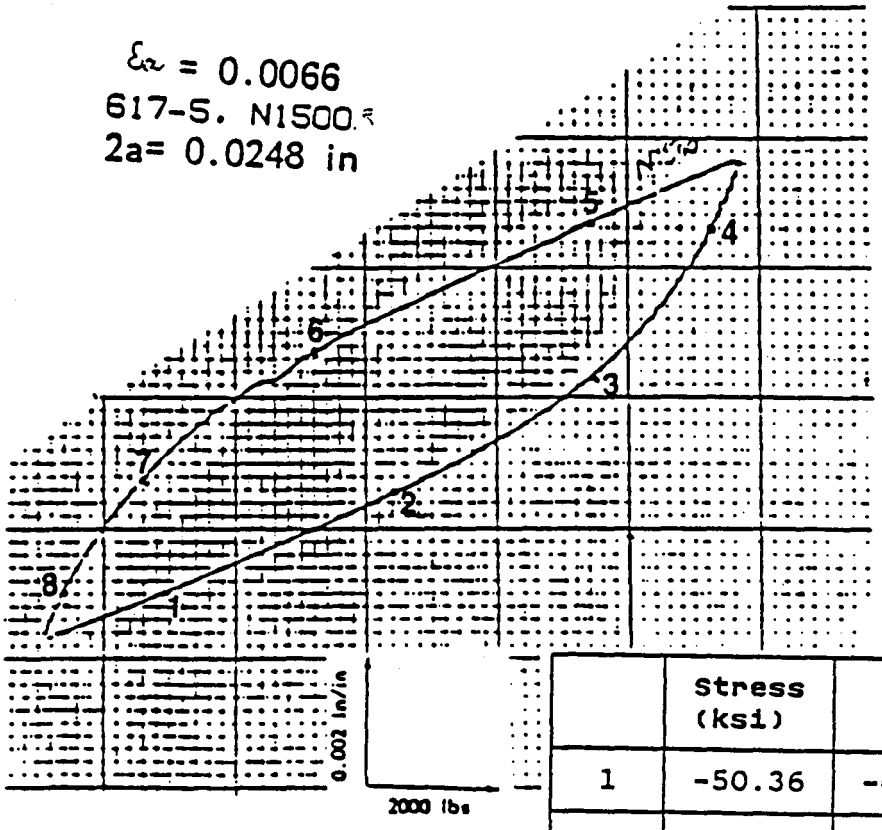


| | Stress (ksi) | Strain |
|---|---|---|
| 1 | -50.36 | -0.006 |
| 2 | 0.00 | -0.0043 |
| 3 | +42.58 | 0.0014 |
| 4 | 68.33 | 0.0038 |
| 5 | 42.44 | 0.006 |
| 6 | -17.40 | 0.0032 |
| 7 | -53.90 | -0.0009 |
| 8 | -71.02 | -0.0050 |

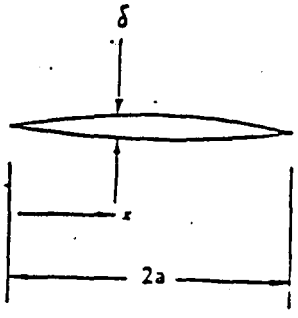


Fig. 29: Crack opening displacements measured in one complete cycle
(a) Load displacement loop as obtained from clip gauge mounted across the grip ends and the points (corresponding stress and strain levels shown in table) where closure observations were made.

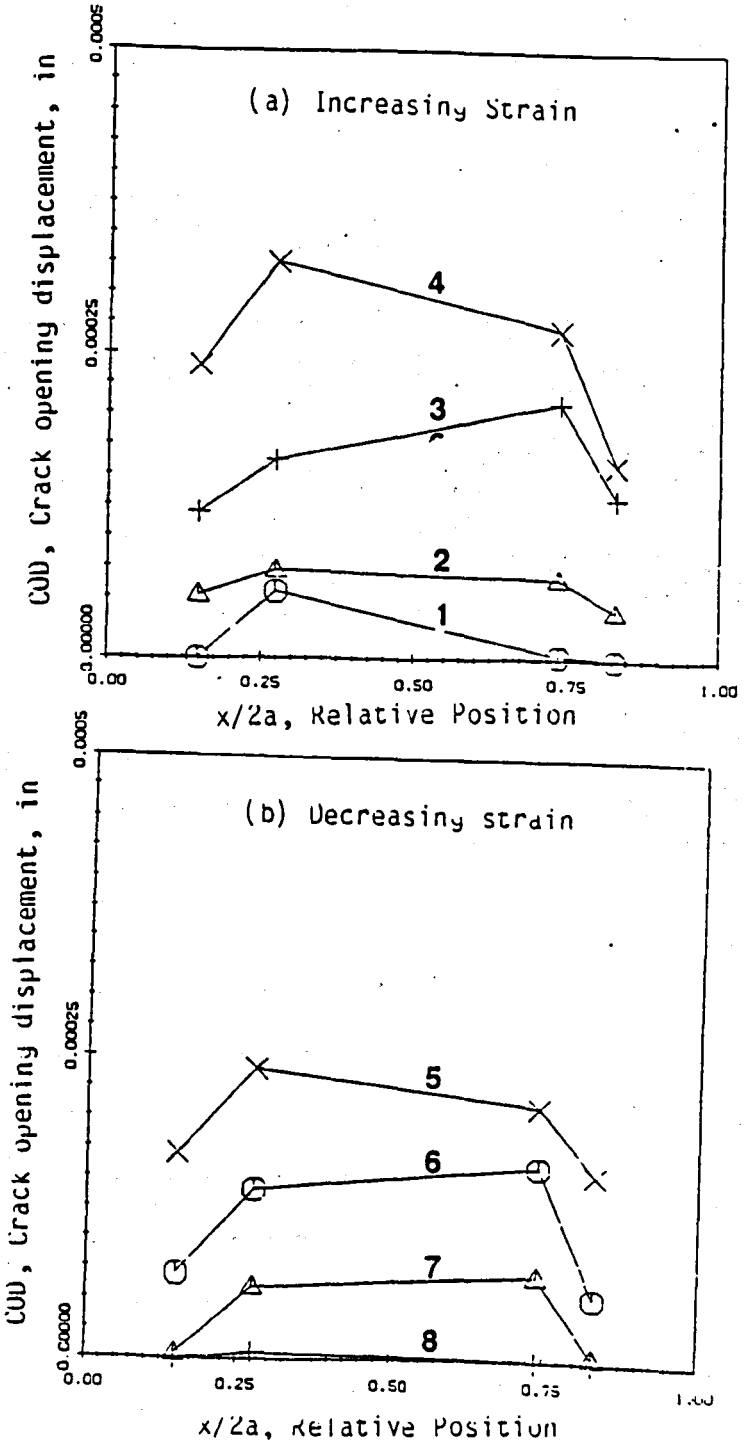


(b) Crack opening displacement during increasing (loading) and decreasing strain (unloading) at different points along the crack length. Different stress (strain) levels correspond to the points shown in load displacement loop.

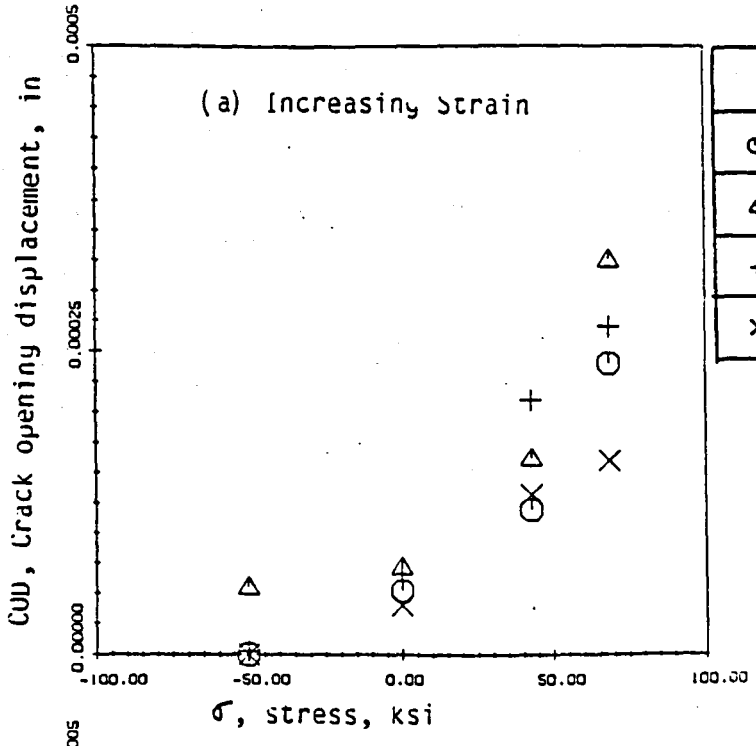


| | x(in) | x/2a |
|---|---|---|
| ⊙ | 0.0037 | 0.1491 |
| △ | 0.0062 | 0.2742 |
| + | 0.0183 | 0.7379 |
| × | 0.0206 | 0.8306 |

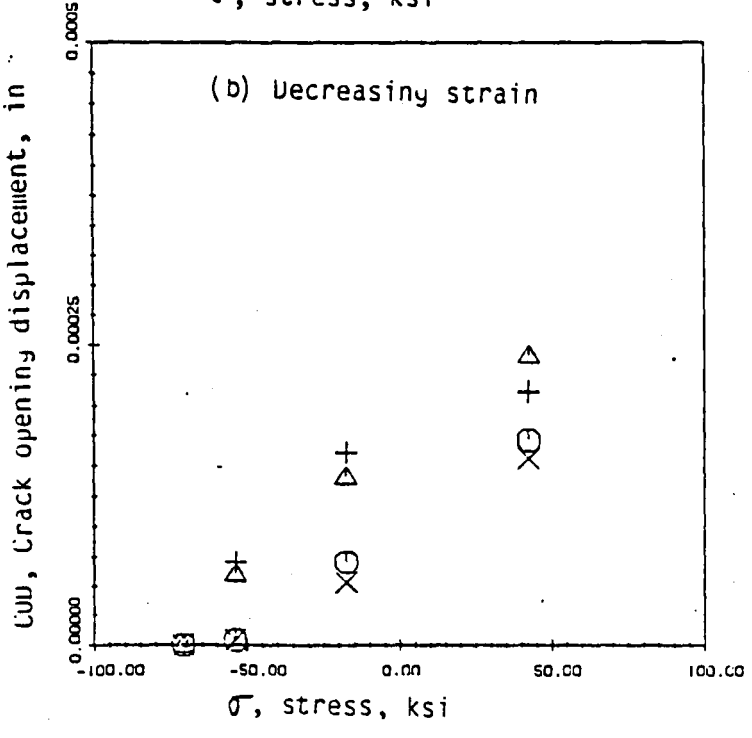


(c) Crack opening displacement as a function of stress at different points along the crack length during increasing and decreasing strain.

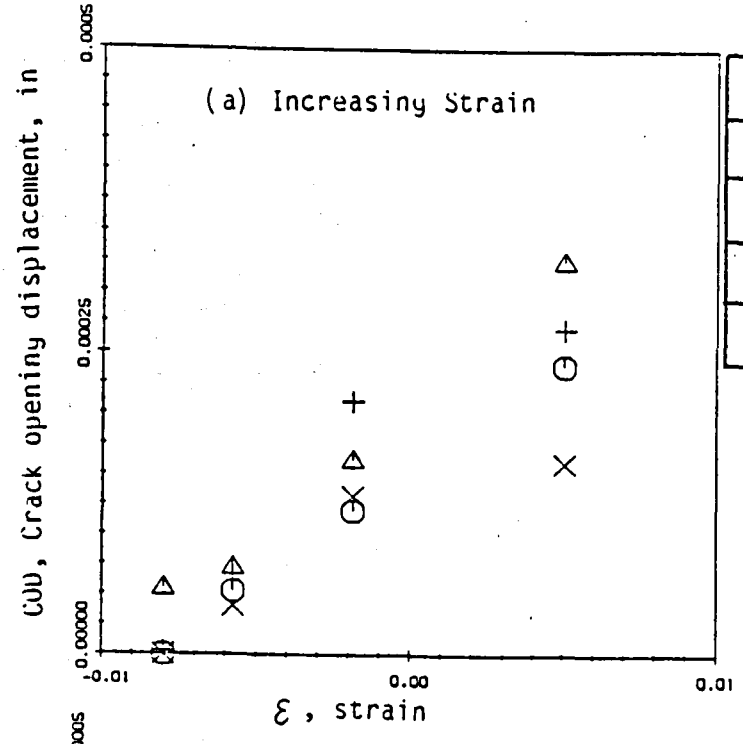


| | x(in) | x/2a |
|---|---|---|
| ⊙ | 0.0037 | 0.1491 |
| △ | 0.0062 | 0.2742 |
| + | 0.0183 | 0.7379 |
| × | 0.0206 | 0.8306 |

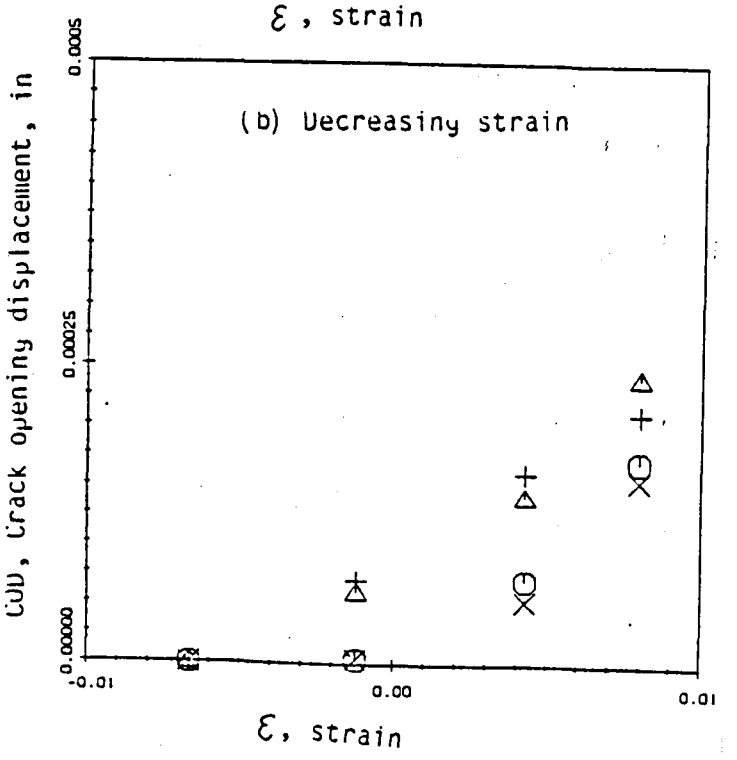


(d) Crack opening displacement as a function of strain at different points along the crack length during increasing and decreasing strain.

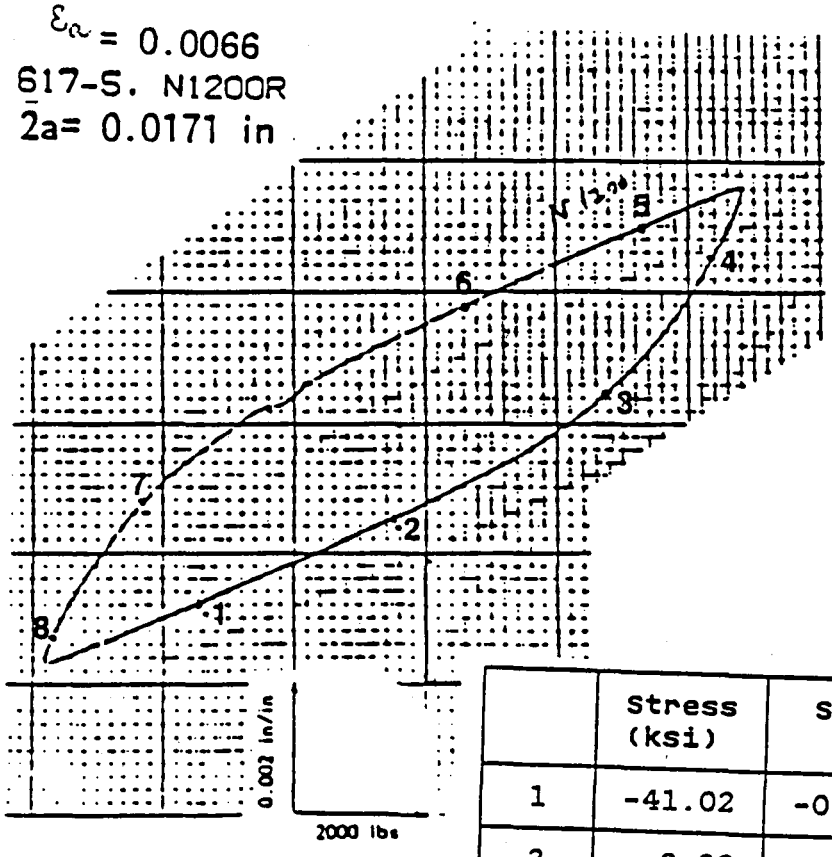


| | Stress (ksi) | Strain |
|---|---|---|
| 1 | -41.02 | -0.0058 |
| 2 | - 0.28 | -0.004 |
| 3 | 44.13 | -0.0011 |
| 4 | 66.33 | 0.0037 |
| 5 | 52.48 | 0.0061 |
| 6 | 14.71 | 0.00464 |
| 7 | -54.60 | -0.00052 |
| 8 | -74.27 | -0.005 |

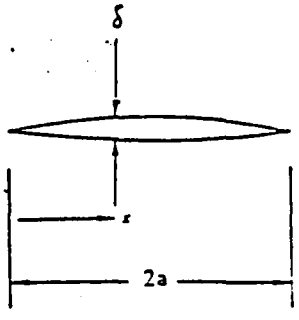


Fig. 30: Crack opening displacements measured in one complete cycle
(a) Load displacement loop as obtained from clip gauge mounted across the grip ends and the points (corresponding stress and strain levels shown in table) where closure observations were made.

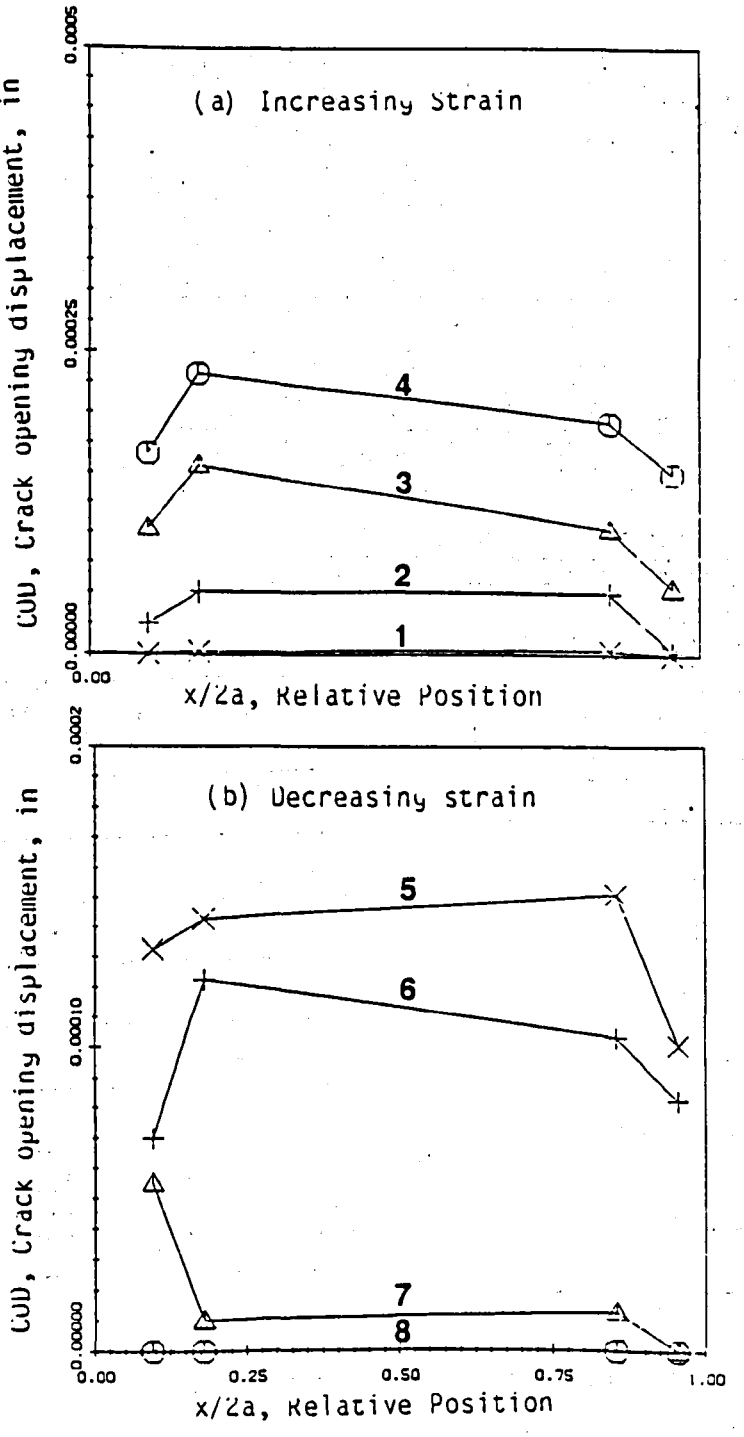


(b) Crack opening disolacement during increasing (loading) and decreasing strain (unloading) at different points along the crack length. Different stress (strain) levels correspond to the points shown in load displacement loop.

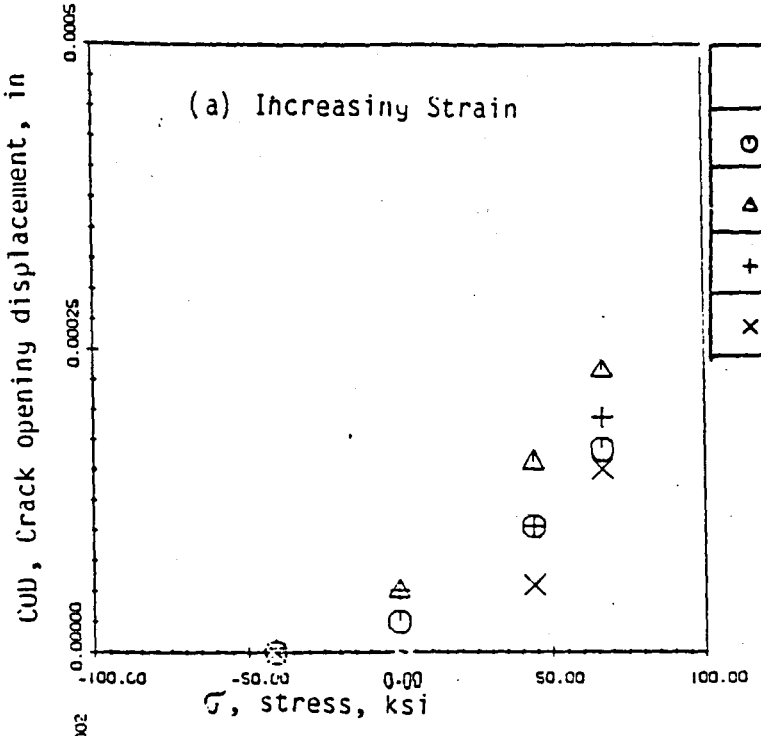


| | x(in) | x/2a |
|---|---|---|
| ⊙ | 0.0017 | 0.0955 |
| △ | 0.0032 | 0.1797 |
| + | 0.0152 | 0.8539 |
| × | 0.0171 | 0.955 |

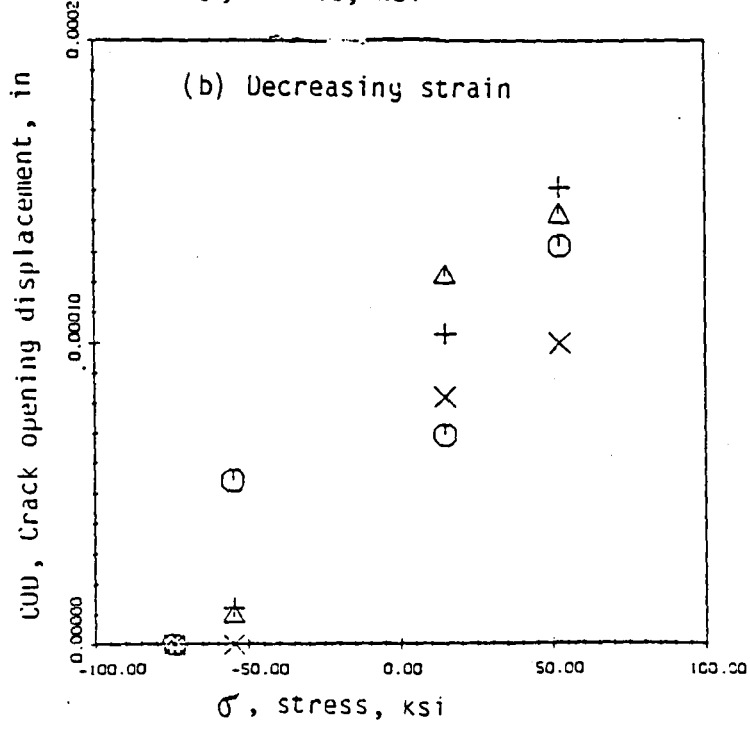


(c) Crack opening displacement as a function of stress at different points along the crack length during increasing and decreasing strain.

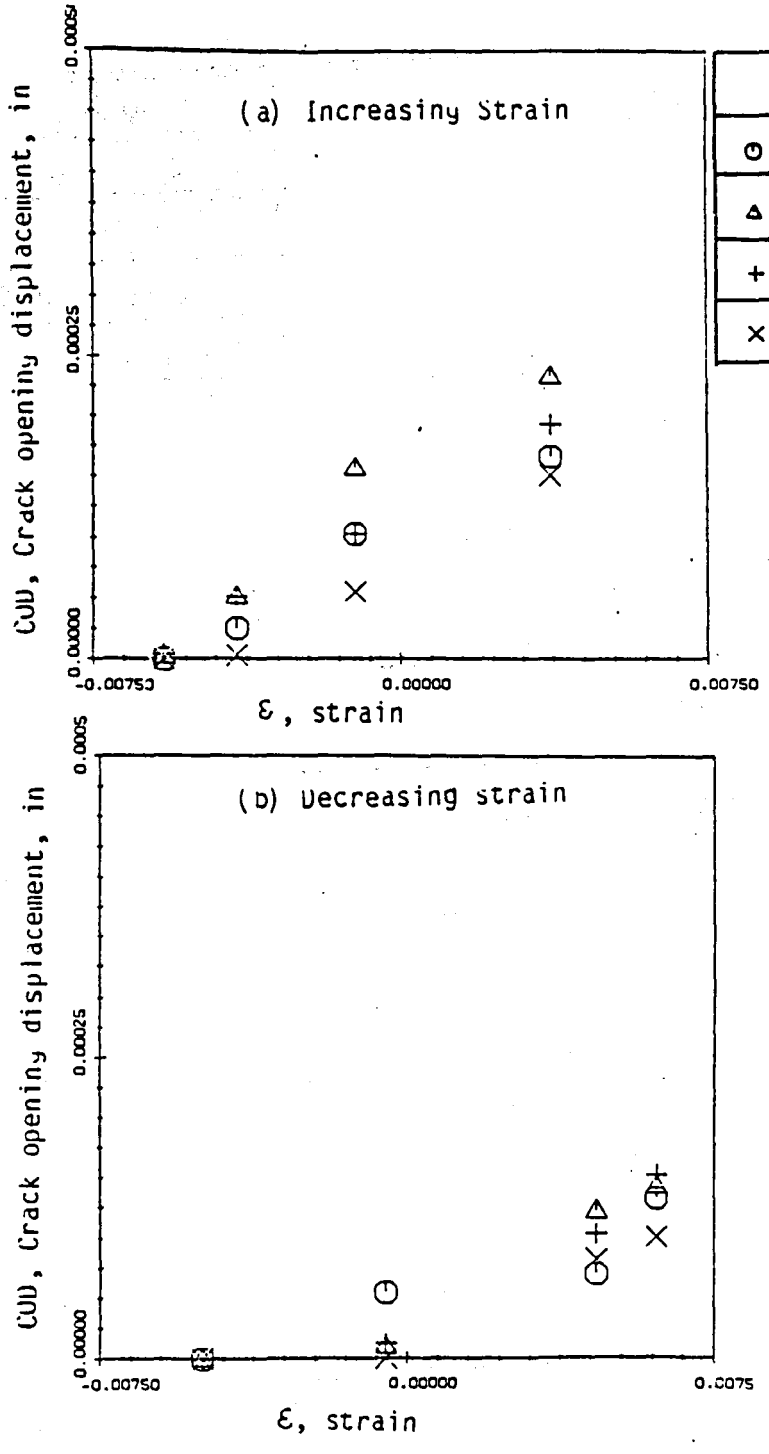


| | x(in) | x/2a |
|---|---|---|
| ⊙ | 0.0017 | 0.0955 |
| △ | 0.0032 | 0.1797 |
| + | 0.0152 | 0.8539 |
| × | 0.0171 | 0.955 |

(d) Crack opening displacement as a function of strain at different points along the crack length during increasing and decreasing strain.

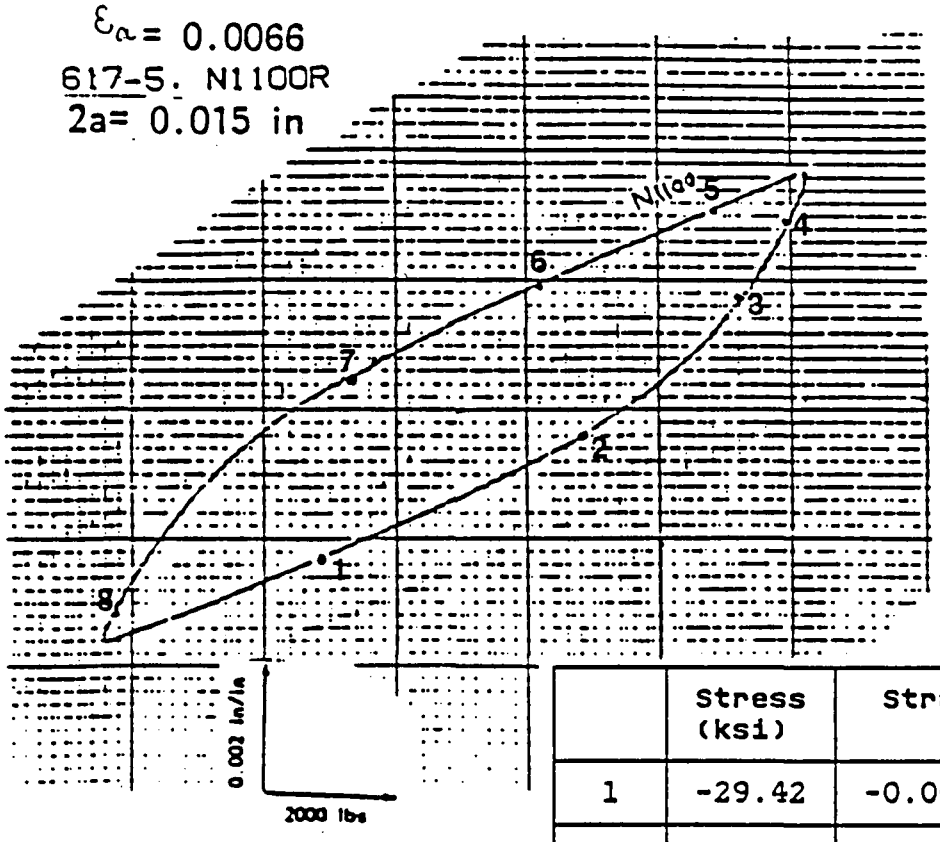


| | Stress (ksi) | Strain |
|---|---|---|
| 1 | -29.42 | -0.0052 |
| 2 | 25.74 | -0.0027 |
| 3 | 58.71 | 0.0009 |
| 4 | 69.03 | 0.0036 |
| 5 | 55.17 | 0.006 |
| 6 | 17.83 | 0.0032 |
| 7 | -22.35 | 0.0027 |
| 8 | -72.99 | -0.0047 |

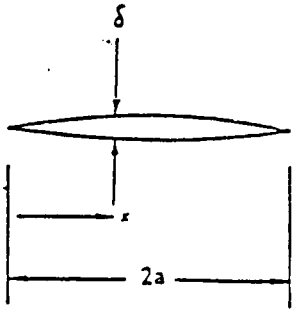


Fig. 31: Crack opening displacements measured in one complete cycle
(a) Load displacement loop as obtained from clip gauge mounted across the grip ends and the points (corresponding stress and strain levels shown in table) where closure observations were made.

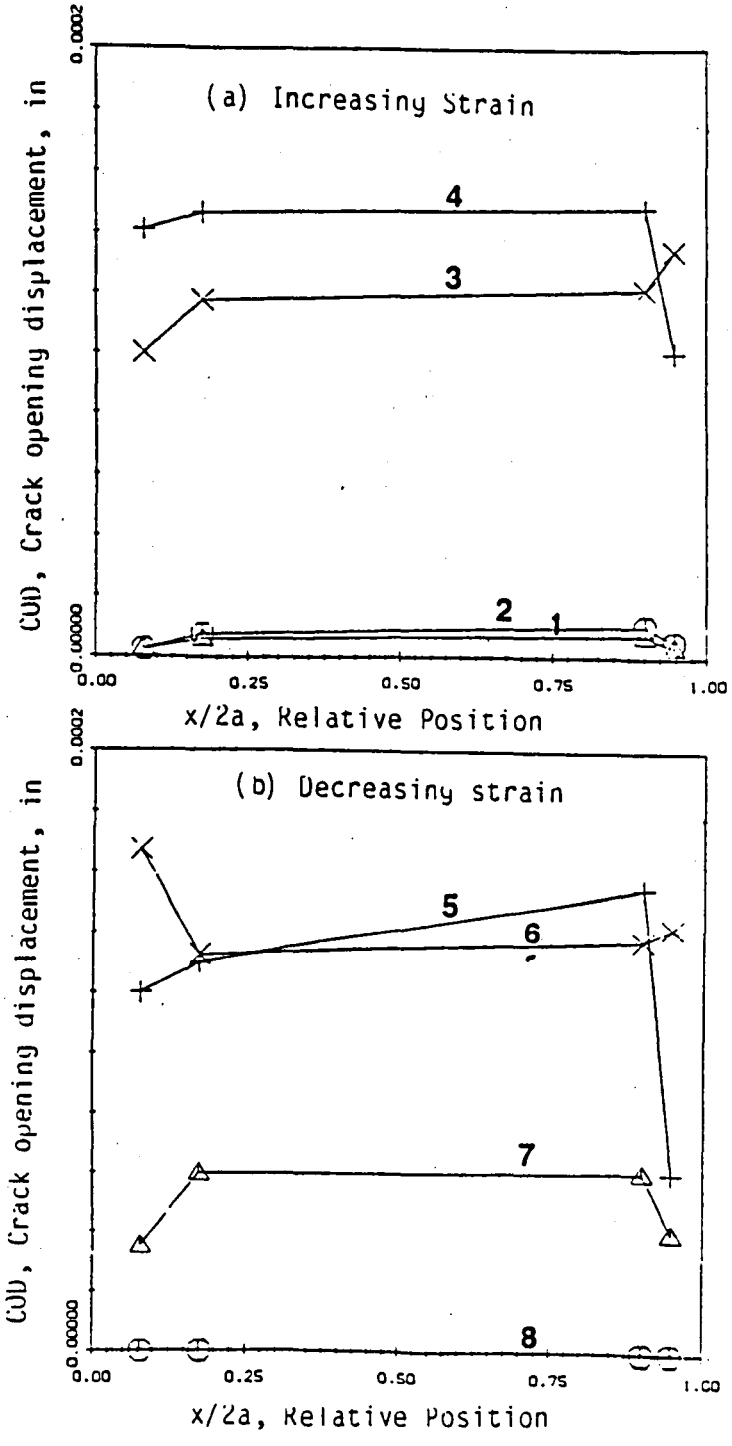


(b) Crack opening displacement during increasing (loading) and decreasing strain (unloading) at different points along the crack length. Different stress (strain) levels correspond to the points shown in load displacement loop.

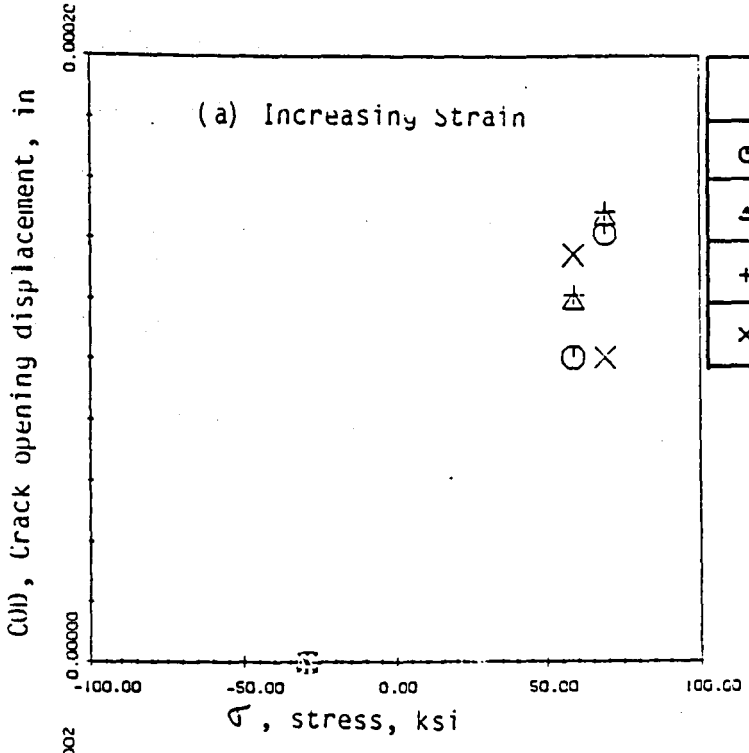


| | x(in) | x/2a |
|---|---|---|
| ⊙ | 0.0012 | 0.0784 |
| △ | 0.0027 | 0.1764 |
| + | 0.0138 | 0.9019 |
| × | 0.0146 | 0.9477 |

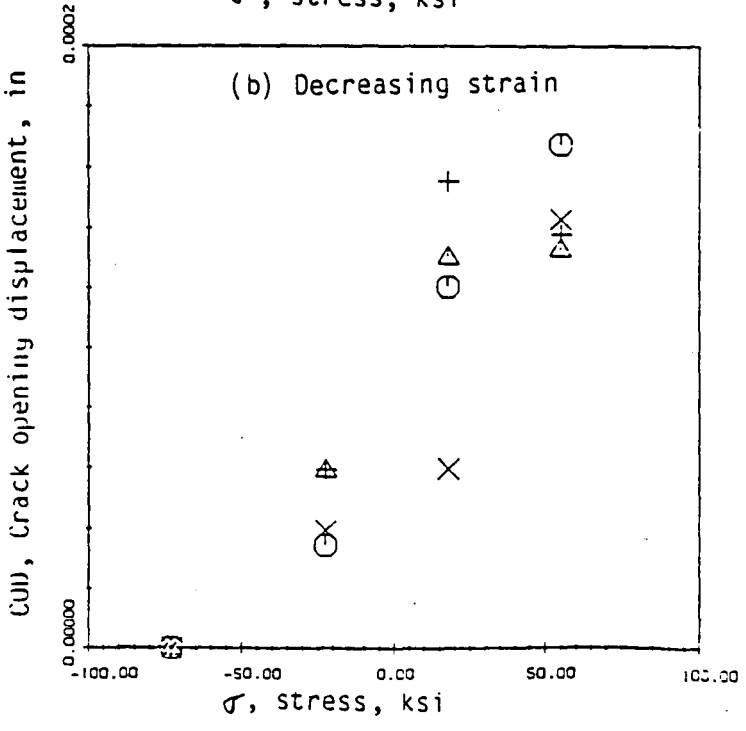


(c) Crack opening displacement as a function of stress at different points along the crack length during increasing and decreasing strain.

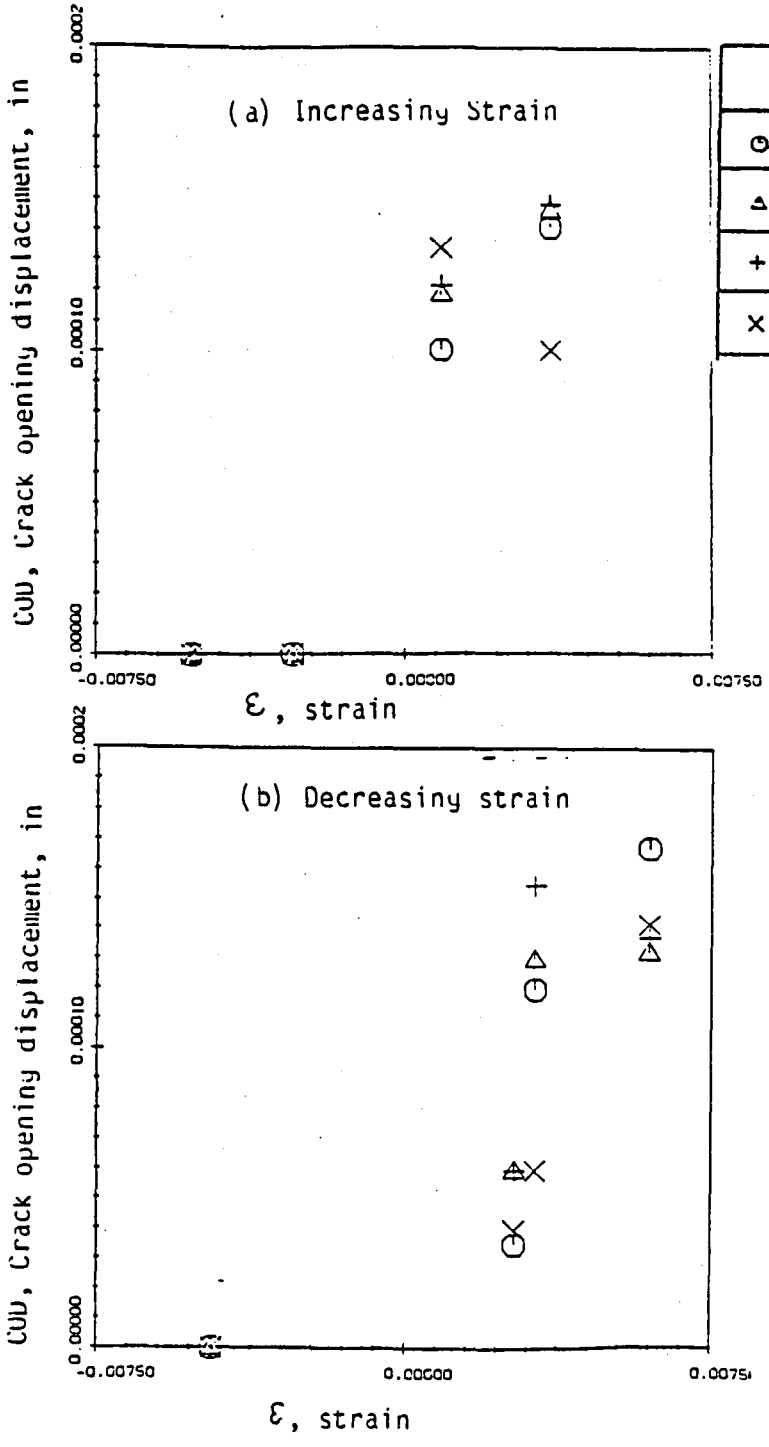


| | x(in) | x/2a |
|---|---|---|
| ⊙ | 0.0012 | 0.0784 |
| △ | 0.0027 | 0.1764 |
| + | 0.0138 | 0.9019 |
| × | 0.0146 | 0.9477 |

(d) Crack opening displacement as a function of strain at different points along the crack length during increasing and decreasing strain.

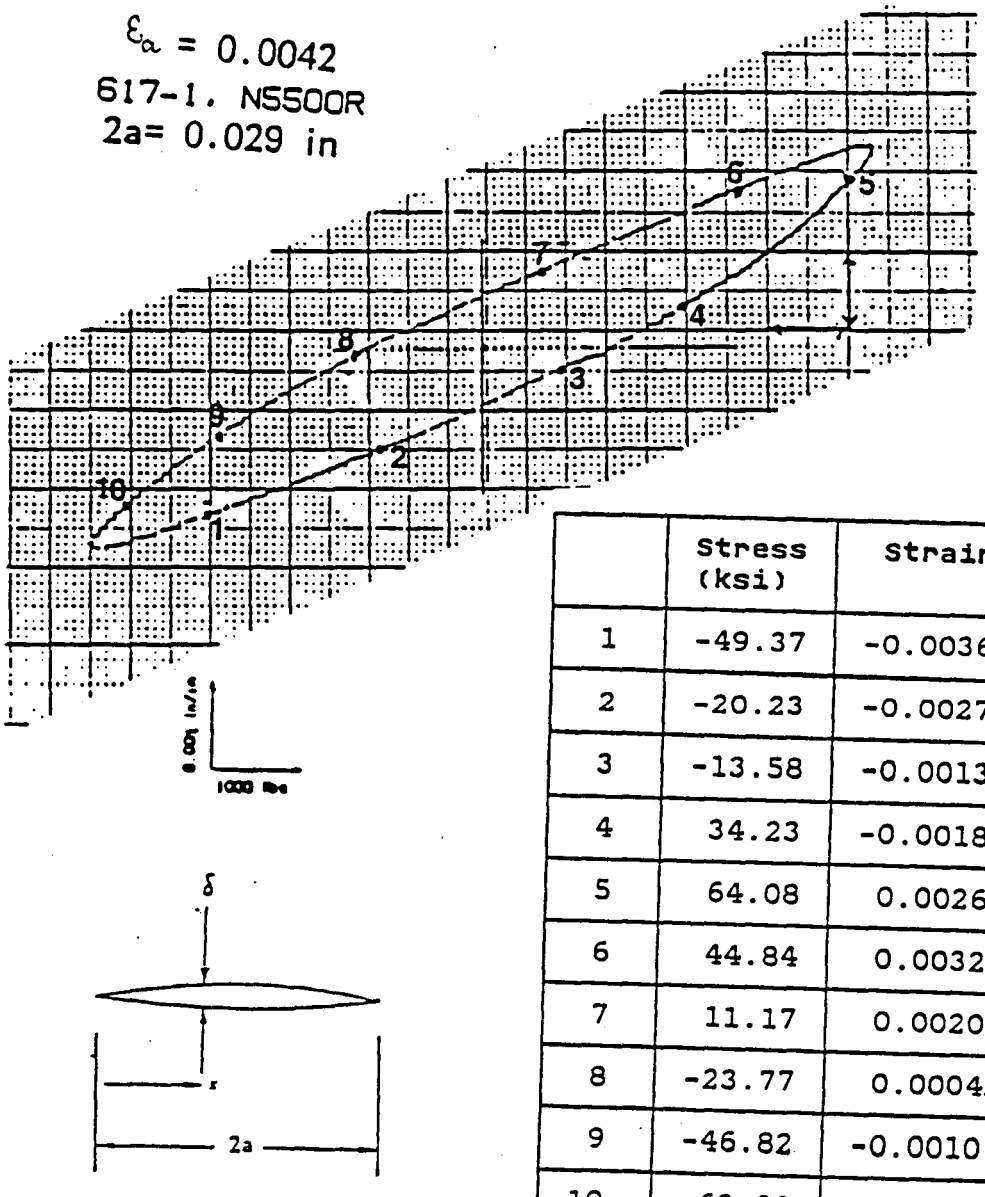


| | Stress (ksi) | Strain |
|---|---|---|
| 1 | -49.37 | -0.00364 |
| 2 | -20.23 | -0.0027 |
| 3 | -13.58 | -0.0013 |
| 4 | 34.23 | -0.0018 |
| 5 | 64.08 | 0.00264 |
| 6 | 44.84 | 0.0032 |
| 7 | 11.17 | 0.0020 |
| 8 | -23.77 | 0.00042 |
| 9 | -46.82 | -0.0010 |
| 10 | -63.80 | -0.00266 |




Fig. 32: Crack opening displacements measured in one complete cycle
(a) Load displacement loop as obtained from clip gauge mounted across the grip ends and the points (corresponding stress and strain levels shown in table) where closure observations were made.

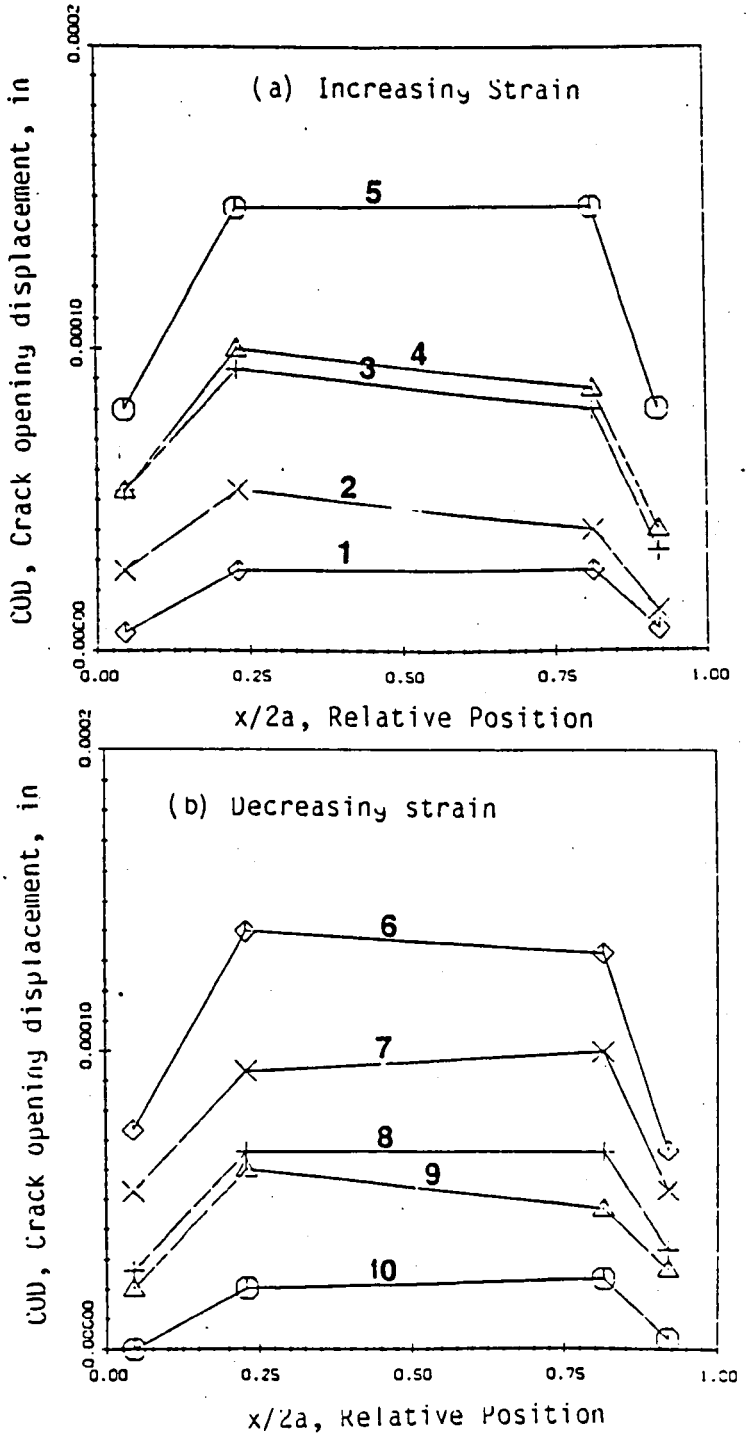


(b) Crack opening displacement during increasing (loading) and decreasing strain (unloading) at different points along the crack length. Different stress (strain) levels correspond to the points shown in load displacement loop.

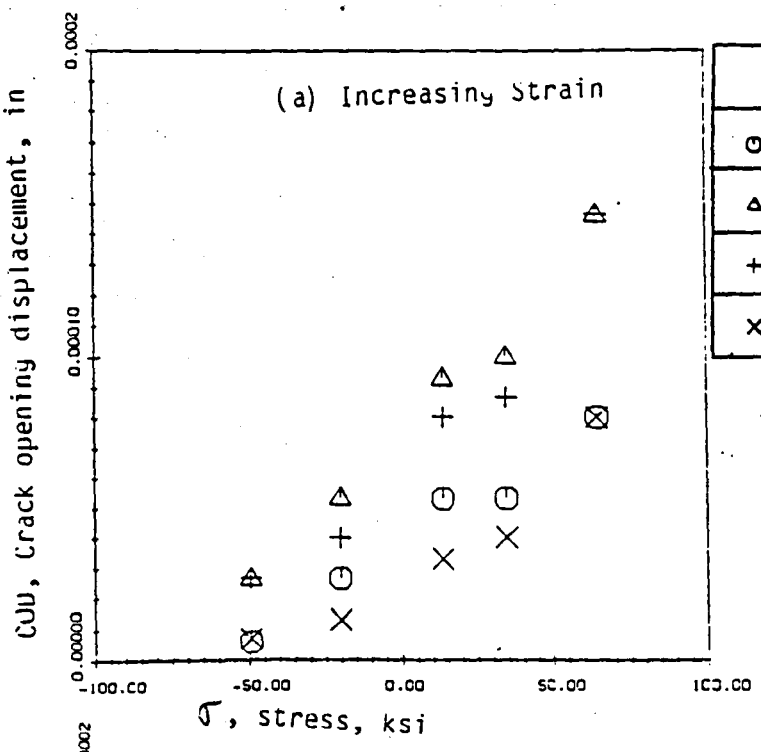


| | x(in) | x/2a |
|---|---|---|
| ○ | 0.0013 | 0.0448 |
| △ | 0.00667 | 0.2306 |
| + | 0.0236 | 0.8138 |
| × | 0.02667 | 0.9196 |

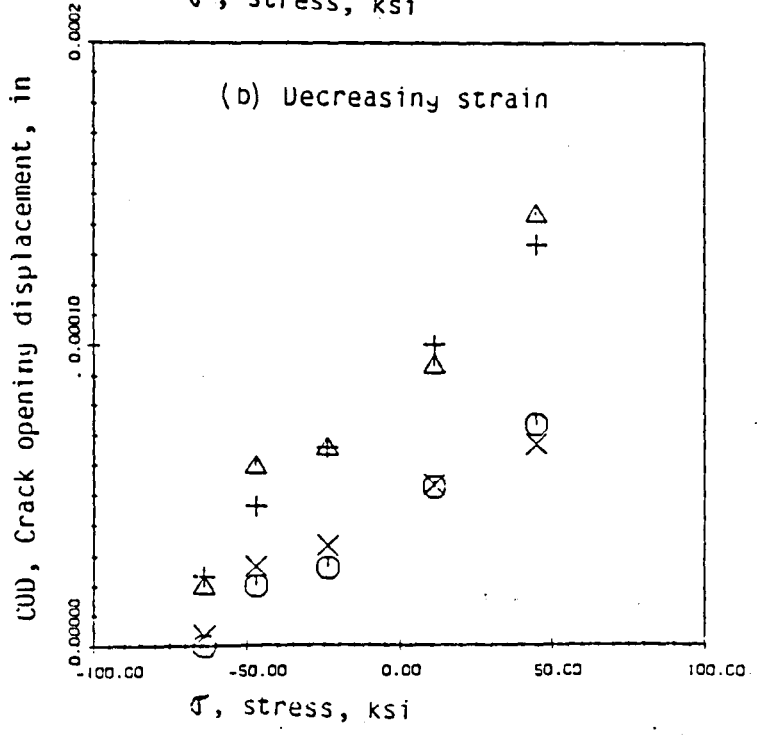


(c) Crack opening displacement as a function of stress at different points along the crack length during increasing and decreasing strain.

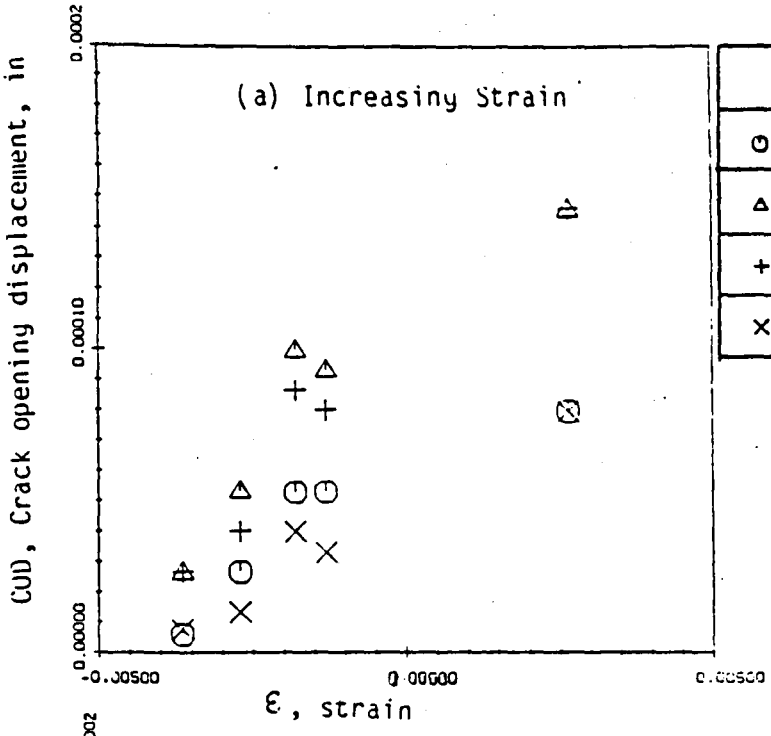


| | x(in) | x/2a |
|---|---|---|
| ○ | 0.0013 | 0.0448 |
| △ | 0.00667 | 0.2306 |
| + | 0.0236 | 0.8138 |
| × | 0.02667 | 0.9196 |

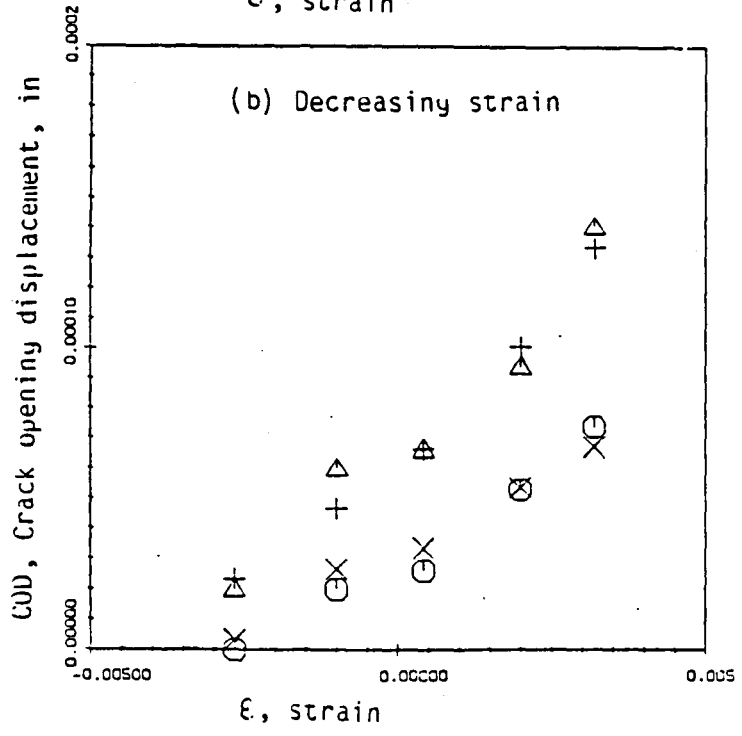


(a) Crack opening displacement as a function of strain at different points along the crack length during increasing and decreasing strain.

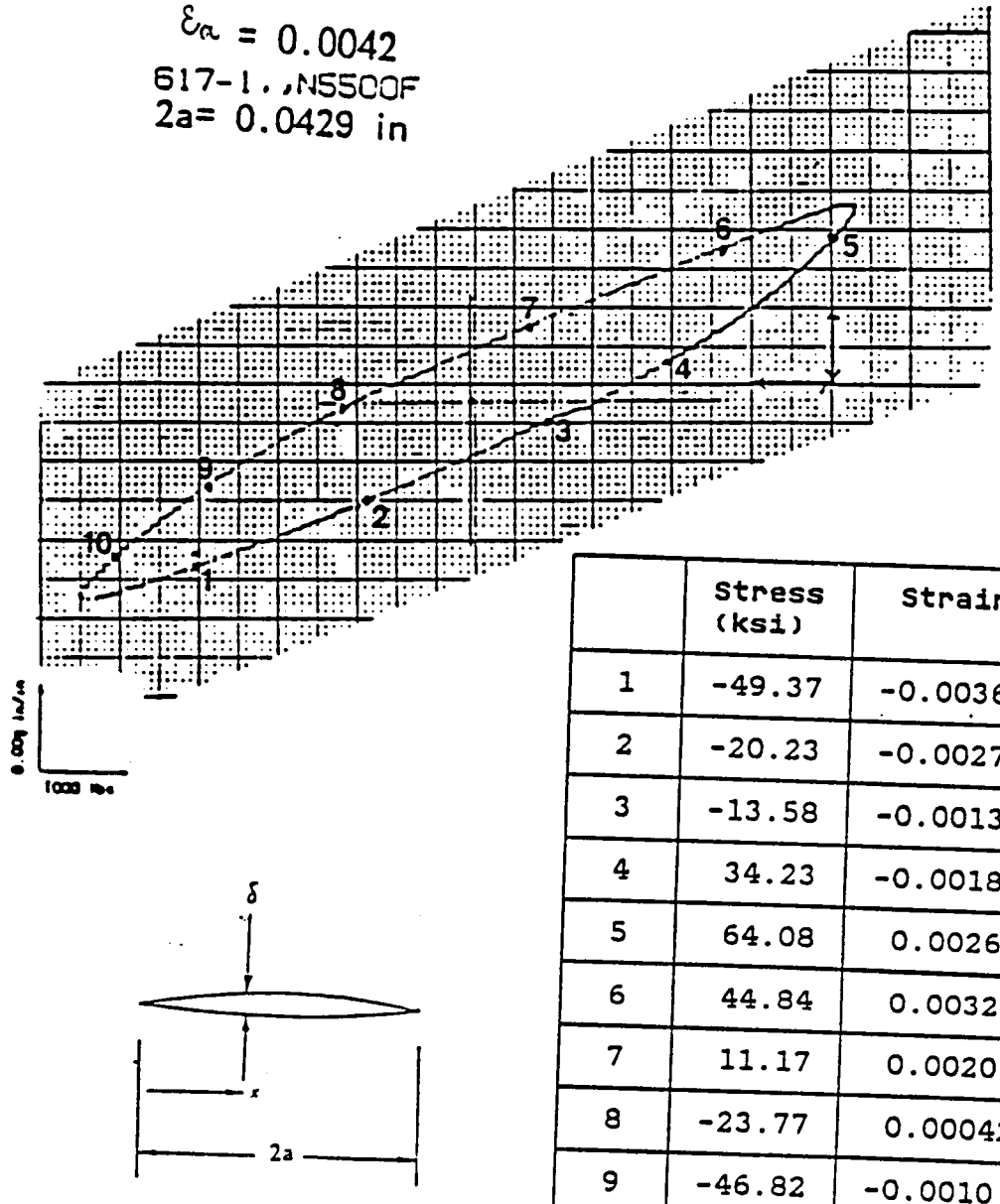


| | Stress (ksi) | Strain |
|---|---|---|
| 1 | -49.37 | -0.00364 |
| 2 | -20.23 | -0.0027 |
| 3 | -13.58 | -0.0013 |
| 4 | 34.23 | -0.0018 |
| 5 | 64.08 | 0.00264 |
| 6 | 44.84 | 0.0032 |
| 7 | 11.17 | 0.0020 |
| 8 | -23.77 | 0.00042 |
| 9 | -46.82 | -0.0010 |
| 10 | -63.80 | -0.00266 |

Fig. 33: Crack opening displacements measured in one complete cycle (a) Load displacement loop as obtained from clip gauge mounted across the grip ends and the points (corresponding stress and strain levels shown in table) where closure observations were made.

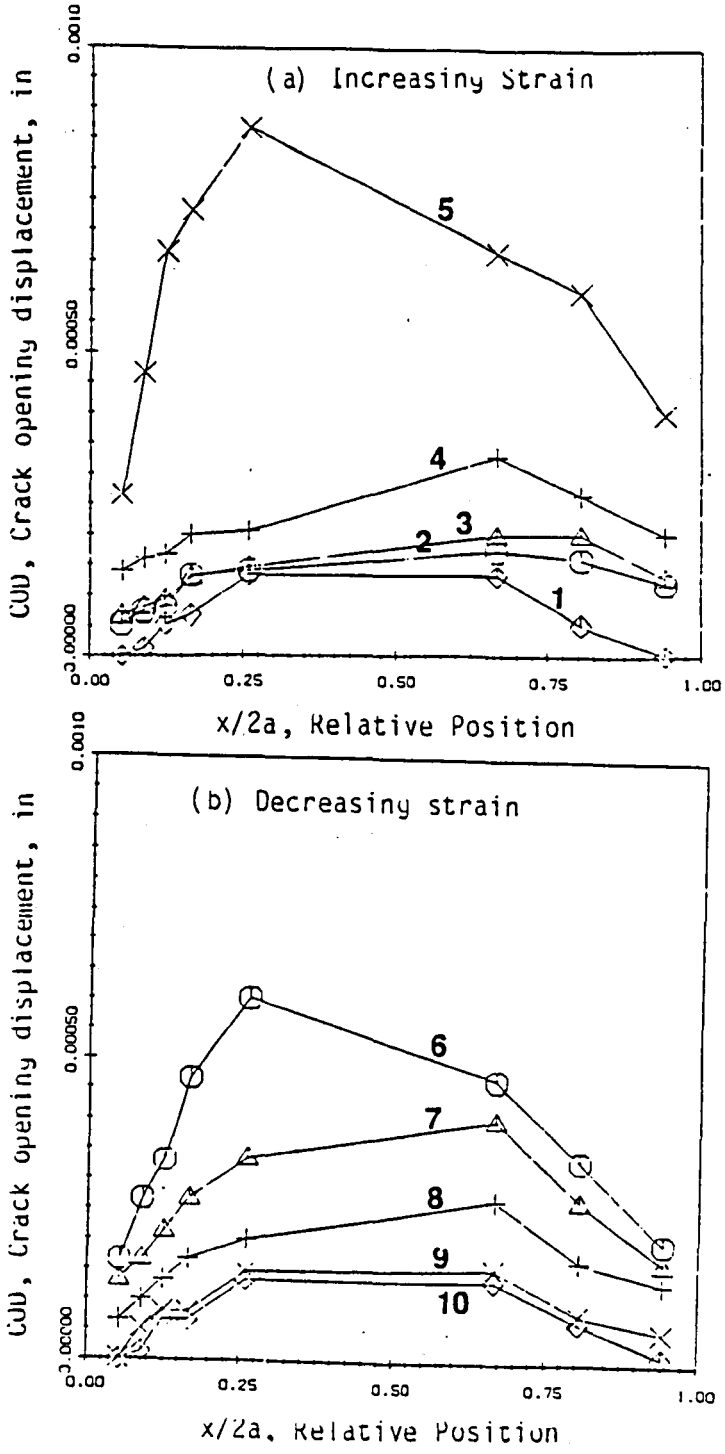


(b) Crack opening displacement during increasing (loading) and decreasing strain (unloading) at different points along the crack length. Different stress (strain) levels correspond to the points shown in load displacement loop.

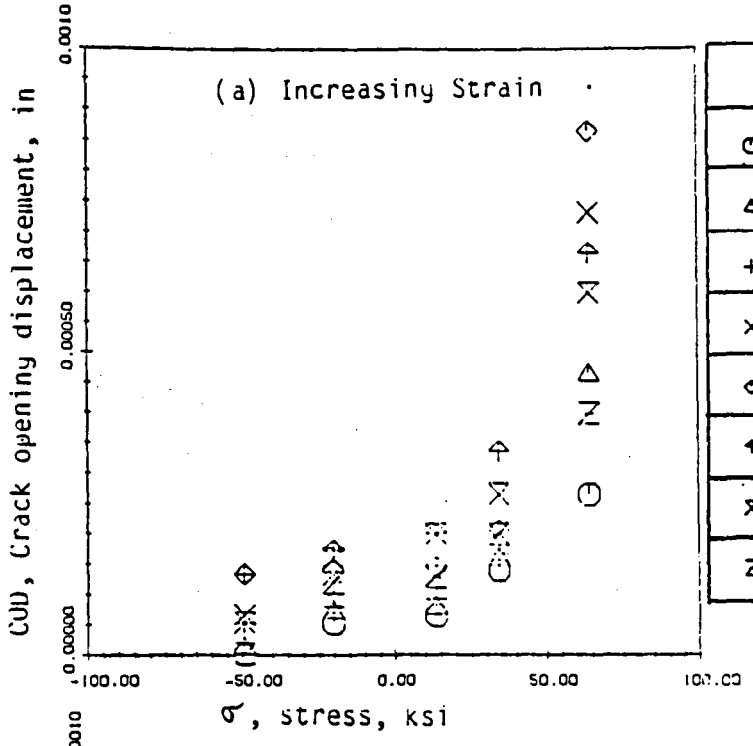


| | x(in) | x/2a |
|---|---|---|
| ○ | 0.0024 | 0.053 |
| △ | 0.004 | 0.0889 |
| + | 0.0056 | 0.1244 |
| × | 0.00746 | 0.1657 |
| ◇ | 0.0117 | 0.26 |
| ✦ | 0.03 | 0.6667 |
| ✳ | 0.0362 | 0.8044 |
| Z | 0.0424 | 0.9424 |

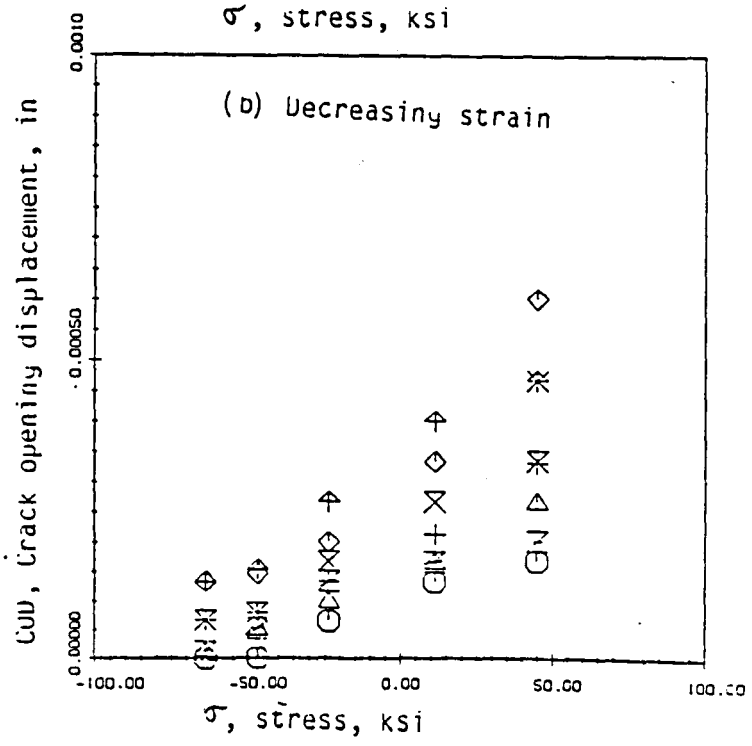


(c) Crack opening displacement as a function of stress at different points along the crack length during increasing and decreasing strain.

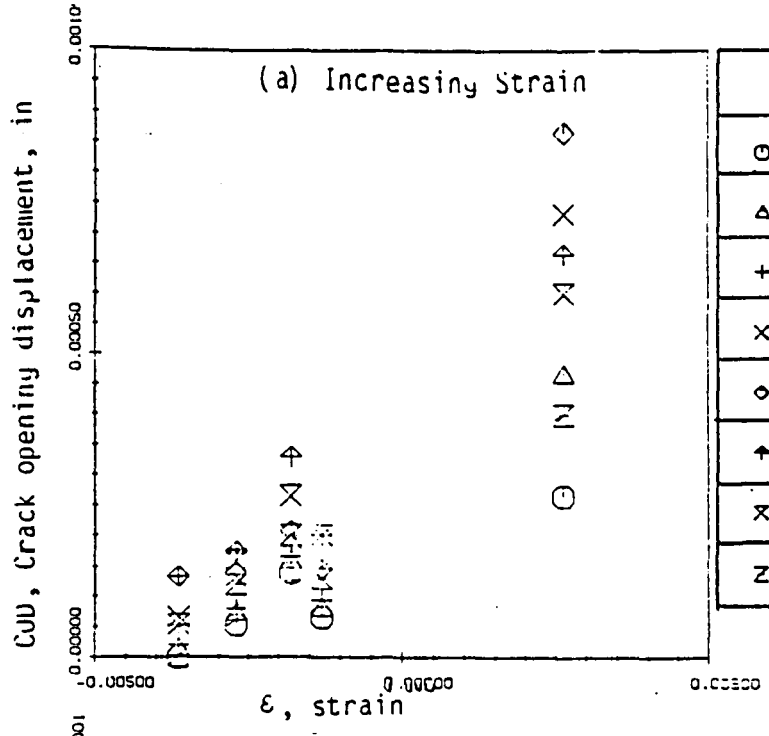


| | x(in) | x/2a |
|---|---|---|
| ⊙ | 0.0024 | 0.053 |
| △ | 0.004 | 0.0889 |
| + | 0.0056 | 0.1244 |
| × | 0.00746 | 0.1657 |
| ◇ | 0.0117 | 0.26 |
| ✦ | 0.03 | 0.6667 |
| ⊠ | 0.0362 | 0.8044 |
| Z | 0.0424 | 0.9424 |

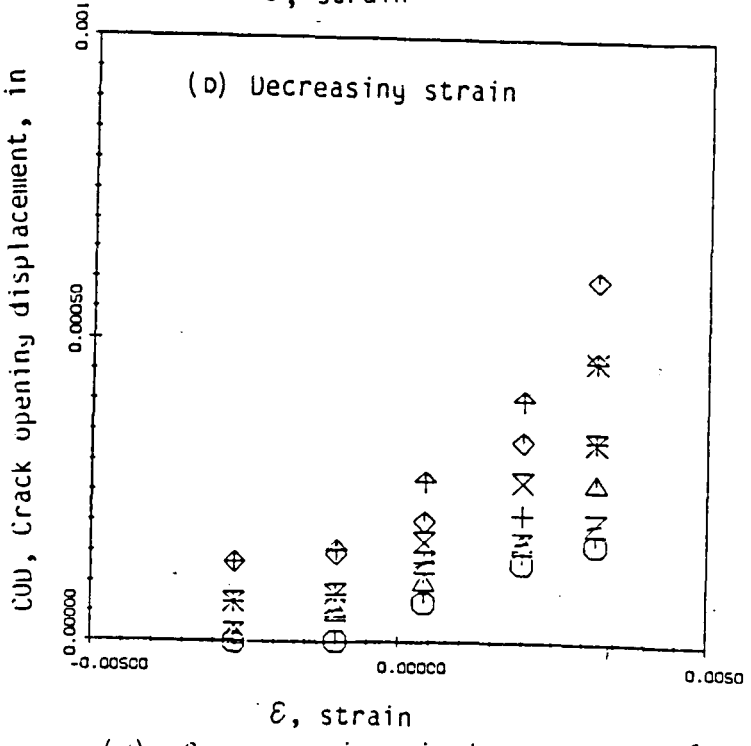


(a) Crack opening displacement as a function of strain at different points along the crack length during increasing and decreasing strain.

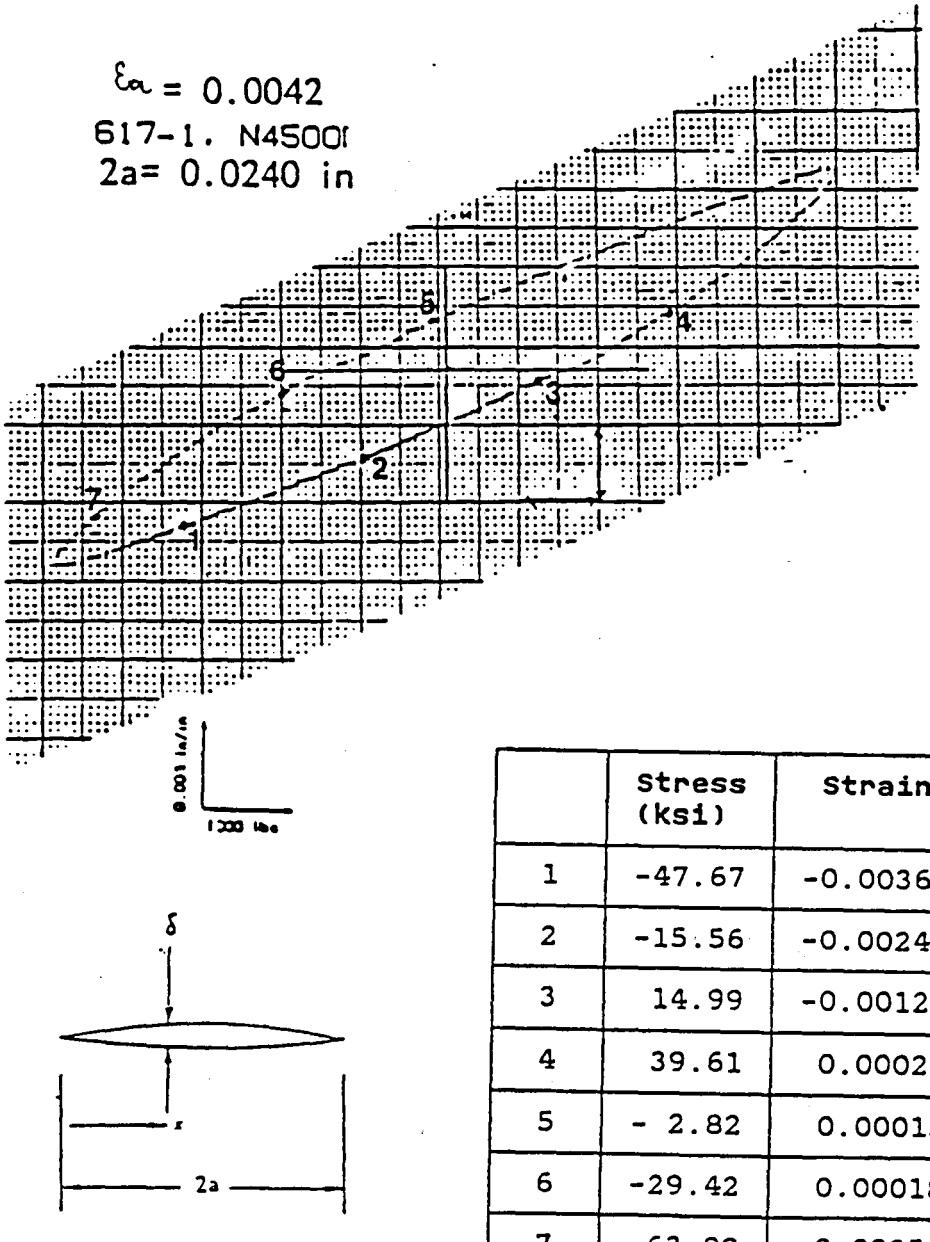


| | Stress (ksi) | Strain |
|---|---|---|
| 1 | -47.67 | -0.00364 |
| 2 | -15.56 | -0.00242 |
| 3 | 14.99 | -0.0012 |
| 4 | 39.61 | 0.00021 |
| 5 | - 2.82 | 0.00013 |
| 6 | -29.42 | 0.00018 |
| 7 | -63.09 | -0.0025 |

Fig. 34: Crack opening displacements measured in one complete cycle (a) Load displacement loop as obtained from clip gauge mounted across the grip ends and the points (corresponding stress and strain levels shown in table) where closure observations were made.

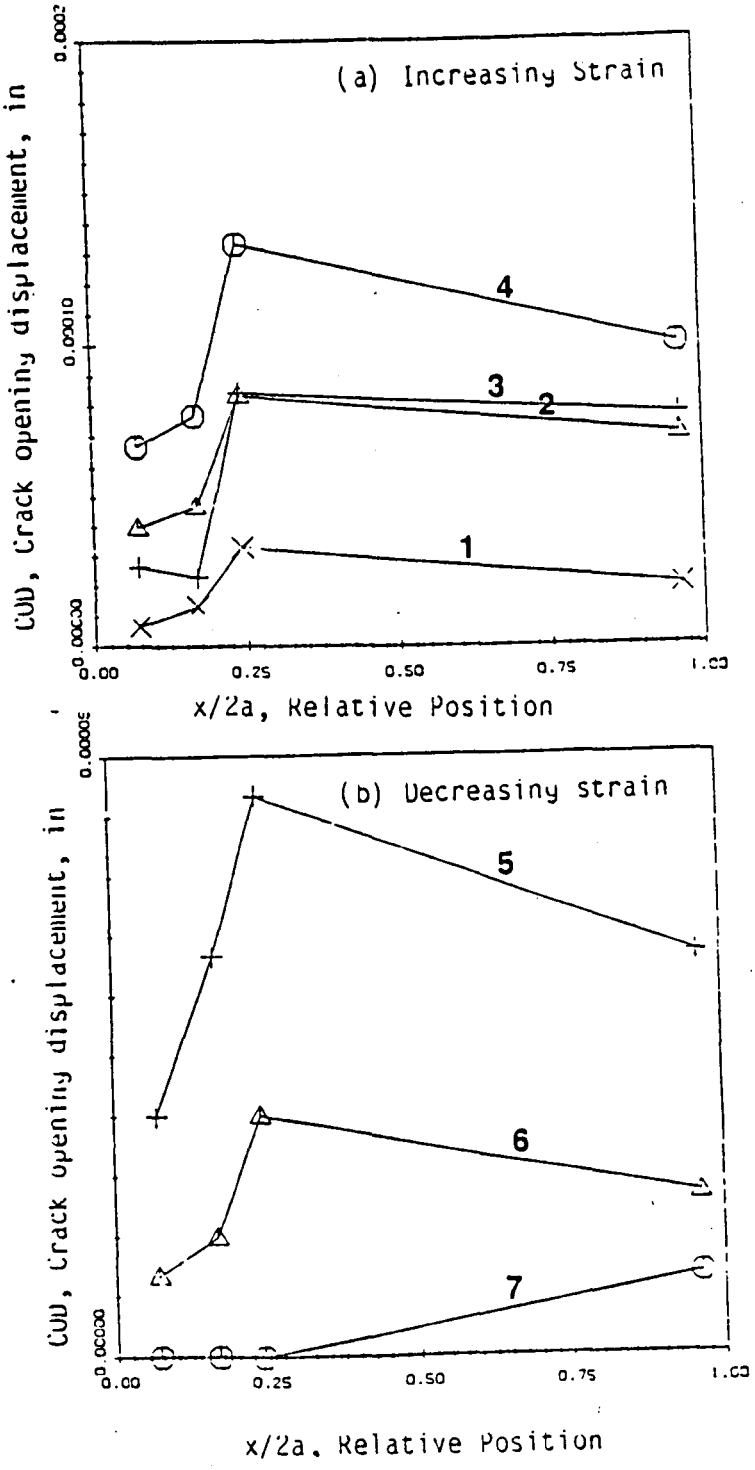


(b) Crack opening displacement during increasing (loading) and decreasing strain (unloading) at different points along the crack length. Different stress (strain) levels correspond to the points shown in load displacement loop.

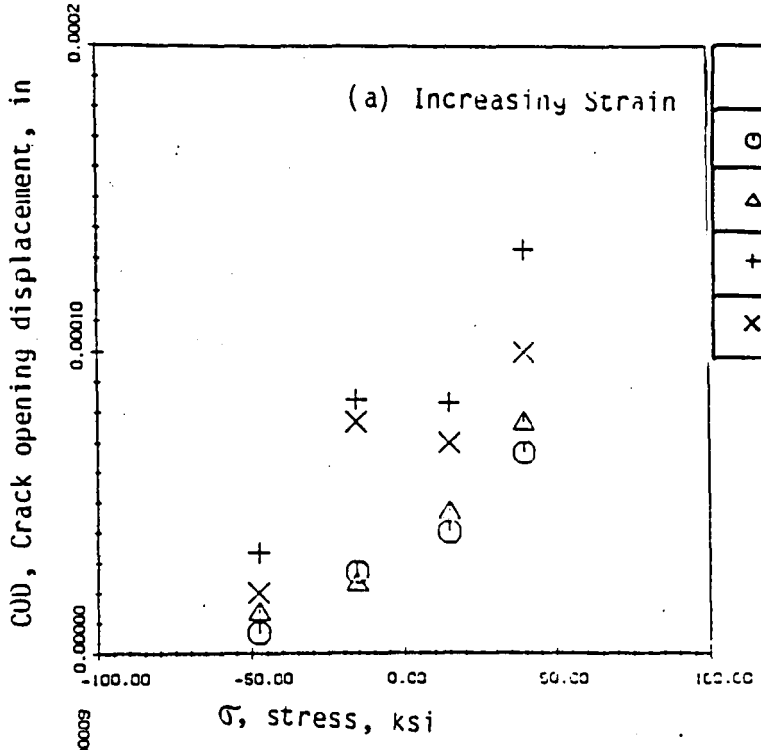


| | x(in) | x/2a |
|---|---|---|
| ⊙ | 0.00173 | 0.0715 |
| △ | 0.00406 | 0.1678 |
| + | 0.00586 | 0.2421 |
| × | 0.0233 | 0.9628 |

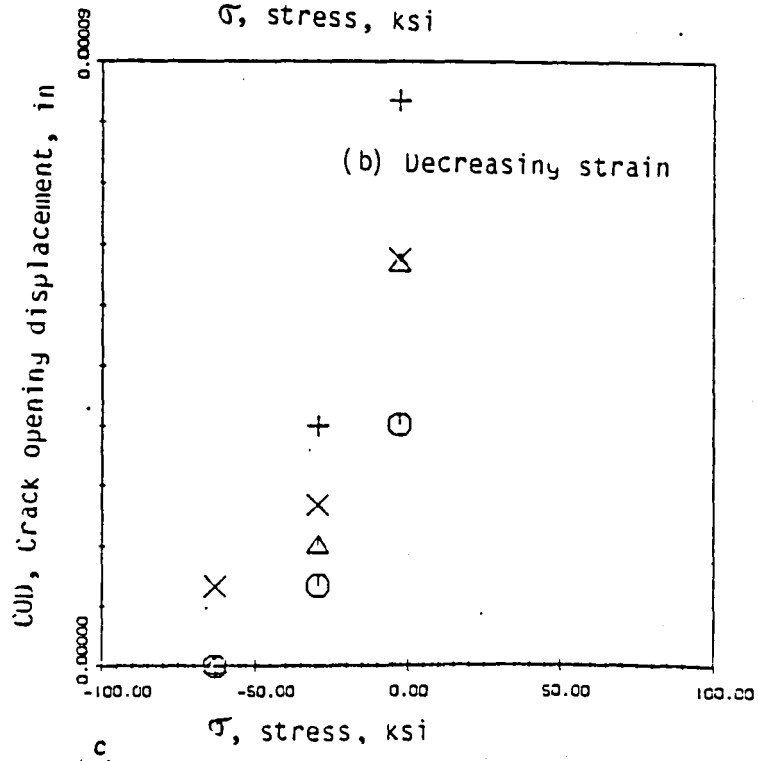


(c) Crack opening displacement as a function of strain at different points along the crack length during increasing and decreasing strain.

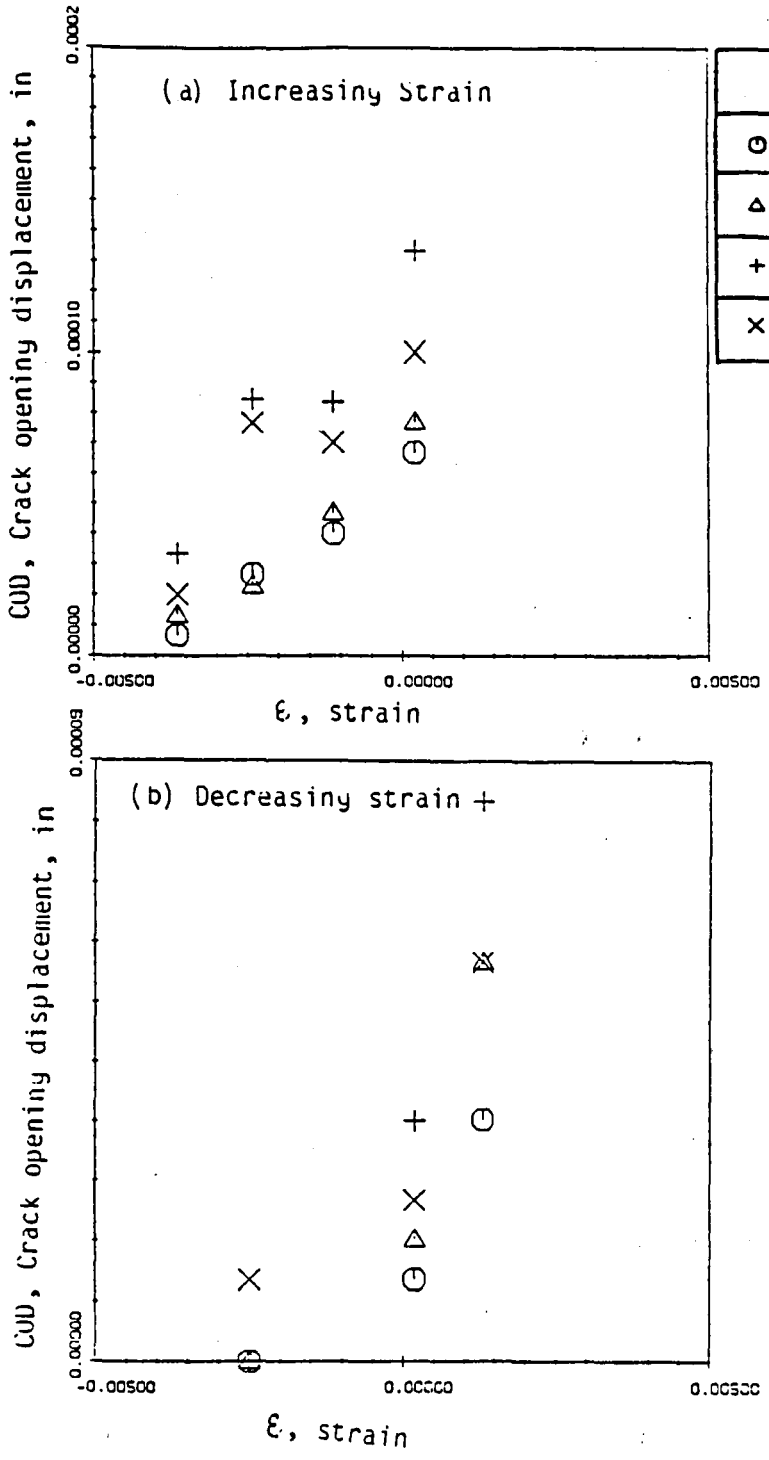


| | x(in) | x/2a |
|---|---|---|
| ⊙ | 0.00173 | 0.0715 |
| △ | 0.00406 | 0.1678 |
| + | 0.00586 | 0.2421 |
| × | 0.0233 | 0.9628 |

(d) Crack opening displacement as a function of stress at different points along the crack length during increasing and decreasing strain.

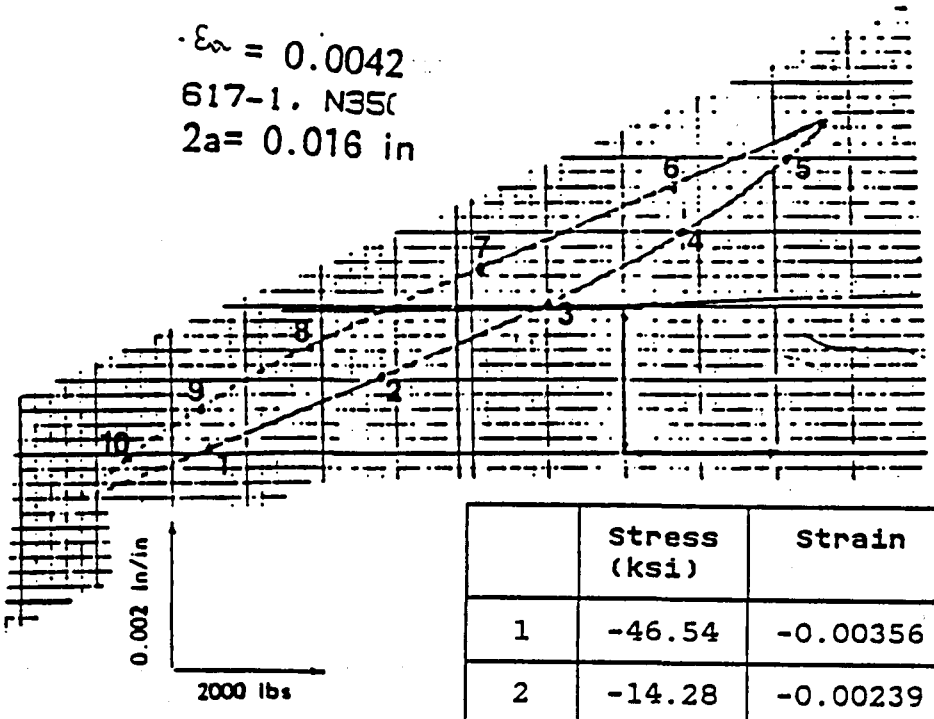


| | Stress (ksi) | Strain |
|---|---|---|
| 1 | -46.54 | -0.00356 |
| 2 | -14.28 | -0.00239 |
| 3 | 16.97 | -0.00106 |
| 4 | 41.16 | 0.00032 |
| 5 | 60.97 | 0.00264 |
| 6 | 40.31 | 0.00296 |
| 7 | 4.10 | 0.00126 |
| 8 | -27.72 | 0.00016 |
| 9 | -48.24 | -0.0013 |
| 10 | -61.82 | -0.00410 |

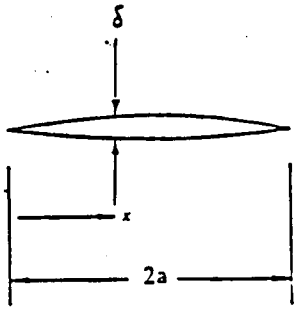


Fig. 35: Crack opening displacements measured in one complete cycle
(a) Load displacement loop as obtained from clip gauge mounted across the grip ends and the points (corresponding stress and strain levels shown in table) where closure observations were made.

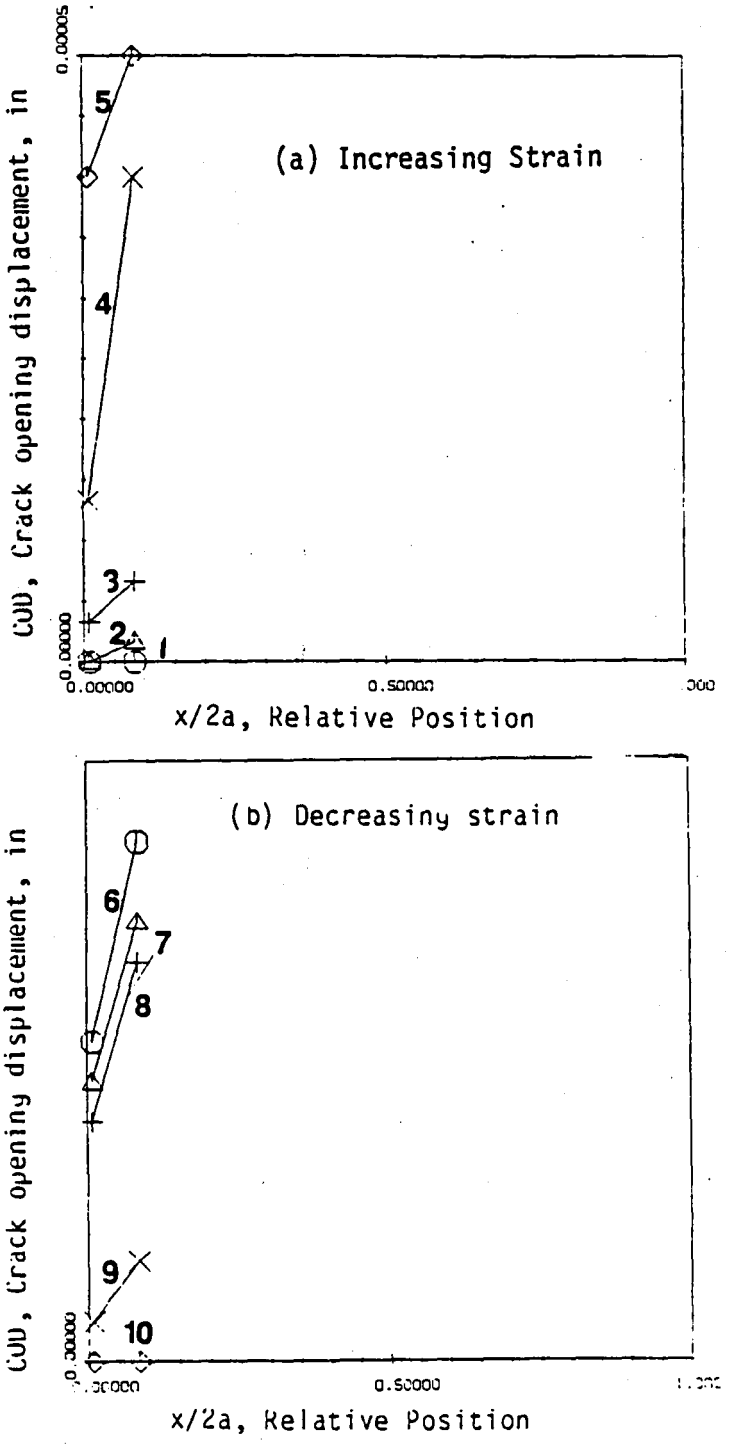


(b) Crack opening displacement during increasing (loading) and decreasing strain (unloading) at different points along the crack length. Different stress (strain) levels correspond to the points shown in load displacement loop.

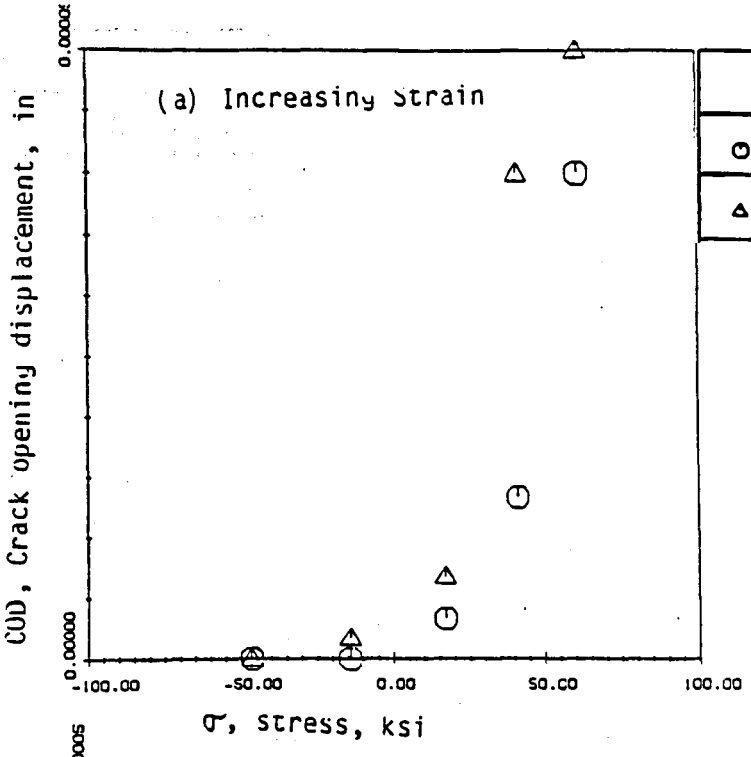


| | x(in) | x/2a |
|---|---|---|
| ○ | 0.00013 | 0.0083 |
| △ | 0.00133 | 0.0838 |

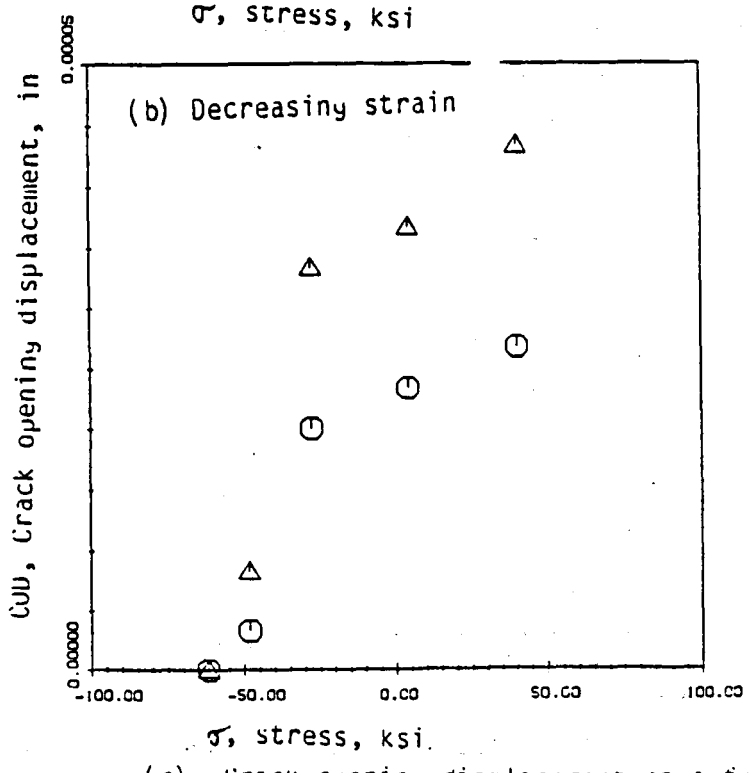


(c) Crack opening displacement as a function of stress at different points along the crack length during increasing and decreasing strain.

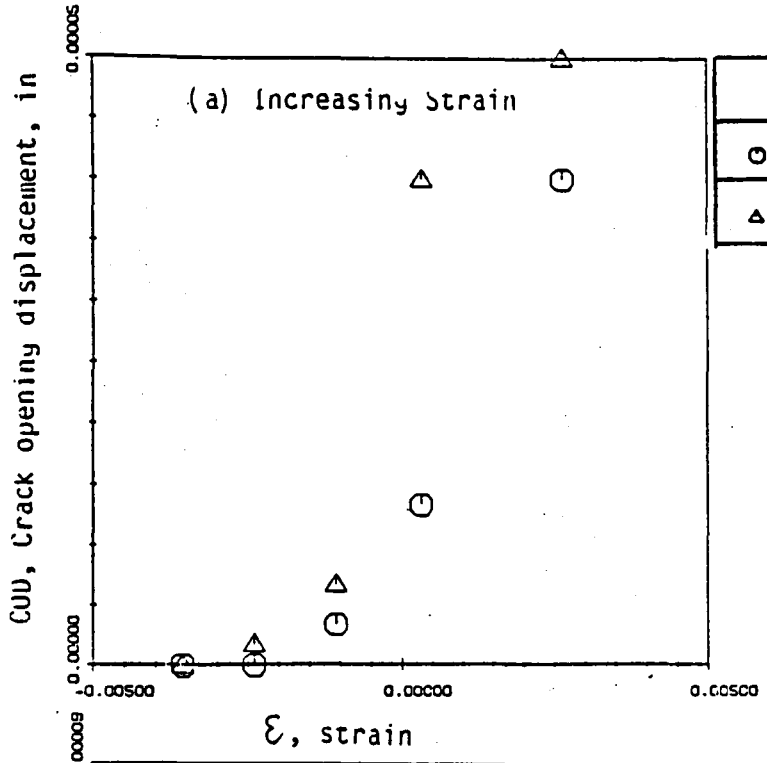


| | x(in) | x/2a |
|---|---|---|
| ○ | 0.00013 | 0.0083 |
| △ | 0.00133 | 0.0838 |

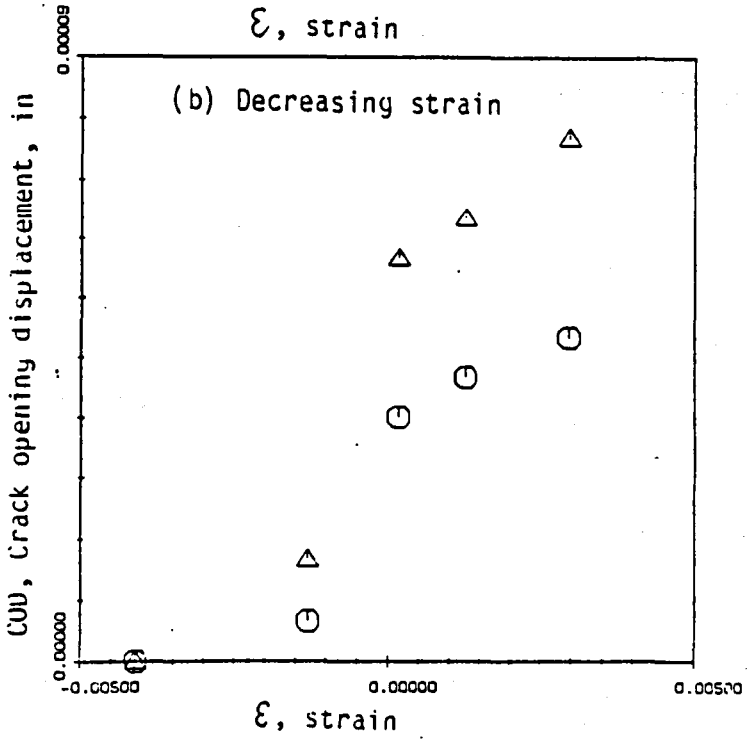


(d) Crack opening displacement as a function of strain at different points along the crack length during increasing and decreasing strain.

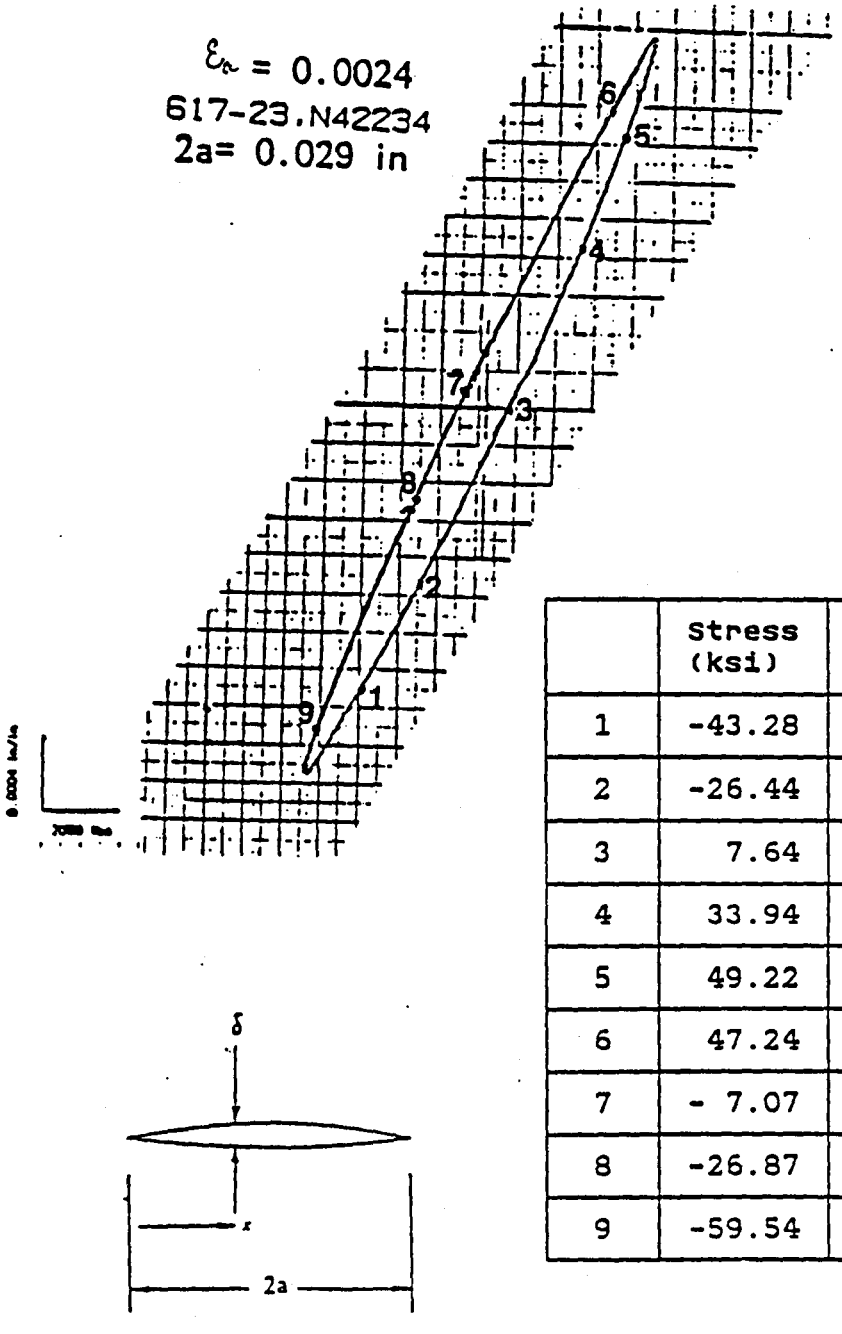


| | Stress (ksi) | Strain |
|---|---|---|
| 1 | -43.28 | -0.001925 |
| 2 | -26.44 | -0.00132 |
| 3 | 7.64 | -0.0002 |
| 4 | 33.94 | 0.00083 |
| 5 | 49.22 | 0.00165 |
| 6 | 47.24 | 0.002 |
| 7 | - 7.07 | 0.00018 |
| 8 | -26.87 | -0.00062 |
| 9 | -59.54 | -0.00205 |

Fig. 36: Crack opening displacements measured in one complete cycle
(a) Load displacement loop as obtained from clip gauge mounted across the grip ends and the points (corresponding stress and strain levels shown in table) where closure observations were made.

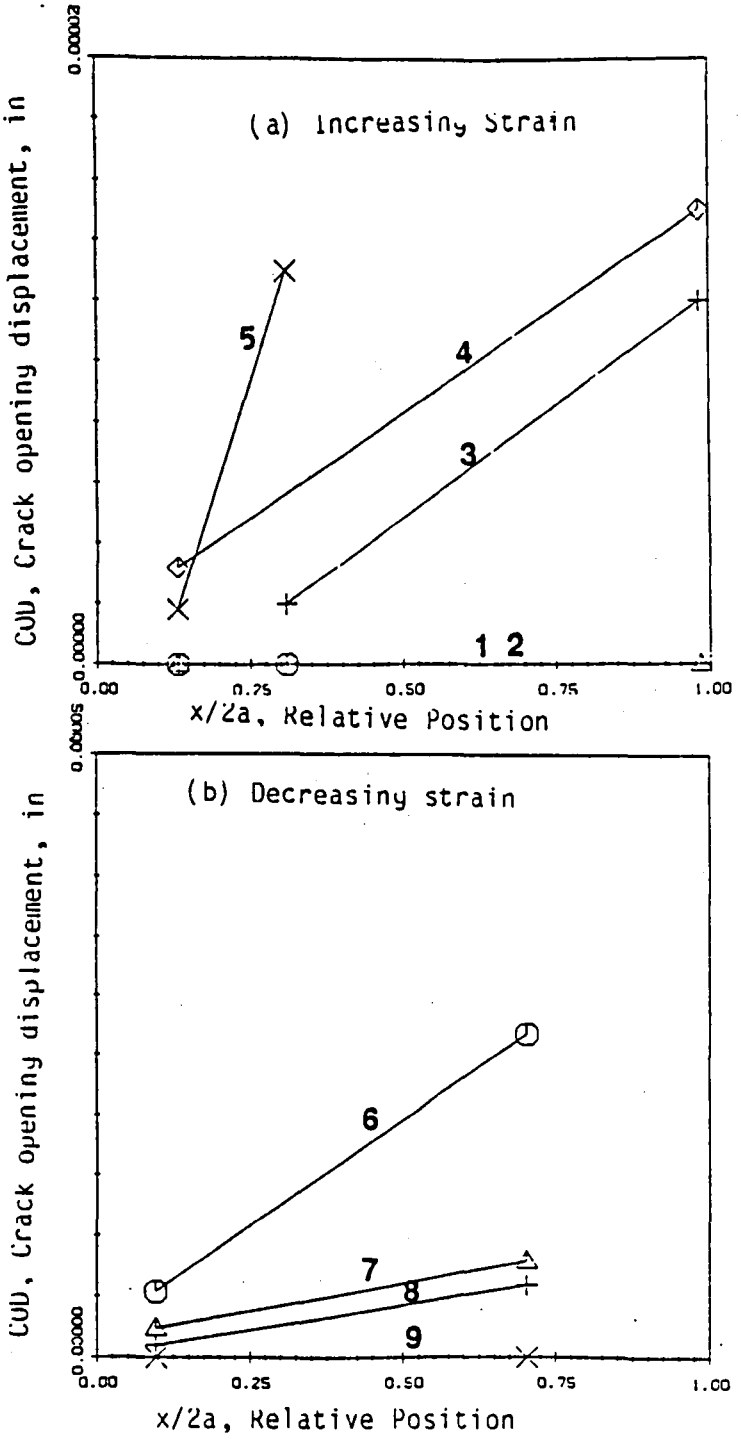


(b) Crack opening displacement during increasing (loading) and decreasing strain (unloading) at different points along the crack length. Different stress (strain) levels correspond to the points shown in load displacement loop.

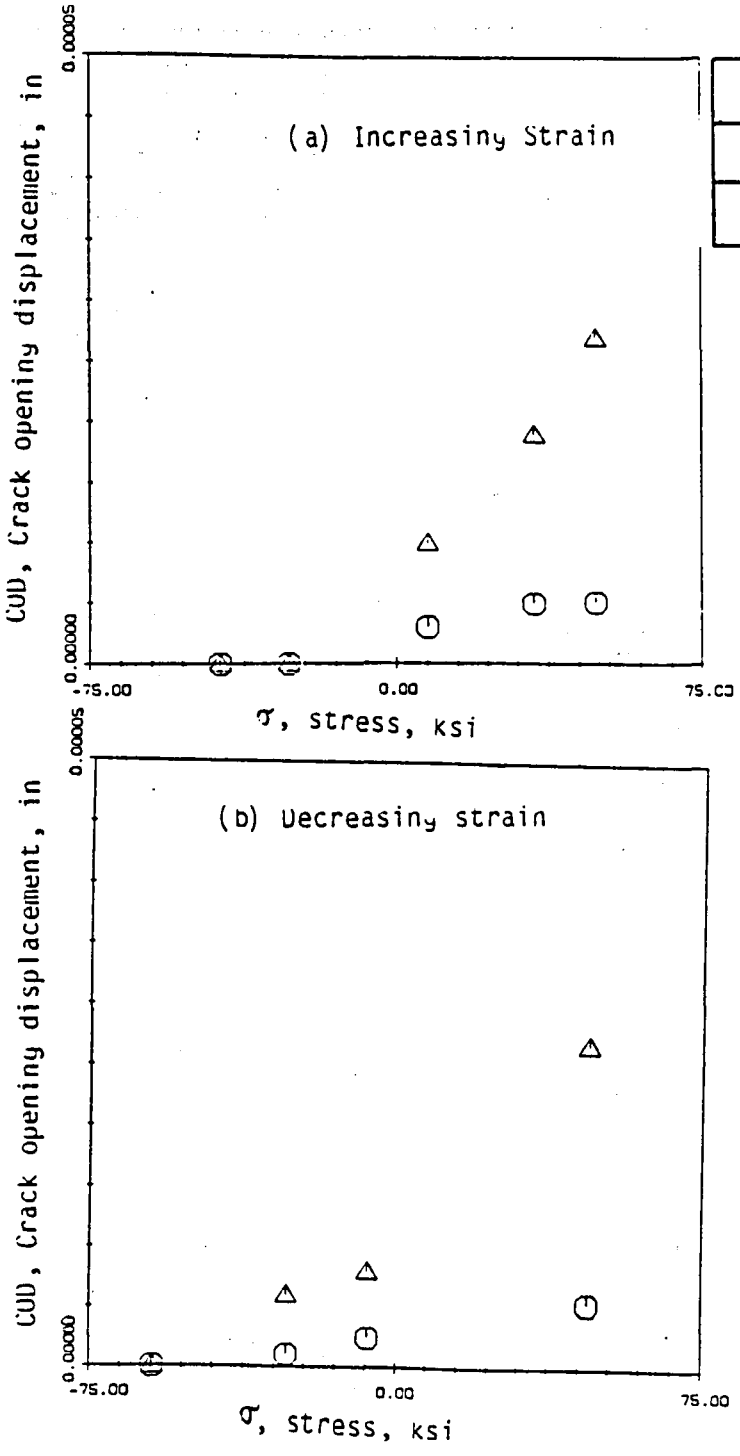


| | x(in) | x/2a |
|---|---|---|
| ○ | 0.0028 | 0.0965 |
| △ | 0.0204 | 0.7034 |

(c) Crack opening displacement as a function of stress at different points along the crack length during increasing and decreasing strain.

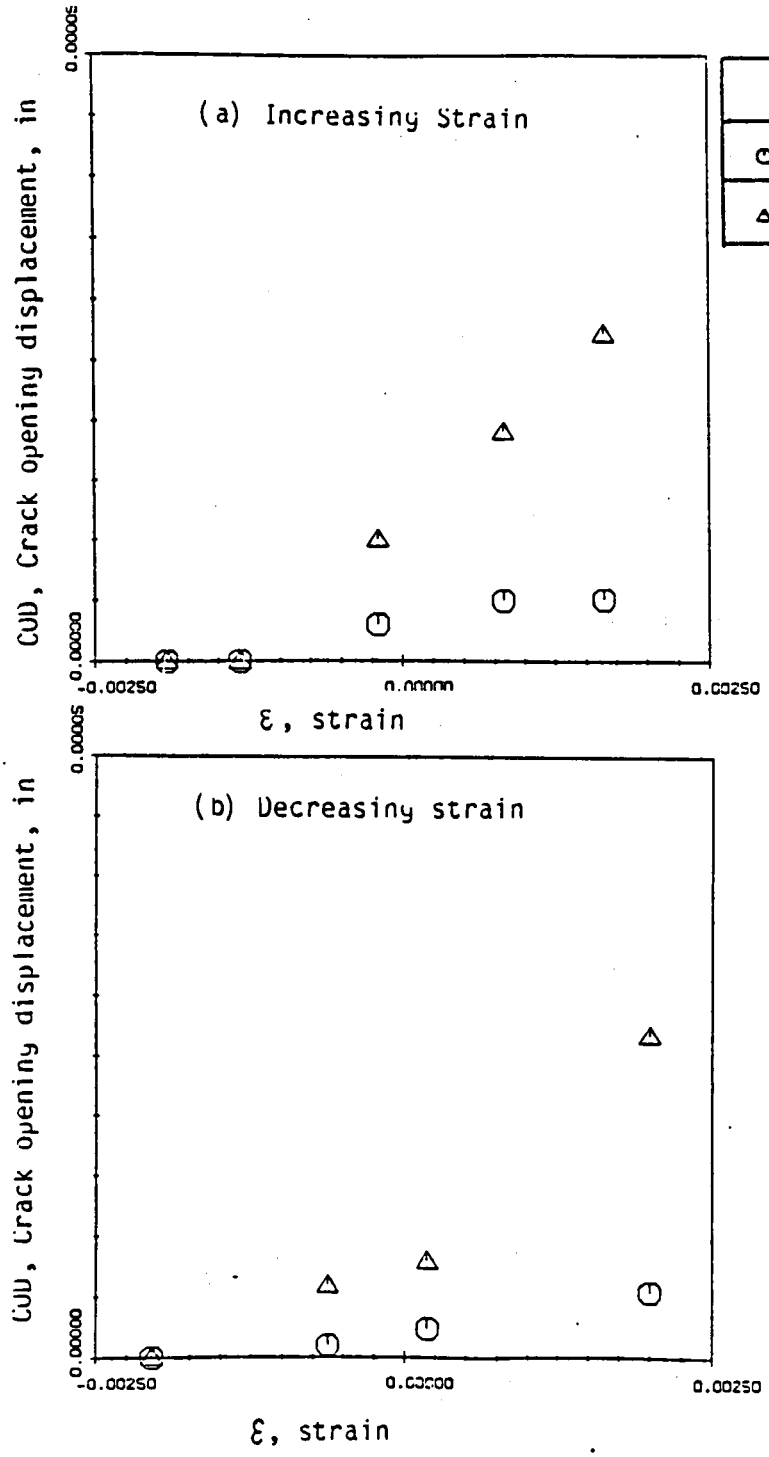


| | x(in) | x/2a |
|---|---|---|
| ○ | 0.0028 | 0.0965 |
| △ | 0.0204 | 0.7034 |

(d) Crack opening displacement as a function of strain at different points along the crack length during increasing and decreasing strain.

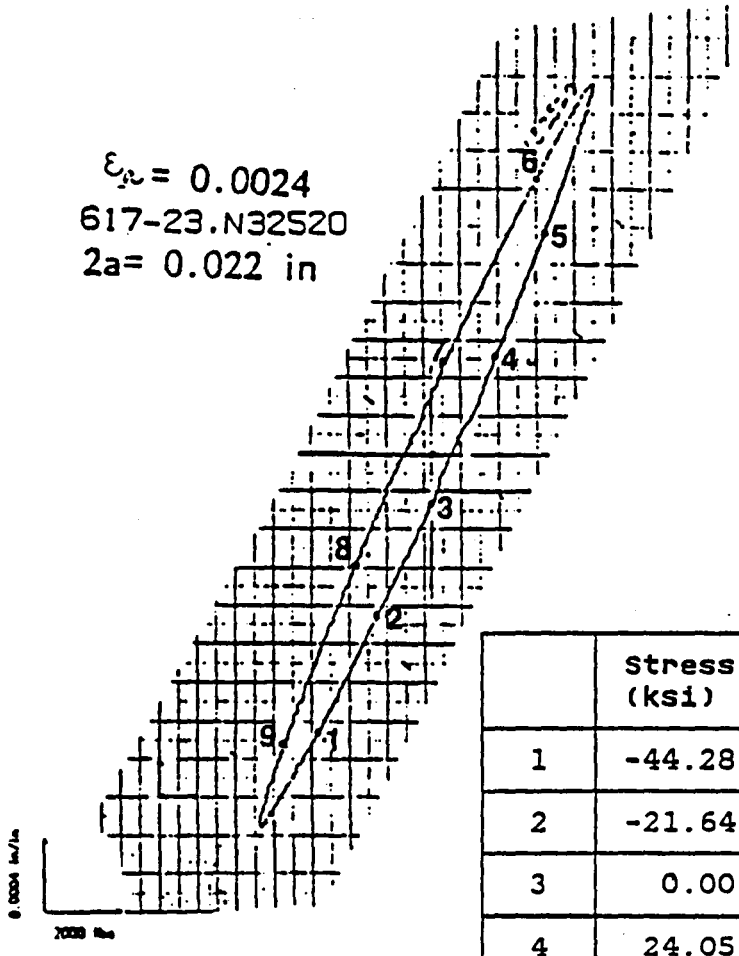


| | Stress (ksi) | Strain |
|---|---|---|
| 1 | -44.28 | -0.00185 |
| 2 | -21.64 | -0.00125 |
| 3 | 0.00 | -0.0005 |
| 4 | 24.05 | 0.0004 |
| 5 | 42.72 | 0.00128 |
| 6 | 39.60 | 0.0018 |
| 7 | 5.65 | 0.00065 |
| 8 | -28.28 | 0.00066 |
| 9 | -55.16 | -0.00192 |

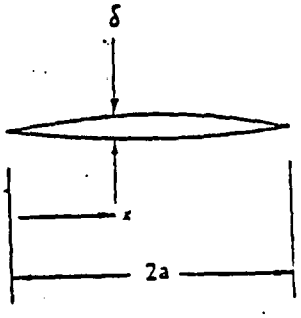


Fig. 37: Crack opening displacements measured in one complete cycle (a) Load displacement loop as obtained from clip gauge mounted across the grip ends and the points (corresponding stress and strain levels shown in table) where closure observations were made.

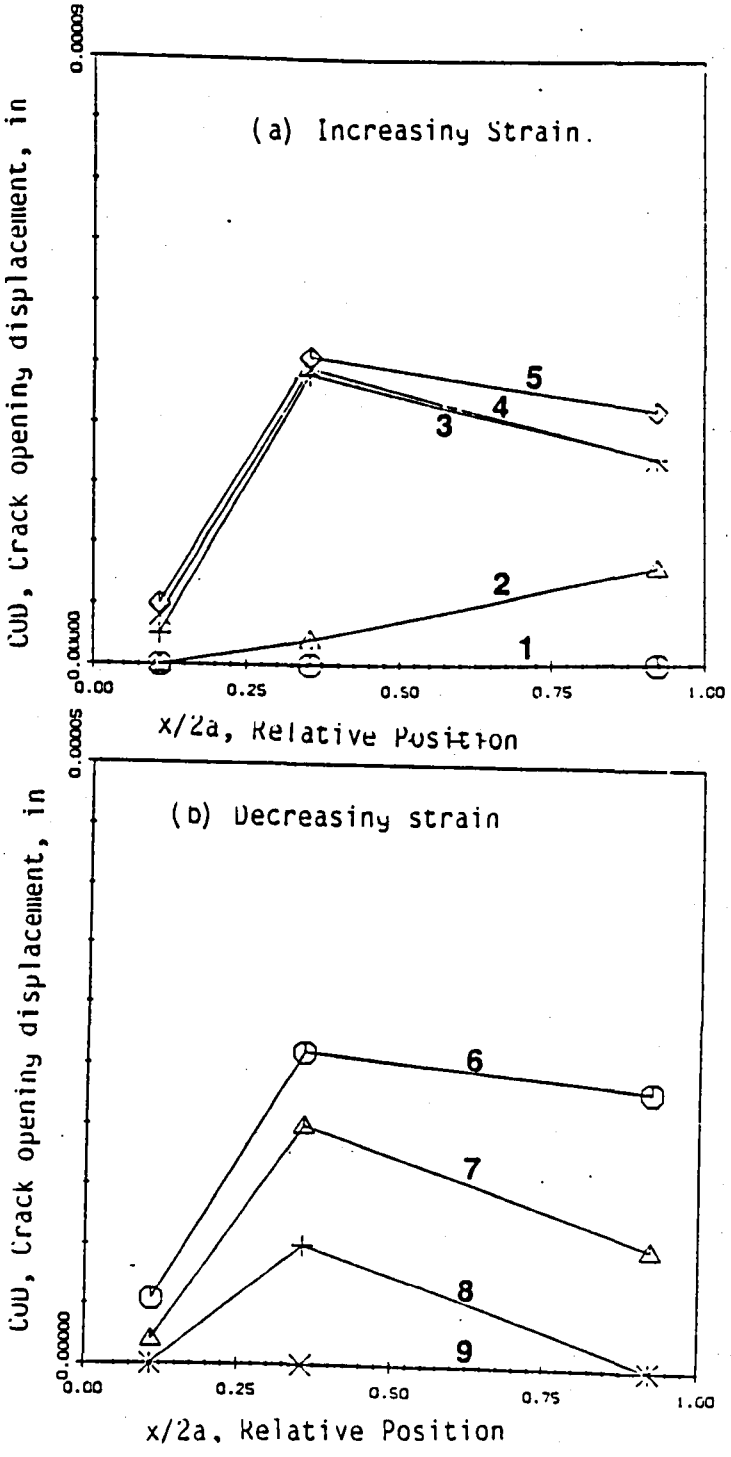


(b) Crack opening displacement during increasing (loading) and decreasing strain (unloading) at different points along the crack length. Different stress (strain) levels correspond to the points shown in load displacement loop.

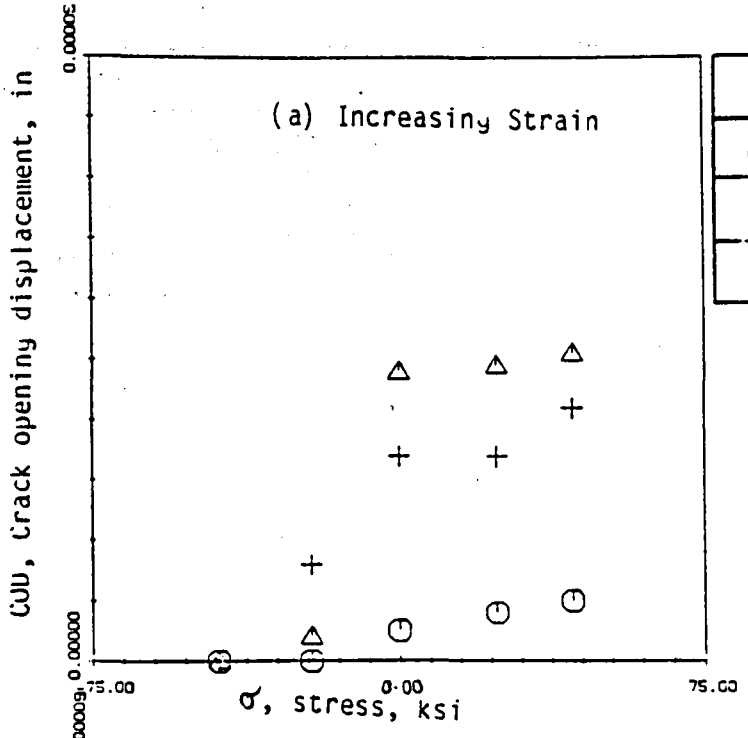


| | x(in) | x/2a |
|---|---|---|
| ⊙ | 0.0024 | 0.1091 |
| △ | 0.0054 | 0.3545 |
| + | 0.0203 | 0.9227 |

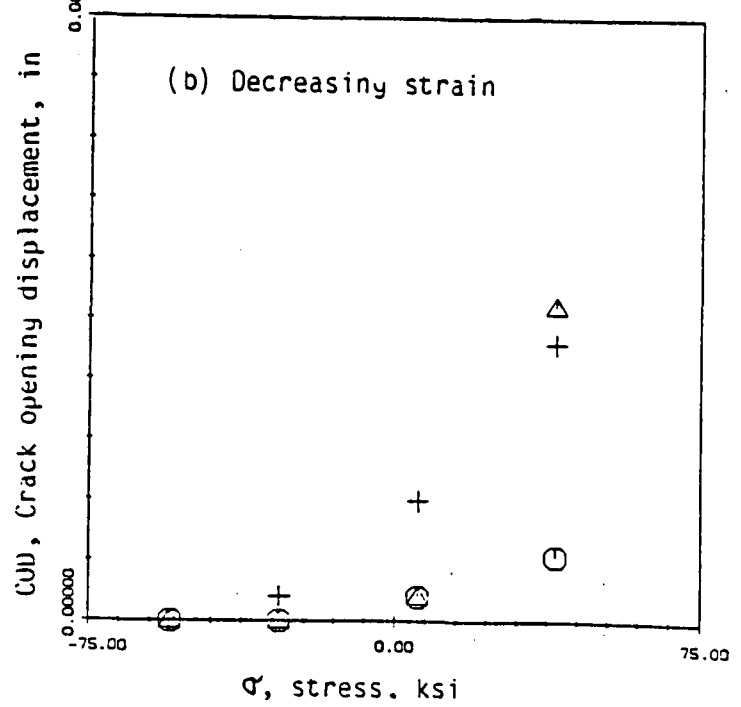


(c) Crack opening displacement as a function of stress at different points along the crack length during increasing and decreasing strain.

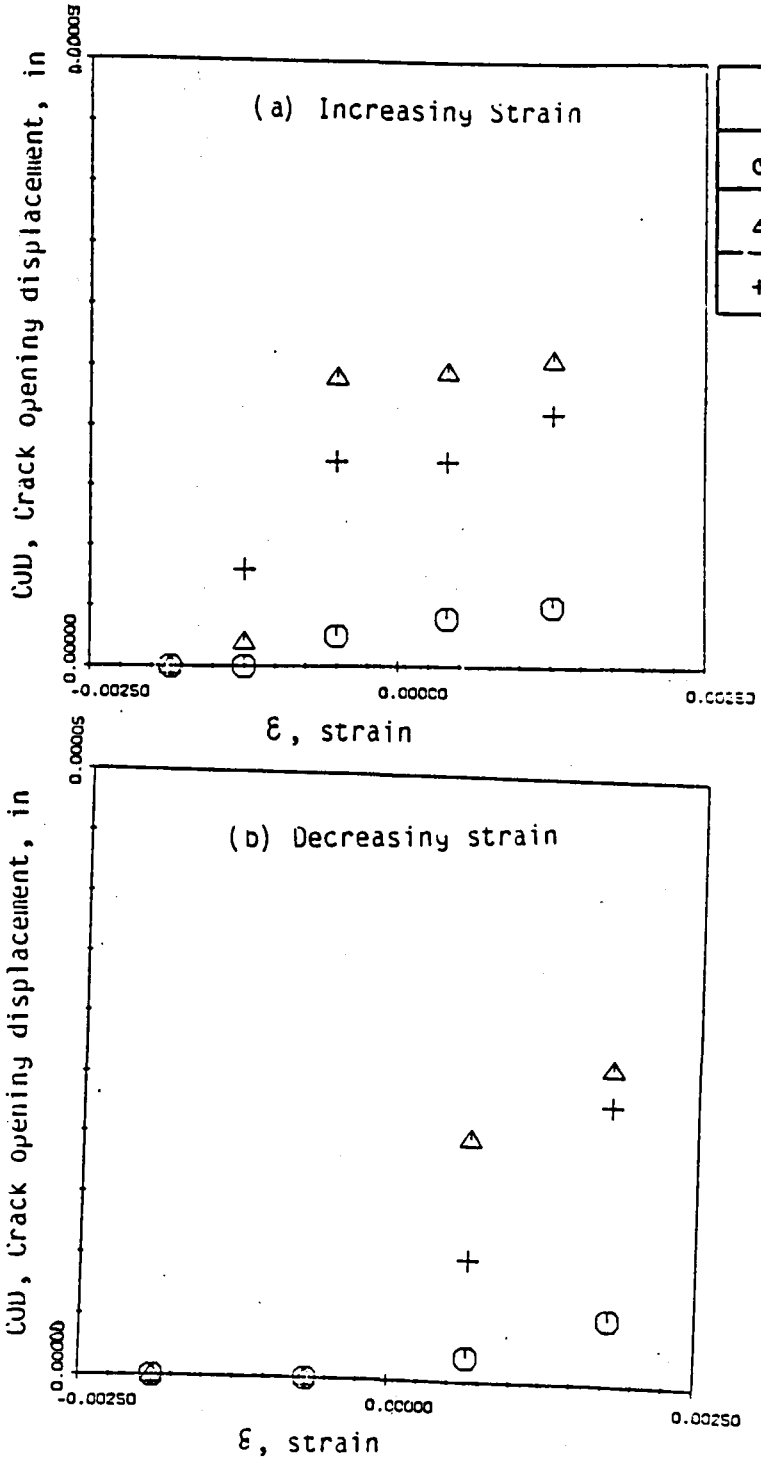


| | x(in) | x/2a |
|---|---|---|
| ⊙ | 0.0024 | 0.1091 |
| △ | 0.0054 | 0.3545 |
| + | 0.0203 | 0.9227 |

(d) Crack opening displacement as a function of strain at different points along the crack length during increasing and decreasing strain.

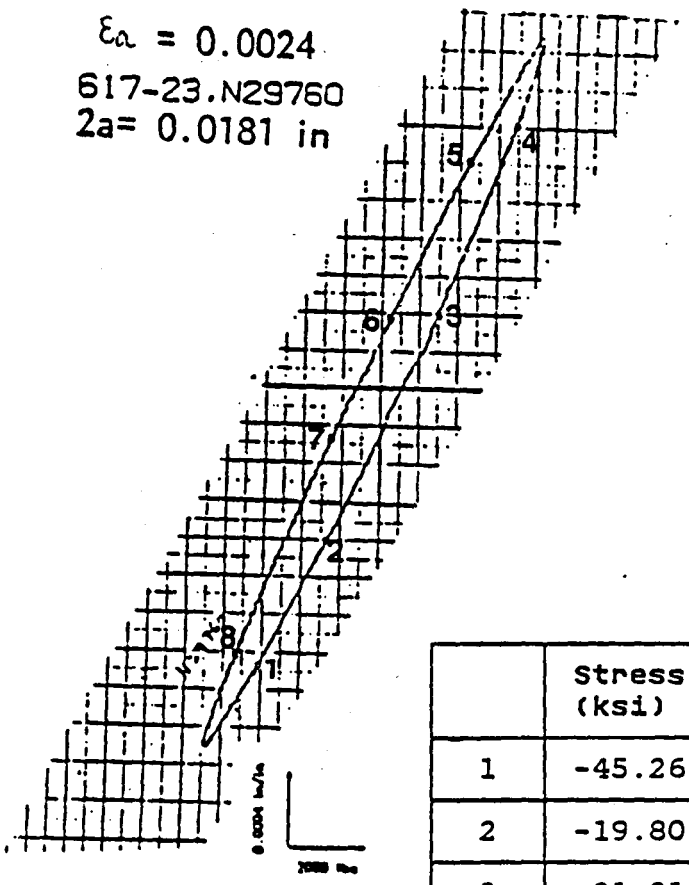


| | Stress (ksi) | Strain |
|---|---|---|
| 1 | -45.26 | -0.001925 |
| 2 | -19.80 | -0.00117 |
| 3 | 21.21 | 0.0003 |
| 4 | 49.50 | 0.00172 |
| 5 | 32.53 | 0.00150 |
| 6 | 4.24 | 0.0005 |
| 7 | -18.38 | 0.00025 |
| 8 | -53.74 | -0.00195 |

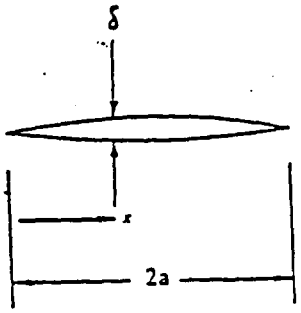


Fig. 38: Crack opening displacements measured in one complete cycle
(a) Load displacement loop as obtained from clip gauge mounted across the grip ends and the points (corresponding stress and strain levels shown in table) where closure observations were made.

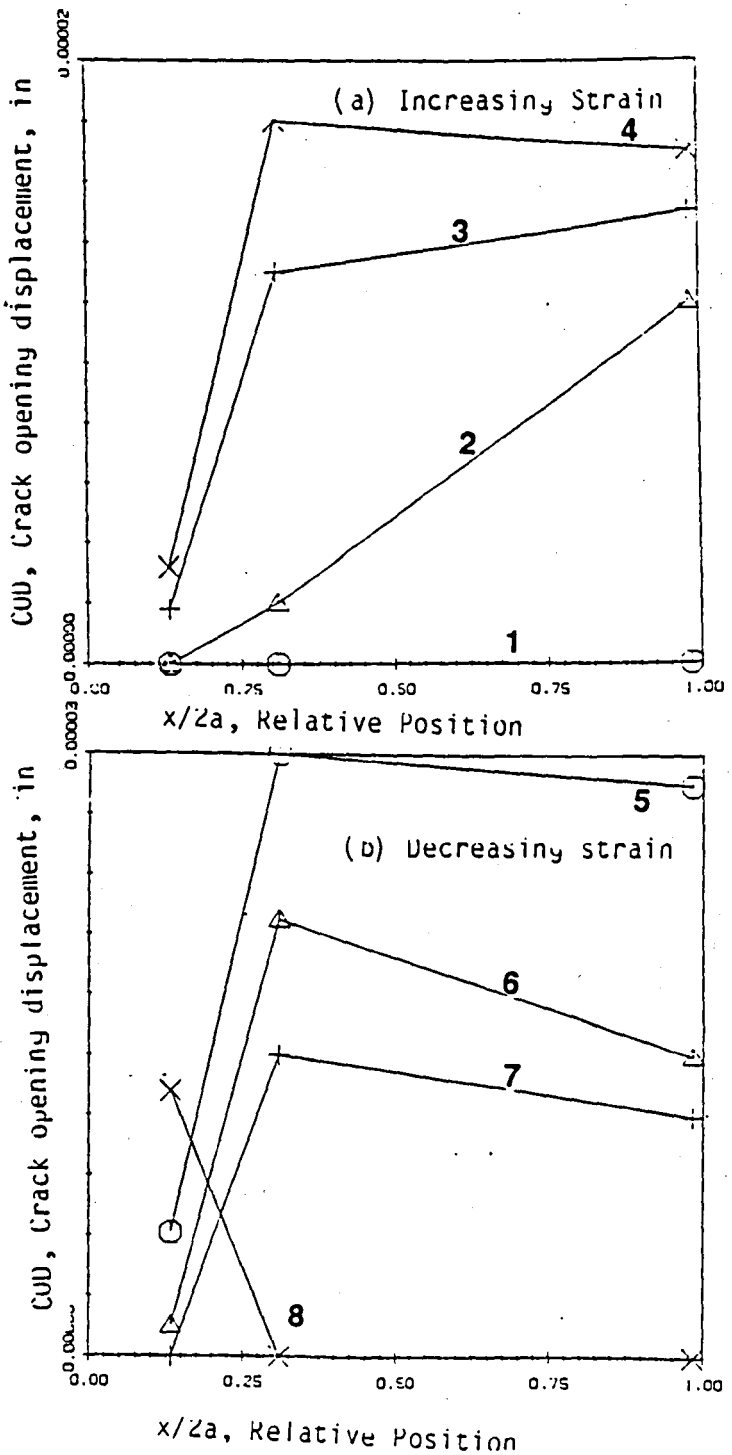


(b) Crack opening displacement during increasing (loading) and decreasing strain (unloading) at different points along the crack length. Different stress (strain) levels correspond to the points shown in load displacement loop.

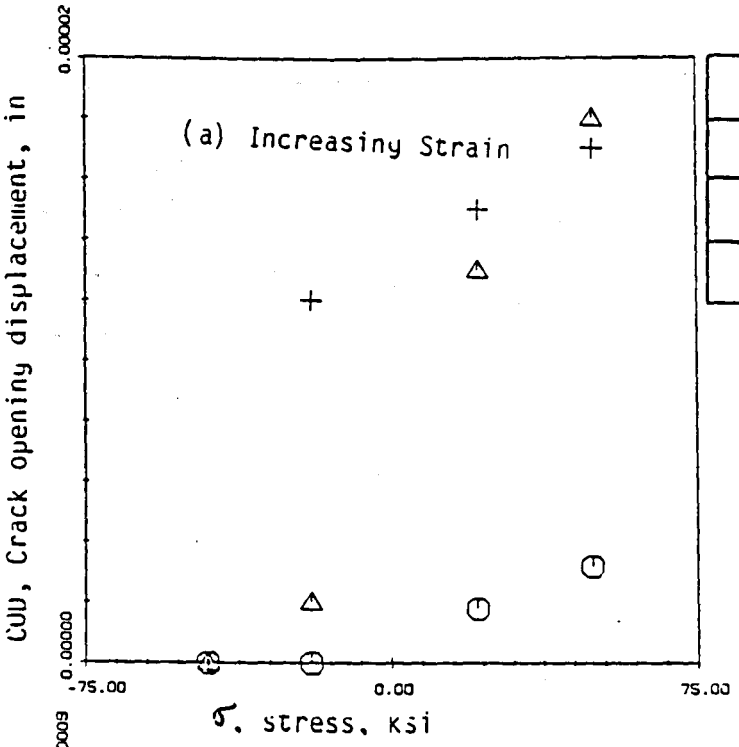


| | x(in) | x/2a |
|---|---|---|
| ○ | 0.0024 | 0.1326 |
| △ | 0.0056 | 0.3093 |
| + | 0.0178 | 0.9834 |

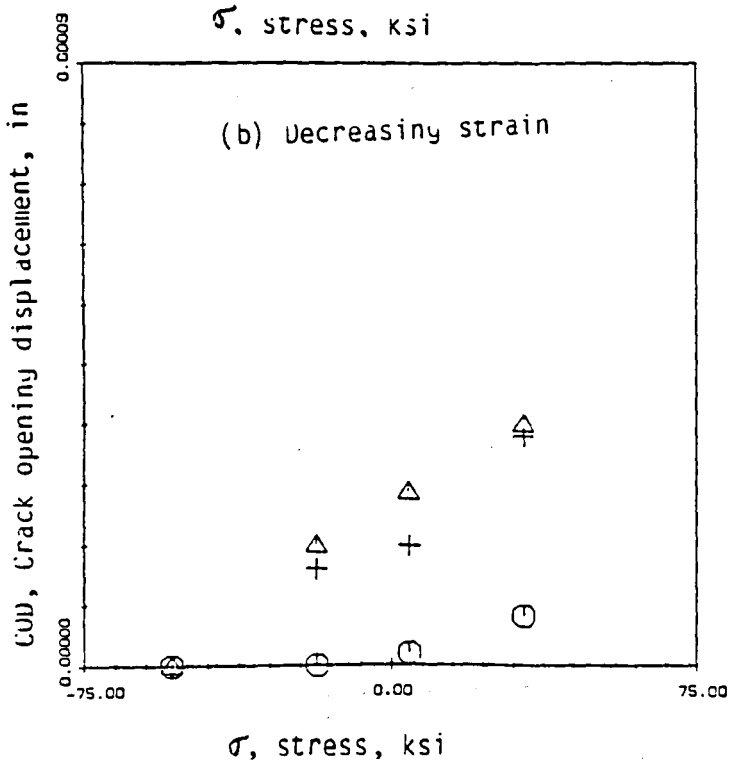


(c) Crack opening displacement as a function of stress at different points along the crack length during increasing and decreasing strain.

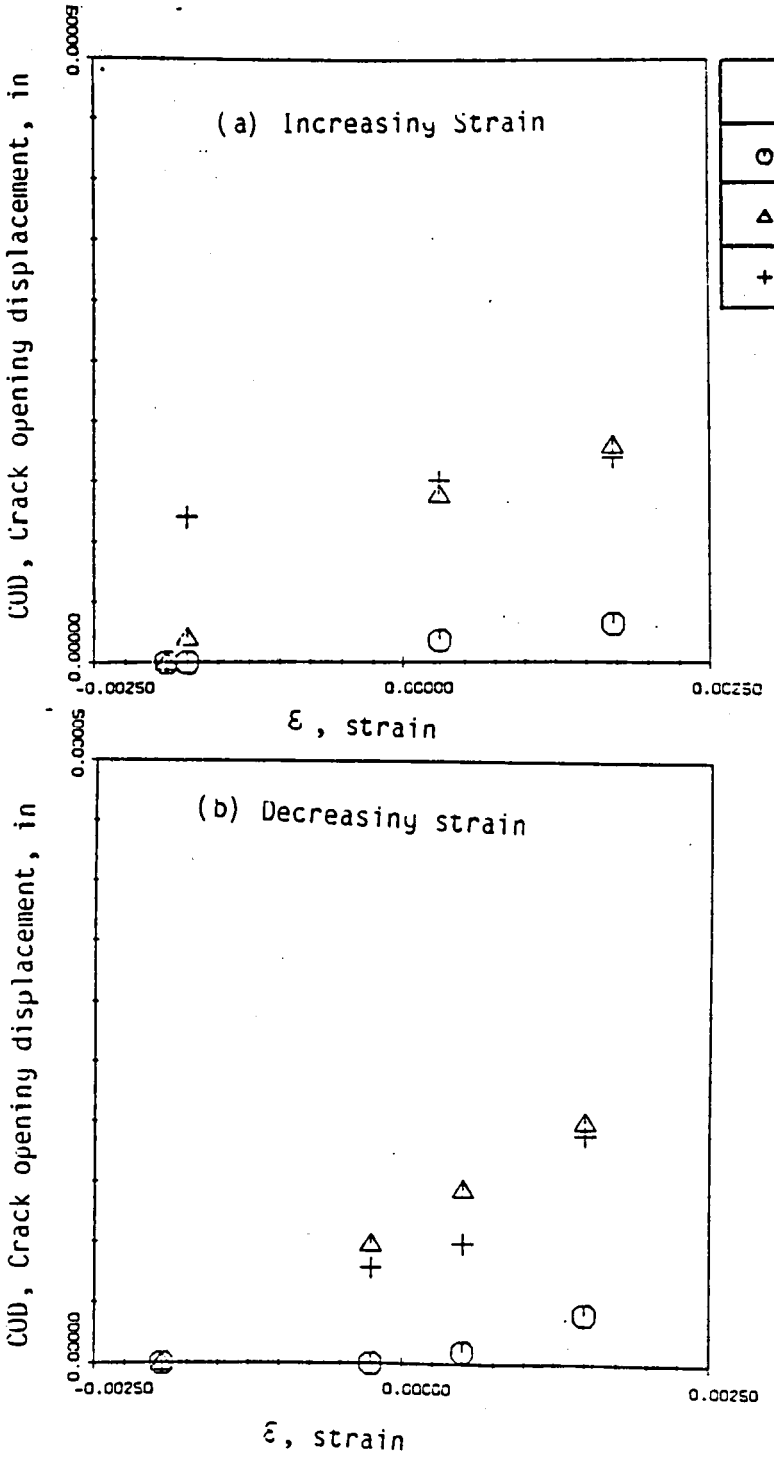


| | x(in) | x/2a |
|---|---|---|
| ○ | 0.0024 | 0.1326 |
| △ | 0.0056 | 0.3093 |
| + | 0.0178 | 0.9834 |

(d) Crack opening displacement as a function of strain at different points along the crack length during increasing and decreasing strain.

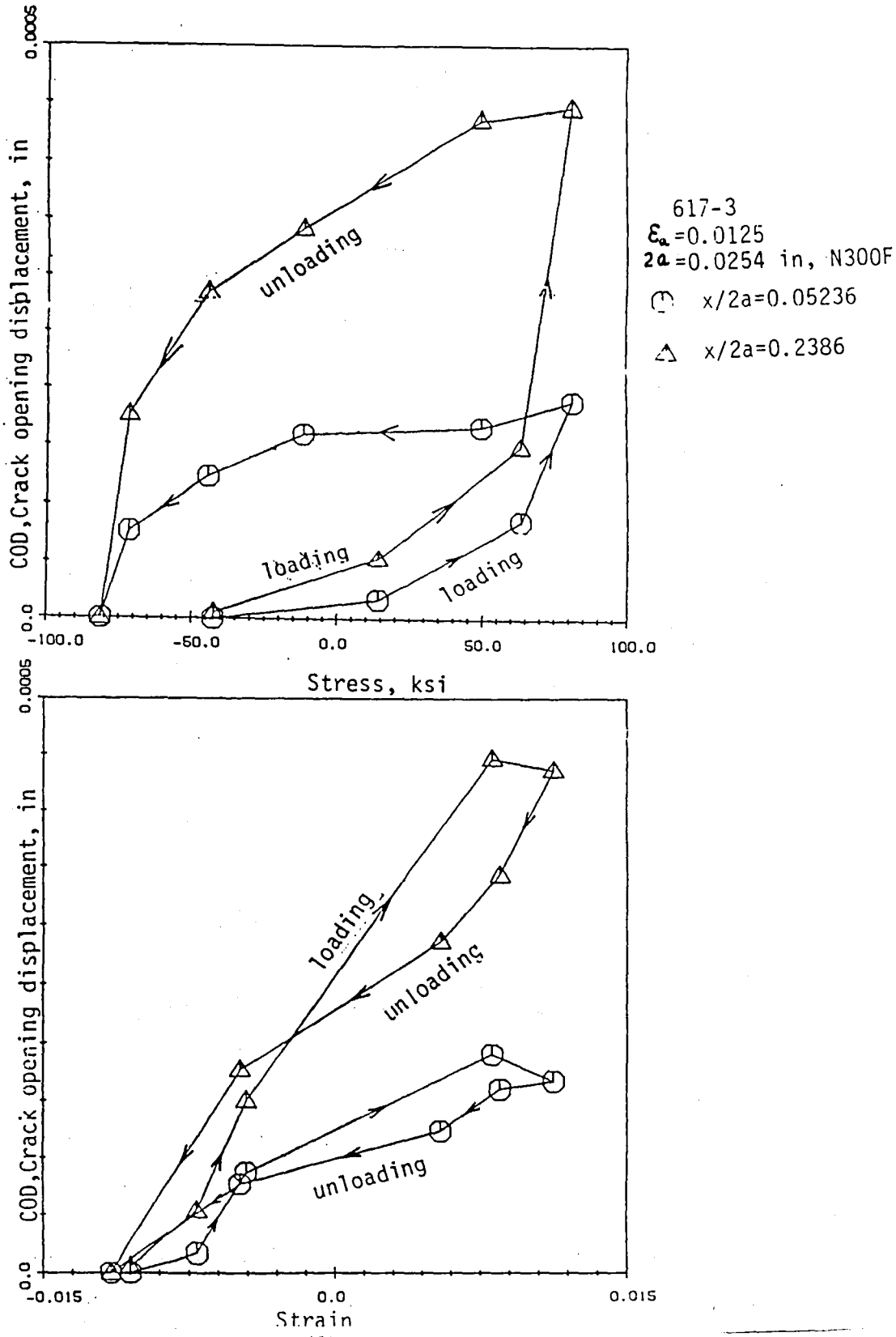


Fig. 39: Loading and unloading paths in a typical COD vs stress, and COD vs. strain plots.

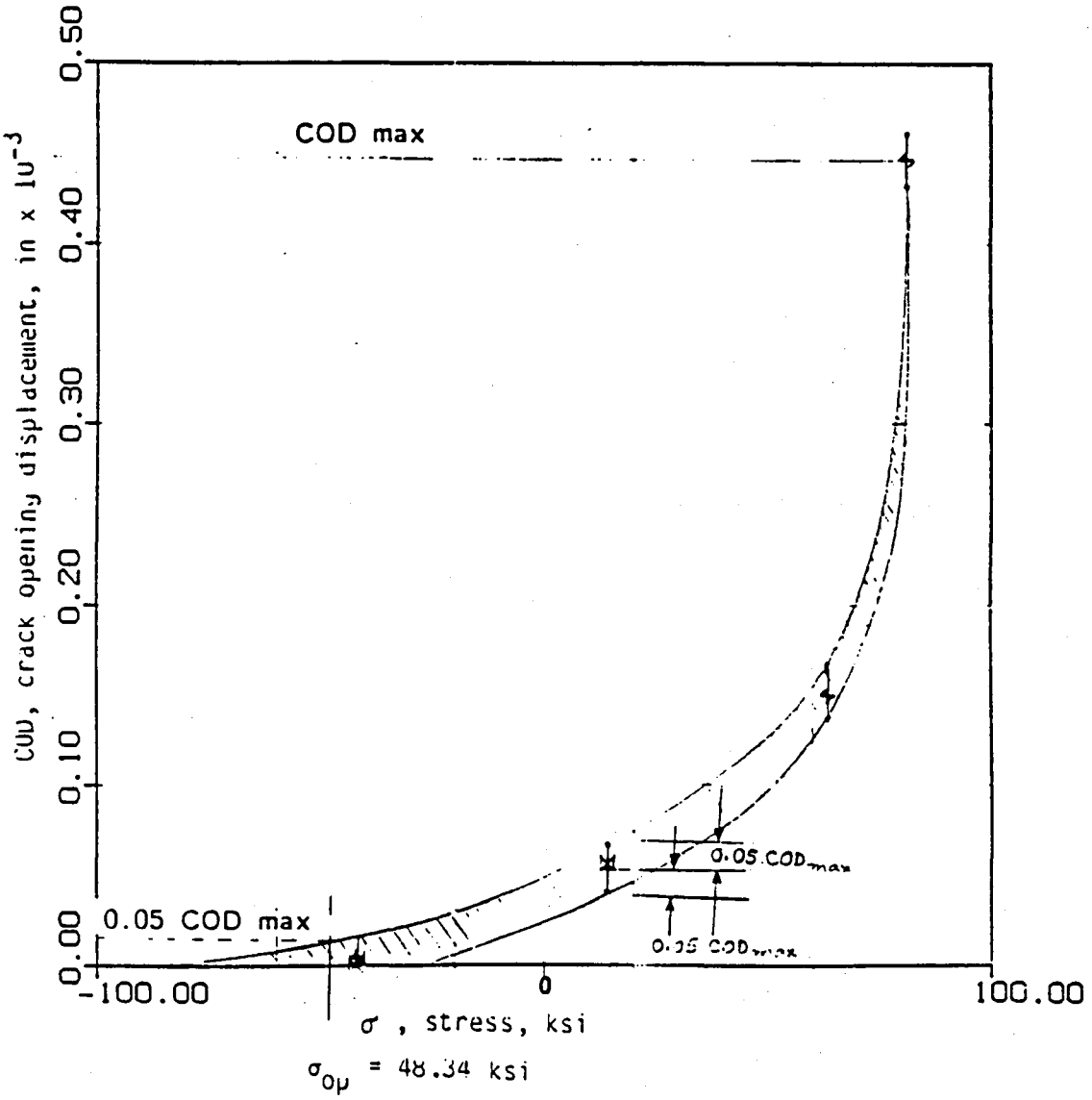


Fig. 40: Typical measurement of the crack opening stress level ($\sigma_{op}$).

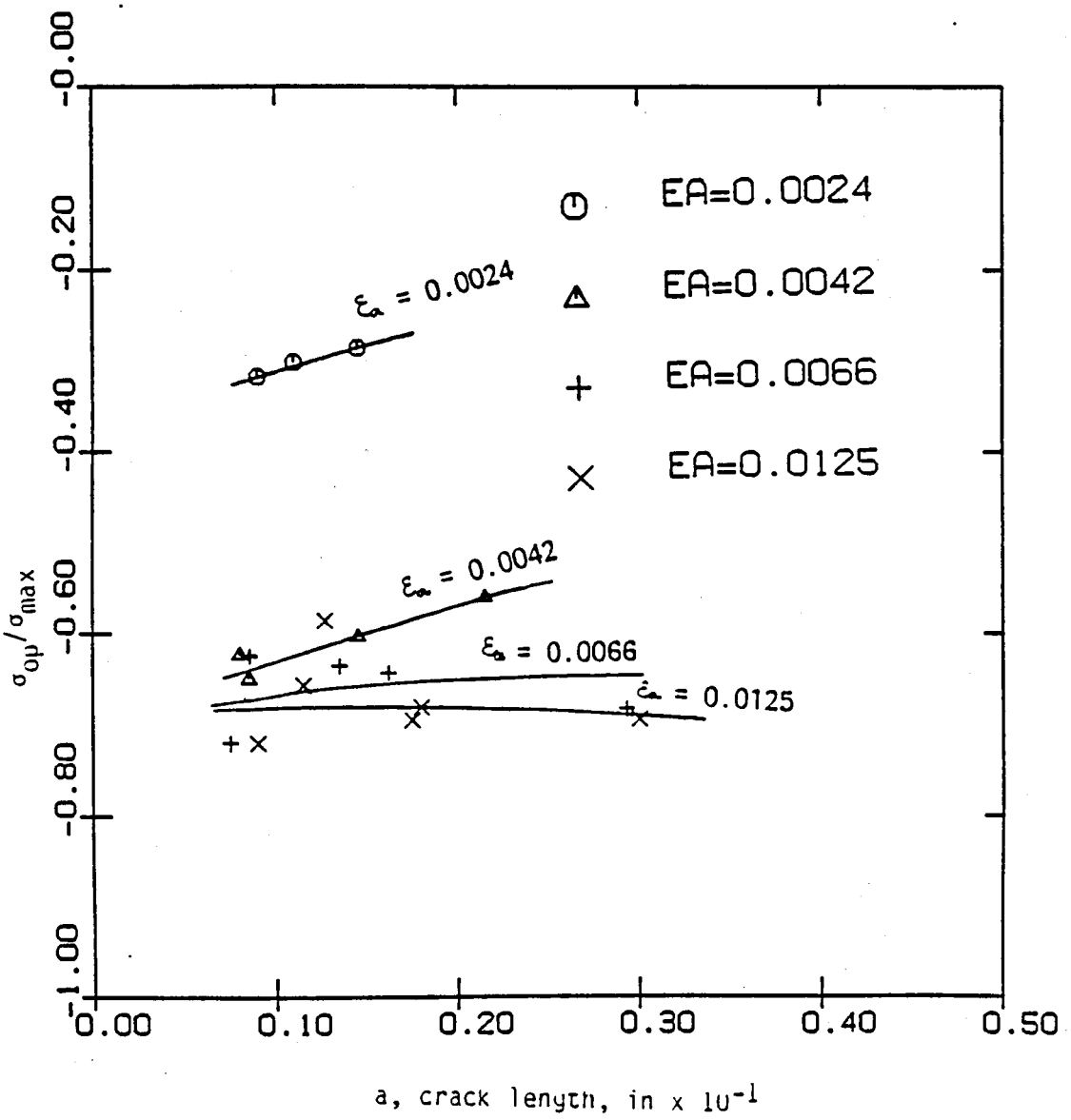


Fig. 41: Crack opening stress level as a function of crack length

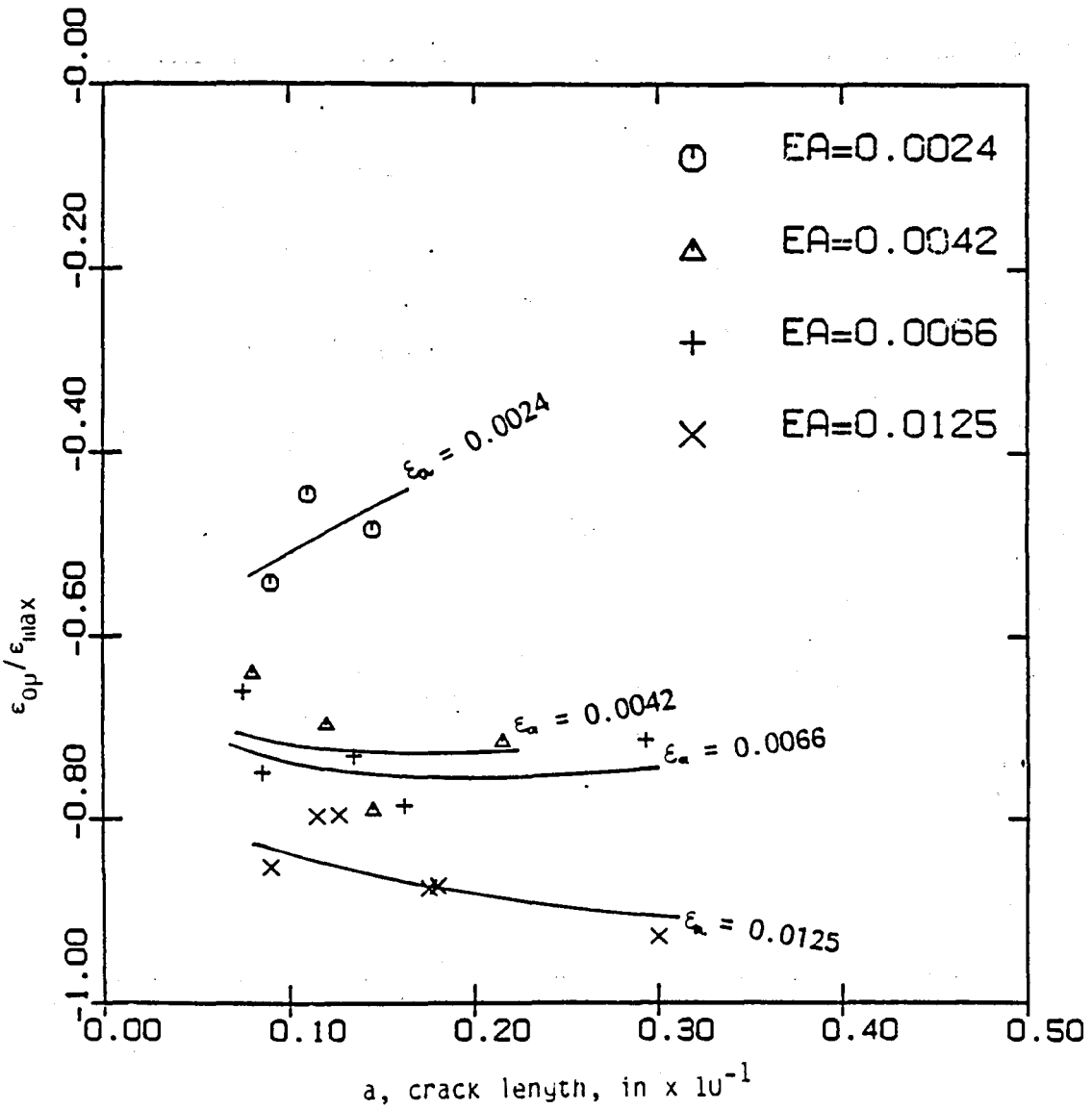


Fig. 42: Crack opening strain level as a function of crack length

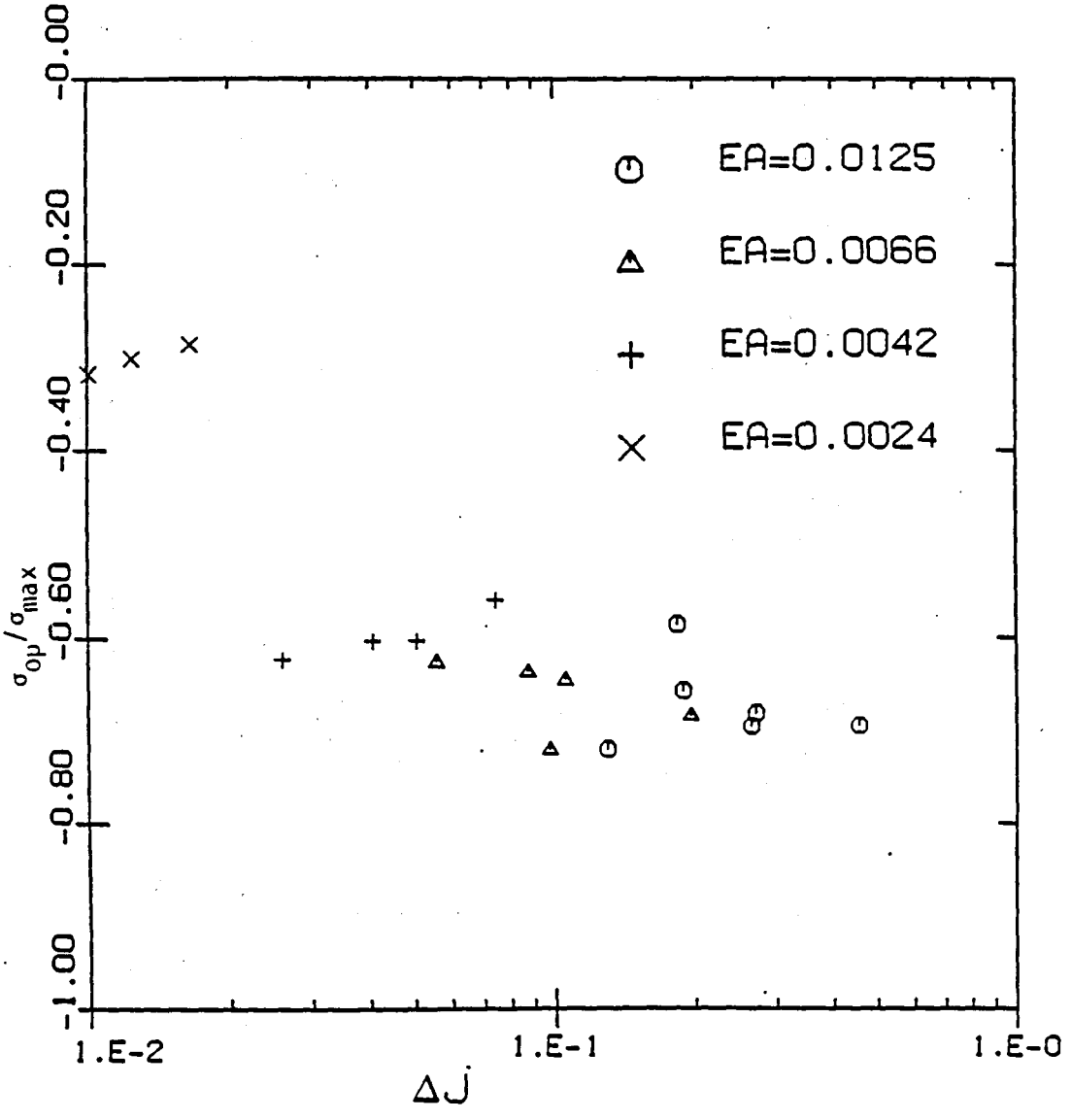


Fig. 43: Crack opening stress level as a function of $\Delta J$

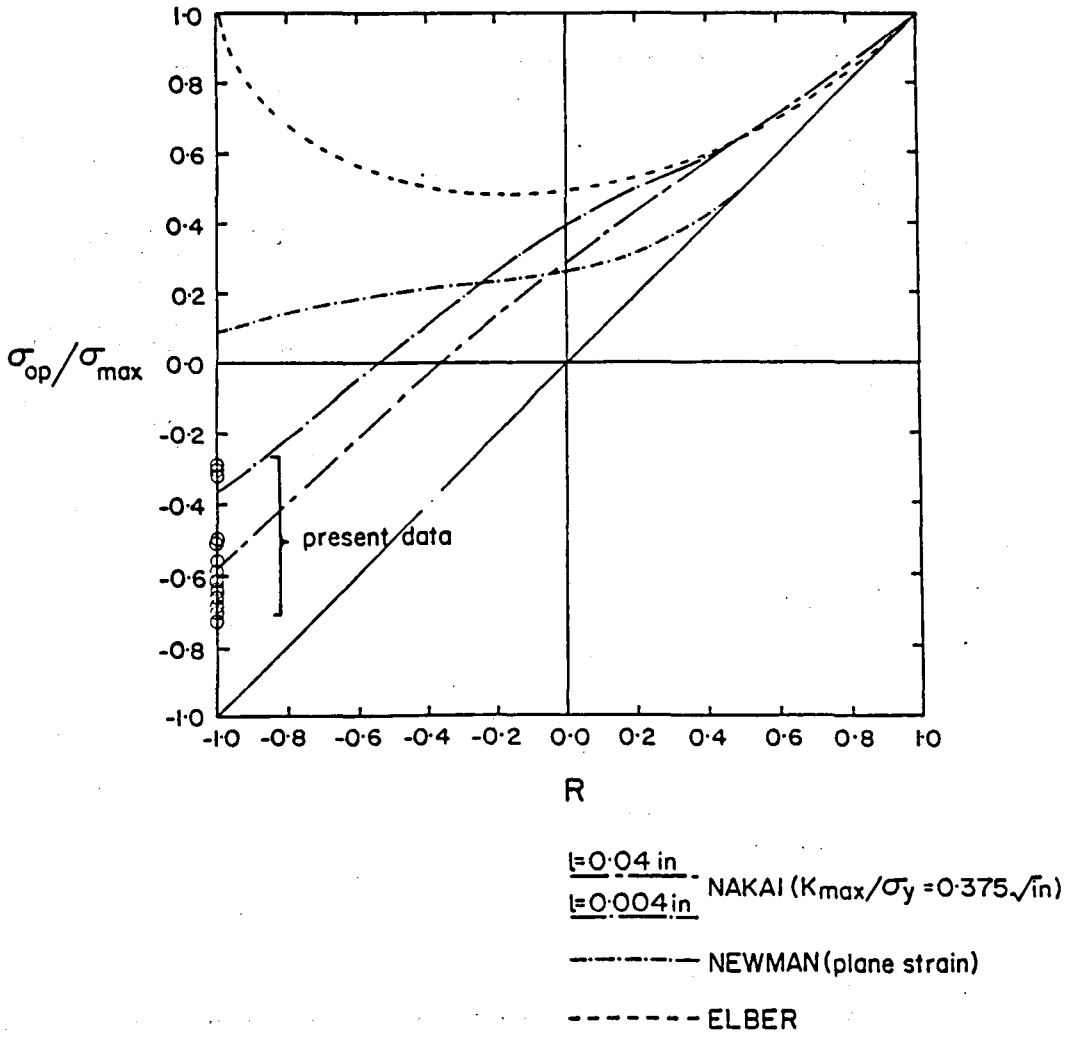


Fig. 44: Crack opening stress level as a function of R

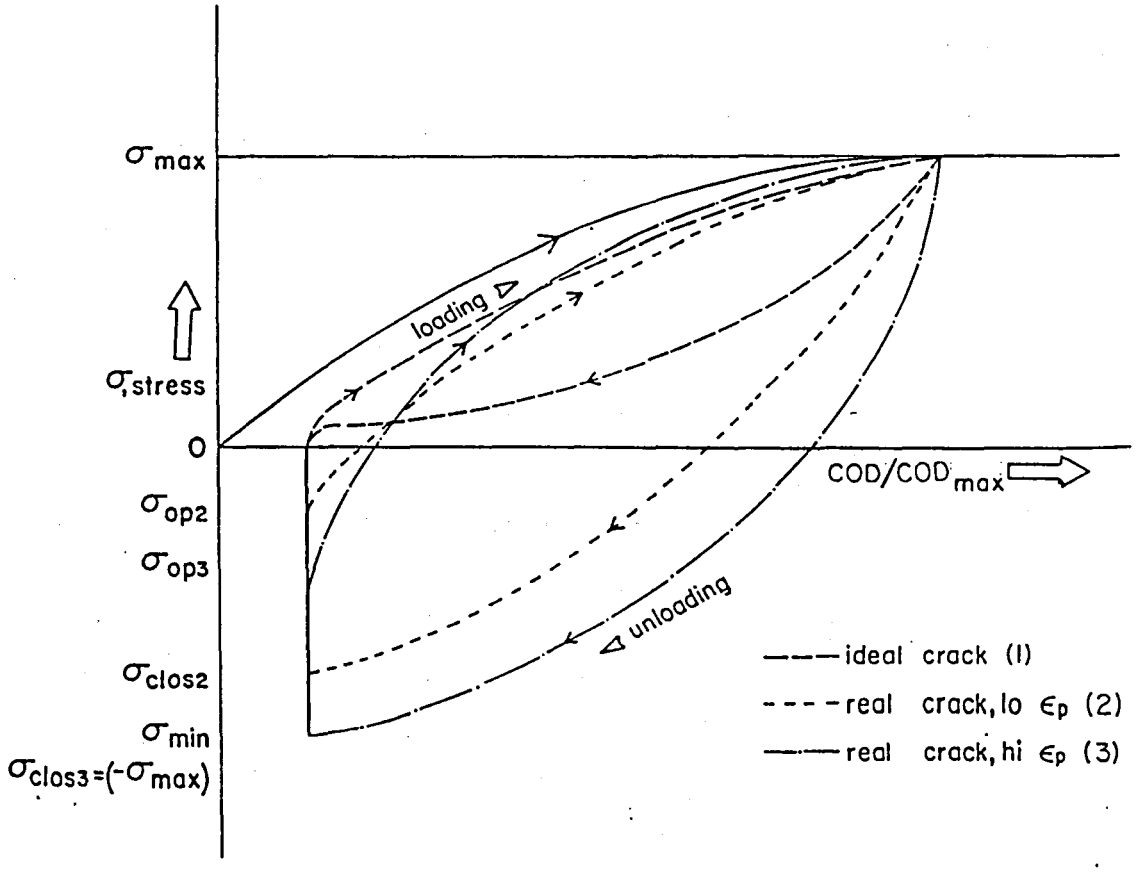


Fig. 45: Schematic diagram of the real crack behavior at high strains and corresponding ideal crack behavior.

| 1. Report No. | 2. Government Accession No. | 3. Recipient's Catalog No. |
|---|---|---|
| NASA CR-175021 | | |

| 4. Title and Subtitle | 5. Report Date |
|---|---|
| Closure of Fatigue Cracks at High Strains | December 1985 |
| | 6. Performing Organization Code |

| 7. Author(s) | 8. Performing Organization Report No. |
|---|---|
| N.S. Iyyer and N.E. Dowling | None |
| | 10. Work Unit No. |

| 9. Performing Organization Name and Address | 11. Contract or Grant No. |
|---|---|
| Virginia Polytechnic Institute and State University<br>Engineering Science and Mechanics Department<br>Blacksburg, Virginia 24061 | NAG 3-438 |
| | 13. Type of Report and Period Covered |
| 12. Sponsoring Agency Name and Address | Contractor Report |
| National Aeronautics and Space Administration<br>Washington, D.C. 20546 | 14. Sponsoring Agency Code |
| | 505-33-7C |

15. Supplementary Notes

Final report. Project Manager, Thomas W. Orange, Structures Division, NASA Lewis Research Center, Cleveland, Ohio 44135.

16. Abstract

Experiments were conducted on smooth specimens to study the closure behavior of short cracks at high cyclic strains under completely reversed cycling. Testing procedures and methodology, and closure measurement techniques, are described in detail. The strain levels chosen for the study cover from predominantly elastic to grossly plastic strains. Crack closure measurements were made at different crack lengths. The study reveals that, at high strains, cracks close only as the lowest stress level in the cycle is approached. The crack opening was observed to occur in the compressive part of the loading cycle. The applied stress needed to open a short crack, under high strain was found to be less than for cracks under small scale yielding. For increased plastic deformations, the value of $\sigma_{op}/\sigma_{max}$ is observed to decrease and approaches the value of R. Comparison of the experimental results with existing analysis has been made and indicates the limitations of the small scale yielding approach where gross plastic deformation behavior occurs.

| 17. Key Words (Suggested by Author(s)) | 18. Distribution Statement |
|---|---|
| Crack; Crack growth; Small cracks;<br>Crack closure; Plasticity; J-integral | Unclassified - unlimited<br>STAR Category 39 |

| 19. Security Classif. (of this report) | 20. Security Classif. (of this page) | 21. No. of pages | 22. Price* |
|---|---|---|---|
| Unclassified | Unclassified | 158 | A08 |

*For sale by the National Technical Information Service, Springfield, Virginia 22161

End of Document